In situ measurement of gas concentrations in working catalytic reactors by HPNMR

UNIVERSITY OF LIVERPOOL

Thesis submitted in accordance with the requirements of the University of Liverpool for the degree of Doctor in Philosophy by *Alexandre Torres Herce*.

January 2009

Acknowledgements

I would like to start thanking my supervisors Jon Iggo and John Satherley for giving me the opportunity of doing this PhD research project with them, and for all the great teaching, support and encouragement given during these four years.

This project could not be done without Graham Eastham and Darren Goby from Lucite International. Thank you very much for giving me this opportunity, your help has been invaluable in the development of this project. Big thanks to Lucite for the funding.

I would like to thank all the staff in the chemistry department of the University of Liverpool, especially to Ritchie and Warren in the mechanical workshop, and Charlie in the electrical workshop. Your work has been essential for this project; it made possible the making of our experiments so many times.

I also want to thank the staff of Lucite International in the Wilton Research Centre; they made me feel comfortable at all times over there.

Thank you to all the colleagues in the lab, especially to Jiankee and Gill for your help with the chemistry.

Big thanks too all the good friends I made in Liverpool: Nacho, Carlos, Fity, Sergio, Victor, Santi, Jesus, Jose, Miriam… and especially to Dan, you all made my days much funnier.

Thank you to all my old friends in Spain: Arenke, Jaime, Blanca, Sarmi, Josiño, Karen, Gil, Juanin, Angel, Iago, el primo Javi… thanks for your visits, we really enjoyed Liverpool together.

I want to give the most felt thanks my family for their support and encouragement in the good and bad moments, we did it, the PhD is finally here.

Finally, thank you very much to the most especial person in my life, Enza, you give me the biggest and most useful support.

Abstract

This thesis describes a new experimental protocol for the determination of the solubilities of gases in liquids in the presence and absence of chemical reaction by NMR.

A new high pressure NMR bubble column system and experimental protocol have been developed for the quantitative measurement of gas solubilities at different temperatures and pressures. This new experimental method consists of a gas flow recycling system in which the liquid phase partially fills the equilibrium cell (sapphire tube) and a gas stream is bubbled through the solvents continuously. The composition of the liquid phase in the equilibrium cell can be measured at all times. This system allows equilibrium to be established rapidly, and the temperature and pressure of the equilibrium cell can be readily varied. Thus, the composition of the liquid phase in equilibrium with the gas phase can be rapidly and reliably determined.

Measurements are taken by charging a known amount of the gas mixture to the HPNMR system and isotherms constructed point by point. The system pressure at each equilibrium condition is also recorded to afford the mole fraction as a function of system pressure at each temperature. The solubilities of CO and C_2H_4 in mixtures of methyl propanoate and methanol in the pressure range 1 to 25 bar and temperature range 323 K to 373 K have been determined. The solubility of the gases in the solvent system has also been modelled using a combination of the UNIQUAC activity coefficient method and Redlich Kwong equation of state.

The new HPNMR bubble column design has been used not only for the determination of the vapour-liquid equilibrium, but also for a kinetic study of the methoxycarbonylation of ethylene for the production of MeP, first stage of the Lucite's Alpha Process for the production of MMA. The experimental system allowed for the determination of the reaction kinetics regime thanks to the simultaneous study of reaction and mass transfer processes by monitoring of reacting solution composition.

Table of contents

Nomenclature:

CO: carbon monoxide

C_2H_4: ethylene

MeOH: methanol

MeP: methyl propanoate

NMR: nuclear magnetic resonance

FID: free induction decay

nOe: nuclear Overhauser effect

Ha: Hatta number

V: volume

P: pressure

p: partial pressure

p^0: vapour pressure

T: temperature

S: entropy

$\bar{s}$: partial molar entropy

H: enthalpy

$\bar{h}$: partial molar enthalpy

R: ideal gas constant

f: fugacity

a: activity

x: mole fraction in liquid phase

y: mole fraction in gas phase

n: moles

Z: compressibility factor

H: Henry's coefficient

T_1: relaxation time constant

I: NMR intensity

C: concentration

k_L: liquid phase mass transfer coefficient

k_G: gas phase mass transfer coefficient

t: time

D : diffusivity

k_{mn} : reaction rate constant

Pd: palladium

Greek symbols:

φ : fugacity coefficient

γ : activity coefficient

μ : chemical potential

$\alpha\alpha$, $\alpha\beta$, $\beta\alpha$, $\beta\beta$: energy levels

ρ : density

Subscripts:

i, j, 1, 2, A, B: component i, j, 1, 2, A, B

c: critical property

r: reduced property

vap: vaporization

i: interface

R: reaction

D: diffusion

Superscripts:

0: standard state

α , β : phase α , β

v: vapour phase

l: liquid phase

Chapter 1

Introduction

Chapter 1: Introduction

1.1. Introduction – Problem summary

The methoxycarbonylation of ethylene to form methylpropanoate (MeP) using a palladium phosphine catalyst is a homogeneous catalytic reaction which has been developed by Lucite International as part of a novel two-stage route to methyl methacrylate (MMA)[1]. A substantial amount of research has been carried out on the mechanisms and catalysts for the homogeneous catalytic methoxycarbonylation of ethylene for the production of methyl propanoate (MeP). Investigations have focused on understanding all the steps that take place during the reaction and on catalyst species used for the carbonylation of alkenes, usually palladium based complexes, and how their chemistry affects the mechanism and the possible final product.

The mechanism, explained later on, shows how carbon monoxide (CO) and ethylene (C_2H_4) molecules must coordinate with the metal centre of the catalyst, dissolved in a liquid mixture of methanol (MeOH) and methyl propanoate (MeP). From an engineering point of view the issue is how to put the components together for the reaction to happen, the CO and the ethylene must dissolve in the liquid mixture so that the concentration of these components is sufficient for the coordination to happen. The

composition of these gaseous components, ethylene and carbon monoxide, dissolved in the liquid phase is governed by vapour-liquid equilibrium (VLE) thermodynamic relations, and so it depends on the composition of the liquid phase, the temperature, the partial pressures of these gaseous components in the gas phase, and the physical properties of each compound present in the equilibrium system. The system under study is a four-component two-phase gas-liquid equilibrium, which is experimentally determined and theoretically resolved using a thermodynamic model based on a combination of the Redlich Kwong equation of state and the UNIQUAC activity coefficient model. Hence, the concentration of the four components in the liquid phase for different equilibrium conditions of temperature and pressure is experimentally measured and theoretically calculated.

When reaction happens, carbon monoxide and ethylene are consumed through coordination with methanol in the catalyst metal centre to produce methyl propanoate. The fact that some components must be transported from a gas phase to a liquid reaction phase makes the process kinetics much more complex; there are two different processes involved which affect one another reciprocally, mass transfer and reaction. For example, as CO and ethylene are consumed by reaction, the equilibrium condition is modified, so more CO and ethylene are dissolved at the same time they react with methanol producing MeP. Thus, the global process kinetics will

depend on these two processes: mass transfer and reaction.

The existence of mass transfer and chemical reaction, which can be thought of as two resistances, lead to different possibilities in the kinetics regime depending on which is the controlling resistance in the overall process. Hence, if the reaction is slower than the dissolution of CO and ethylene in the liquid phase, the overall process rate will be controlled by the slower step in chemical reaction mechanism. In contrast, if mass transfer is slower than the reaction, the controlling step will be the dissolution of the gaseous components in the liquid phase, and the reaction would not happen until enough CO and ethylene are present in the reaction mixture. Hence, it is crucial to get the gaseous components dissolved in the liquid phase properly and as fast as possible to obtain true reaction kinetics and to avoid limiting the reaction rate due to inefficient mass transfer. Without a proper method for dissolving the gases, and having them present in the liquid reaction phase in enough concentrations, the mechanism defined for the reaction may not represent the real process.

In summary, this project can be roughly described as the study of a homogeneous catalytic gas-liquid reaction. The determination of gas solubilities and vapour-liquid equilibrium is crucial for a good understanding and design of the two-phase catalytic reaction. Therefore, the VLE study based on experimental solubility determinations and theoretical thermodynamics will be the central topic of the project. This

thesis consists of three main parts: the design of an experimental system allowing gas solubility determinations in a working catalytic reaction as well as in an equilibrium steady state without reaction (Chapters 2 and 3); the four-component vapour-liquid equilibrium study (Chapter 4); and the kinetic study of the palladium catalysed methoxycarbonylation of ethylene (Chapter 5). This introduction chapter gives basic concepts and literature review on: homogeneous catalysis and the methoxycarbonylation of ethylene; determination of solubilities of gases in liquids and a detailed description of the vapour-liquid equilibrium calculation applying thermodynamics; and nuclear magnetic resonance (NMR), analytical method used for the determination gas solubilities.

1.2. Homogeneous catalysis – Methoxycarbonylation of ethylene

Catalysis plays a crucial role in the industrial production of liquid fuels and bulk chemicals. In recent times producers of fine chemicals started to apply catalytic conversions also in their processes. Heterogeneous catalysts are usually preferred for oil processes, except for alkylations in which liquid acids are used. In petrochemicals conversion, both heterogeneous and homogeneous catalysis are used, but homogeneous catalytic processes have grown significantly through the 1980's and 1990's.

A catalyst is usually added to the reactants as a catalyst precursor which subsequently must become active for the catalytic reaction to happen. A catalyst brings the reactants together in a reactive state providing a new reaction pathway with a low barrier of activation, which may involve many intermediates and many steps. These different steps define the mechanism of the reaction, which is a detailed description of the reaction at a molecular bonding level. During a catalytic cycle the catalyst participates in different complexes (intermediates) cycling continuously from one species to another, and in this sense it remains unchanged during a catalytic conversion. Substrates are normally in larger amounts than the catalyst, and the ratio of substrate to catalyst is an important figure in catalytic reactions.

Selectivity is a crucial property in catalytic reactions as it helps to reduce

waste, to reduce the work-up equipment of a plant, and to ensure a more effective use of feedstocks. The other essential property is the reaction rate, which can be increased by many orders of magnitude by slight changes in the catalyst. Rates represent a cost factor, i.e. higher rates allow the use of smaller reaction vessels because of the increase in space-time yields (kg of product per time and reaction volume). Higher rates and catalyst yields (mass of product per unit mass of catalyst) decrease the contribution of catalyst costs per unit mass of product generated.

1.2.1. Homogeneous Catalysis[2] – Organometallic complexes

Homogeneous catalysis refers to catalytic systems in which the reagents and the catalyst components are brought together in one phase, usually a liquid phase. Most recent homogenous catalytic processes generally use organometallic complexes as catalysts, but there are many important processes employing non organometallic complexes as homogeneous catalysts.

Homogeneous catalysis using transition metal complexes has attracted a lot of attention for researchers in recent years. Many discoveries have been reported by investigators from industry and academia. Reactions thought to be optimised and completely developed have now been modernized with the application of completely new catalysts providing better product selectivity.

Organometallic catalysts involve a central metal surrounded by organic and inorganic ligands. Transition metals have the unique property that their *d* shells are only partially filled with electrons, providing them with the distinctive ability to exist in several oxidation states. Therefore, the use of organo-transition-metal complexes offers pathways for an extraordinary range of reactions. A typical transition metal atom has nine valence shell orbitals: one *s*, three *p*, and five *d*, in which it accommodates valence electrons that bond with other moieties known as ligands to form two types of bonds, covalent and coordinated. In a typical covalent bond, one or more electrons are shared between two atoms. However, the electrons that constitute a bond can be unequally shared; in fact, all of the electrons can come from just one of the atoms. This latter kind of bond is usually regarded as a subcategory of the covalent bond and is called a coordinate bond. This capacity to form these two types of bonds with a number of ligands is responsible for the exceptional catalytic properties of the transition metals and their complexes.

The properties of the catalyst are defined by the metal and the different ligands around it. Organometallic catalysts' success is due to the possibility of simple modifications by changing the ligand environment. Hence, critical properties can be changed, and consequently reaction rate and selectivity, by changing the ligands surrounding the metal centre. Therefore, ligand electronic, steric, and bite angle effects are crucial in

homogeneous catalysis by metal complexes.

Historical notes on homogeneous catalysis

Since 1870 numerous heterogeneous catalytic processes have been developed and applied in industry[3]. What was considered to be the first homogeneous catalyst employing organometallic intermediates in industry was mercury sulphate, used in the 1920's[4] for the conversion of acetylene to acetaldehyde. This process involves the addition of water to acetylene with no oxidation occurring. Industrially it is the precursor of the Wacker chemistry, in which acetaldehyde is formed by an oxidative conversion of ethylene, and started to be applied when the coal based economy changed to oil in the 1950's. The oligomerisation of ethylene[5] using cobalt complexes is another process that came on stream in the 1950's.

In the 1960's, the number of homogeneously catalysed processes were still low, nevertheless four more important processes came on stream: the nickel catalysed hydrocyanation (DuPont);[6] the cobalt catalysed carbonylation of methanol (BASF);[7] cobalt catalysed hydroformylation (Shell);[8] and the molybdenum catalysed epoxidation of propene (Halcon Corporation).[9] The 1970's were better times for homogeneous catalysis and the proportion of homogeneous catalysts has been increasing since then with successful processes such as the rhodium catalysed carbonylation of methanol (Monsanto),[10] the rhodium catalysed hydroformylation (Union

Carbide Corporation),[11] Shell's higher olefins process,[12] asymmetric hydrogenation to l-dopa (Monsanto),[13] and ring-opening polymerisation of cyclooctene using tungsten metathesis catalyst (Huels).[14]

Since only large volumes of product justify the expenditure necessary for the development of new homogeneous catalysts and the engineering involved, most of the homogeneous catalytic processes were developed for bulk chemicals. Fine chemicals production using homogeneous catalysis started in the 1990's due to the research results in the bulk chemicals area and the large academic effort that has been expended in this area recently.

1.2.2 Characterisation of the catalyst

The most convenient technique available in laboratories for the characterisation of organometallic complexes is NMR spectroscopy[15]. The latter is also the best method for the study of catalyst precursors and organometallic catalysts and intermediates. In situ observation of a catalyst is not straightforward, NMR requires relatively high concentrations and some species observed may not be involved in the catalytic process. Many designs of high pressure NMR experimental systems for in situ studies of reacting systems in which gas is consumed have been developed, as explained in section 1.4.2. Only in a few laboratories in the world, equipment has been developed allowing good gas-liquid mixing and hence real in situ NMR measurements[16,17,18,19]. In this project a new experimental

system for the monitoring of homogeneous catalytic reactions with gas consumption by high pressure NMR is developed, explained in detail in Chapter 2.

Another technique applied for the study of organometallic catalyst is IR spectroscopy. IR might be more practical, an IR-cell can be used as an on-line detector connected to a reaction vessel. The problem of gas consumption and limited replenishment occurs also in IR cells. This technique has the disadvantage that the structural information that can be obtained is much less than that for NMR. Both IR and NMR spectroscopic techniques play a very important role in the study of the variations of the ligand environment surrounding a metal centre of a catalytic complex in a controlled way. Both techniques can be used at high pressures using appropriate tubes or cells.

1.2.3 Methoxycarbonylation of ethylene

The methoxycarbonylation of ethylene is a homogeneous palladium catalyzed reaction for the production of methyl propanoate. This particular catalytic reaction, where the catalyst is a palladium diphosphine complex, arises from investigations on palladium based catalyst systems for carbonylation of alkenes aimed at the production of polyketones. Hence, for a clear understanding of the reaction it is necessary to know about the catalytic reaction for the formation of polyketones consisting of alternating

molecules of alkenes and carbon monoxide, and then look at the formation of esters (methyl propanoate), which can be produced under the same conditions with the use of similar catalysts from alkenes, CO, and alcohols. The production of polyketones and methyl propanoate from ethylene/CO has received a lot of industrial attention.[20] The basic reactions implicated are the same for both products: formation of initiating species, insertions of ethylene and CO, and a termination step. Hence, polymers are obtained from multiple alternating insertions, while a 1:1:1 stoichiometry for CO, ethylene, and methanol leads to methyl propanoate.

Polyketone

Polyketones are thermoplastics with high performance properties, covering a large range of performance and production costs, and always in demand. Relevant properties of thermoplastics include strength, toughness, wear resistance, chemical resistance, heat resistance, UV stability, etc.

First polyketones obtained from copolymerization of ethylene and carbon monoxide were made via radical polymerisations[21]. Coordination polymerization of ethylene/CO was discovered by Reppe[22] using nickel cyanide catalysts, but the products' molecular weights were too low. The first palladium catalyst producing an alternating polymer of CO and ethylene was reported in 1967,[23] and similar catalysts were used later by Union Oil and Shell[24,25] but with some problems in polymer stability

during processing.

In 1982 Sen[26] found out that weakly coordinated anions and phosphine ligands together with palladium yielded much more stable and active catalyst complexes for the formation of polyketone from CO and ethylene in alcoholic solvents. In 1984 Drent[27] reported that cationic palladium complexes containing chelating bidentate diphosphine ligands produced alternating polymers of ethylene and CO with 100% selectivity, high molecular weight, and high yields (kg per g of Pd per hour). Hence it was possible to produce alternating polymers with high melting points (>260 °C) containing just ppm quantities of palladium in a process at relatively mild conditions (30-60 bar and 80-100 °C).

Ligand effects. Methyl propanoate formation

Knowing the important effect of ligands in organometallic catalysts performance it is of interest to look at the effect of the bridge of bidentate phosphine ligands on the rate and product molecular weight in the carbonylation of ethylene reaction.

In the 1980's, at Shell Research in Amsterdam, cationic palladium complexes containing tertiary phosphine ligands and weakly coordinating anions, similar to those studied by Sen[26], were studied in methanol as catalysts for the methoxycarbonylation of ethylene to give methyl propanoate. They found that no methyl propanoate was produced using

bidentate tertiary phosphine ligands, but high molecular weight polyketone was formed at high rates[28]. A little later, Drent reported that under conditions of polyketone formation, cationic palladium (II) catalysts modified with excess monodentate phosphine and Bronsted acids of weakly coordinating anions, selectively gave methyl propanoate with high rates[29]. He suggested that bidentate ligands are always *cis* coordinated, meanwhile monodentate ones can also coordinate in a *trans* fashion. Hence, if bidentate ligands are used, the starting polymer chain and the empty fourth coordination site are always *cis* to each other, which is the most favourable position for ethylene and CO insertion reactions.

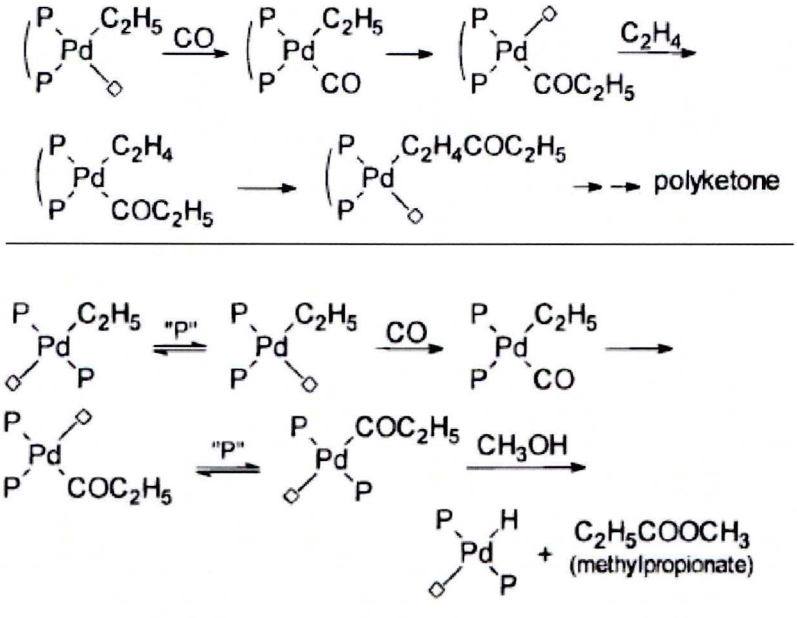

Figure 1.4. Drent's idea of the effect of monodentate and bidentate phosphine ligands for the carbonylation of ethene.[27]

On the other hand, when monodentate phosphines are used, both Pd-alkyl and Pd-acyl species prefer a *trans* orientation of the phosphine ligands for steric reasons, and *cis-trans* isomerisation is expected to be fast because of the presence of excess ligand. Hence, he considered it reasonable to assume that both the insertion of ethylene in Pd-H and the insertion of CO in Pd-alkyl could only occur when the phosphine ligands were *cis*.

However, later in 1999, it was found that several bidentate ligands give high selectivity to methyl propanoate with high reaction rates, and so the initial idea that monodentates were the best ligands for the production of ester had to be abandoned[30]. At the beginning it was thought that these bulky ligands could easily lead to the formation of *trans* diphosphine complexes, which could explain the results. Surprisingly, it was found that acyl complexes containing rigid *trans* coordinating ligands do not undergo alcoholysis[31], hence showing that *cis* coordination is a prerequisite for ester formation, and it was finally concluded that a *cis* coordinated intermediate undergoes methanolysis as the termination step of the reaction. This methanolysis can be viewed as an intermolecular nucleophilic attack of the methoxy group on the acyl carbon atom[32] (Figure 1.5). But others,[33, 34] have evidence for intramolecular proton-transfer/reductive-elimination mechanism.

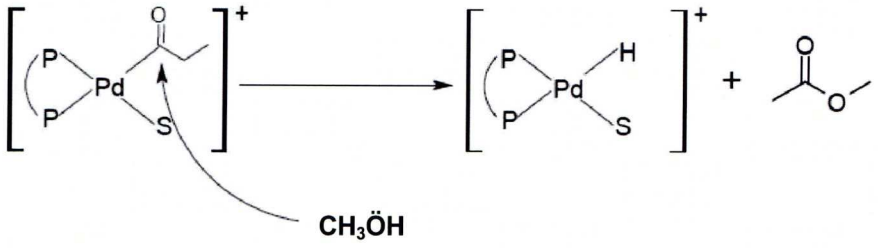

Figure 1.5. Methanolysis as termination step for the production of methyl propanoate (intermolecular mechanism).

Hence, process conditions and catalysts systems are very similar for both polyketone and ester formations, and so is the ligand, which makes the difference in chain growth versus termination. The best ligand for methyl propanoate production found is dtbpx, applied in a new MMA production process developed by Lucite International, and investigated in this project.

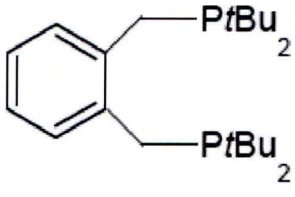

Figure 1.6. dtbpx ligand.[2]

Looking now at the mechanism of the palladium catalysed methoxycarbonylation of ethylene, stepwise reactions had shown the feasibility of two mechanistic pathways[30].

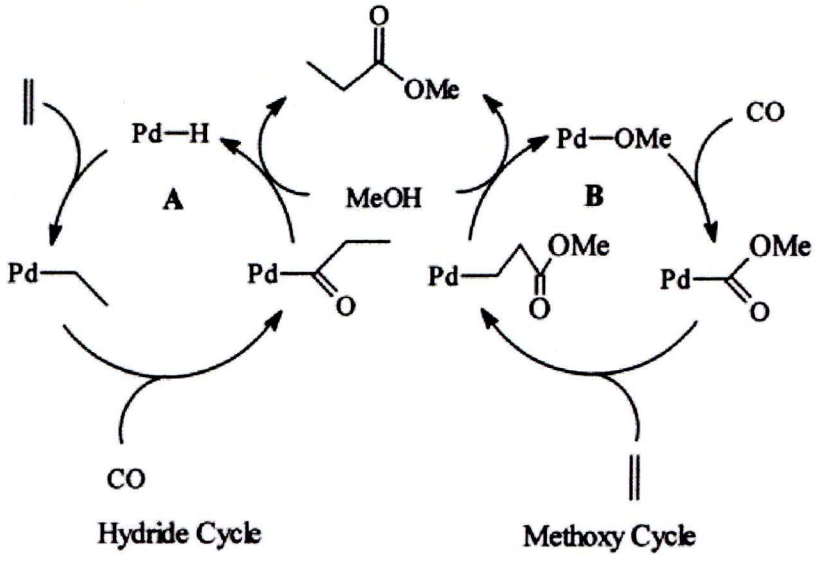

Figure 1.7. The two mechanisms for the methoxycarbonylation of ethylene.[30]

The methoxy cycle starts with a migratory insertion of CO in the palladium methoxy bond. This is followed by an insertion of ethylene in the Pd-carbon bond of the alkoxycarbonyl-palladium complex, and finally a methanolysis produces the methyl propanoate regenerating the initial alkoxy palladium complex. On the other hand, the hydride cycle starts with palladium hydride and a fast migratory insertion of ethylene in the Pd-H bond forming an alkyl complex. Then coordination and migratory insertion of CO produce an acyl complex. In the final step, methanolysis of the Pd-acyl regenerates the Pd hydride and yield the methyl propanoate.

There is a lot of evidence and general agreement that the catalytic cycle leading to esters starts with a palladium hydride;[35] in copolymerisation, both cycles are known to operate.[27]

1.2.4 MMA production processes[36]

World production of MMA has greatly increased in the last 15 years, and is now about 2.2 million tonnes per year. The large demand comes from production of Perspex (polymethyl methacrylate, PMMA), MMA's main application. Methacrylic polymer, which has the characteristics of good transparency and weather resistance, is used in many fields such as signboards, building materials, vehicles and lighting equipment. It is also used to produce resins, plastics, coatings, adhesives, lubricating agents, introfiers for timber and soft wood, impregnants for electric motor coils, glazing agents for paper, printing / dyeing assistants and insulation filling materials.

The acetone-cyanohydrin (ACH) process

The first production process for MMA was developed by ICI in 1937, based on the process for the production of methacrylic ester developed by Rohm & Hass Co. in 1933. The acetone-cyanohydrin (ACH) process was the only operational process until 1982, and still is the most used process for the production of MMA nowadays.

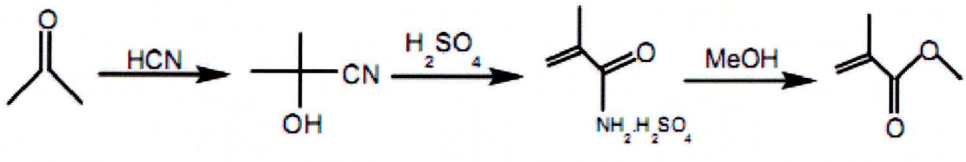

Figure 1.8. ACH process for the production of MMA.

The ACH process starts with a base catalysed reaction between acetone and HCN producing the intermediate ACH, which in a successive stage, using concentrated sulphuric acid, is converted to 2-hydroxy-2-methyl propionamide and its sulphate. A final acid catalysed esterification with methanol yields MMA. This process has environmental issues, i.e. handling of HCN and the great waste of ammonium bisulphate. Furthermore it requires high capital and energy costs for the intensive acid recovery and regeneration.

In 1997, Mitsubishi Gas Chemicals improved the ACH process. Now, acetone cyanohydrin is firstly hydrated to α-hydroxy isobutylamide with a manganese oxide catalyst, instead of sulphuric acid, and then esterified by methylformate to methyl α-hydroxy isobutylate in the absence of methanol. Methylformate is then converted to formamide, which is

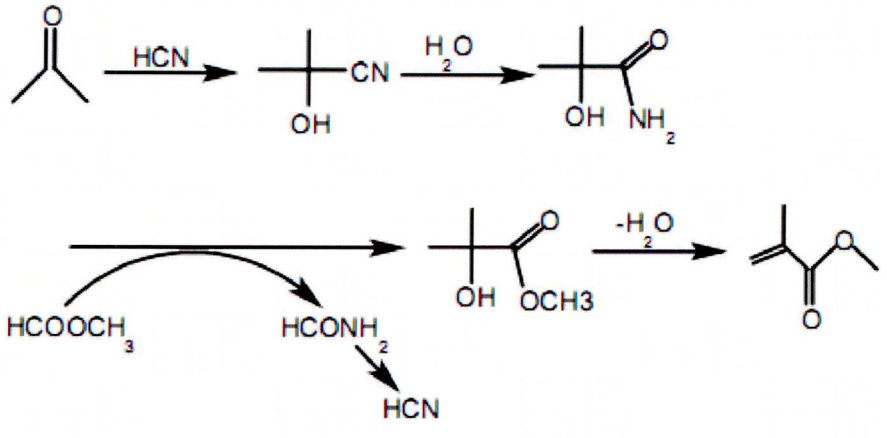

Figure 1.9. Improved ACH process for the production of MMA.

hydrated to give HCN, recycled in the ACH preparation process. Finally, methyl α-hydroxy isobutylate is converted to MMA in a dehydration reaction. This process eliminates the use of sulphuric acid and methanol, and reduces the amount of HCN used; the major disadvantage is the numerous reaction steps involved in the process.

BASF's hydroformylation of ethene

This process consists of a homogeneously rhodium-catalysed hydroformylation of ethene yielding propanal. This process was developed by BASF and commercialised in 1989 with a 40,000 t per year of MMA production plant.

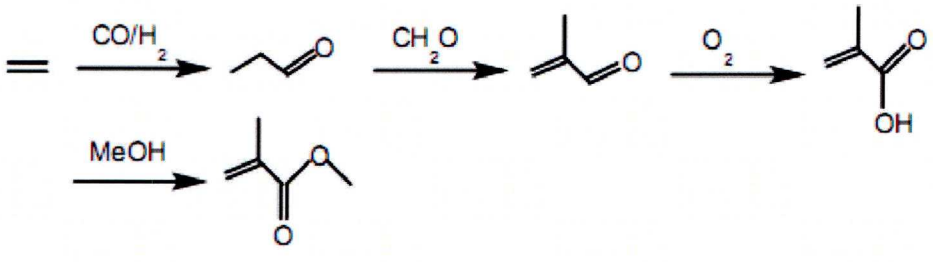

Figure 1.10. BASF's hydroformylation of ethene to MMA.

In this route, MMA is made from ethylene via propionaldehyde, methacrolein and methacrylic acid. The main drawbacks of this process are the moderate yields (< 85 % moles based on propanal) and the limited availability of cheap propanal.

Direct oxidation of isobutylene

The isobutene oxidation route was commercialised in the 1980's by Mitsubishi-Rayon and Asahi Chemical. A C_4 feedstock is catalytically oxidised by air in a two-step vapour phase reaction yielding methacrylic acid which is esterified with methanol to yield MMA. The disadvantages of this process are the low conversion per pass, and the limited availability and high cost of the feedstock.

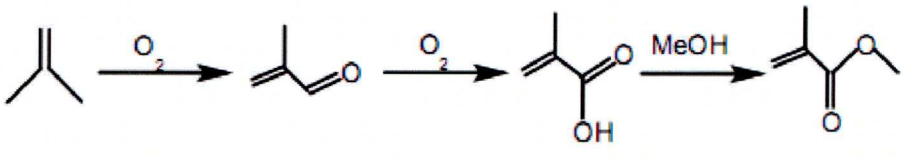

Figure 1.11. Direct oxidation of isobutylene route to MMA.

Methacrylonitrile (MAN) process

Asahi Chemical developed this process, in which methacrylonitrile (MAN) is produced by an ammoxidation, and then hydrated by sulphuric acid to methylamide in the same process as the original ACH route, and finally esterified with methanol to MMA.

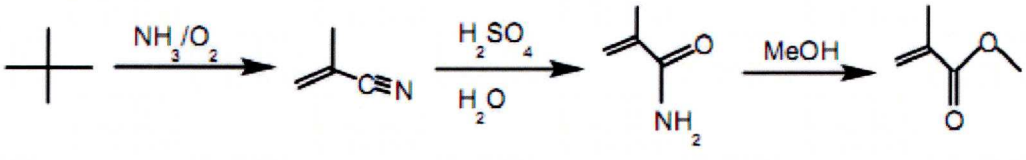

Figure 1.12. MAN process to MMA.

The total yield is greater that for the two-step oxidation process, but the

formation of ammonium bisulphate waste and the use of NH_3 make the process less attractive.

Mitsubishi Gas Company improved the MAN process, developing a new route which excludes the use of sulphuric acid, where the MAN is hydrated to methacrylamide, and then esterified by methylformate to obtain MMA in the same way as the new ACH process.

Direct oxidative esterification process

In 1998, Asahi Chemical developed a process that does not produce ammonium bisulphate as a by-product by modifying the direct oxidation route. The raw material is isobutylene or *tert*-butanol, the same as in the direct oxidation route, and via gas phase catalytic oxidation methacrolein is produced and simultaneously oxidised and esterified in liquid methanol to give MMA with a higher yield and in less steps than in the direct oxidation route.

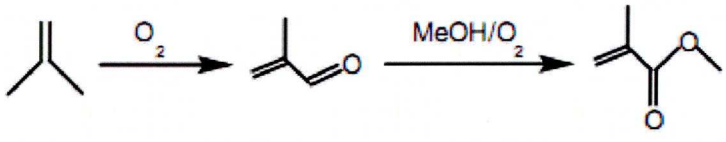

Figure 1.13. Direct oxidative esterification route to MMA.

Although these processes described above are chemically, and some even environmentally viable, they are not economically good enough to

overtake the ACH process.

Lucite's Alpha Process

Acrylics market leader Lucite International has reached commercialisation of a process which can cut the cost of making methyl methacrylate by 40 per cent. The two-stage Alpha Process does not use acetone, HCN or isobutylene as feedstock, but instead is based on ethylene, methanol and carbon monoxide. The Alpha Process relies on combined carbonylation and esterification of ethylene to methyl propanoate, which is then reacted with formaldehyde under almost anhydrous conditions to form methyl methacrylate in an industrial plant, built in Singapore with a production of 120,000 tons per year (2008 start up). This is the only process existing nowadays to compete with the ACH in economic and productive terms. The Alpha Process first stage, methoxycarbonylation of ethylene, is investigated in this project.

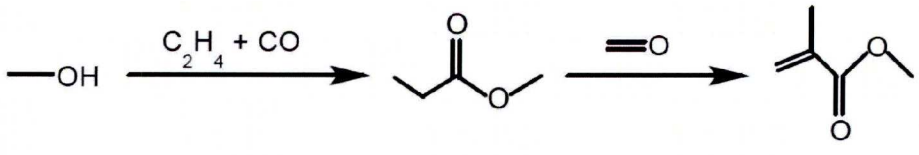

Figure 1.14. Lucite's Alpha process for the production of MMA.

1.3 Vapour-Liquid Equilibrium (VLE)

In a gas-liquid reaction, such as the methoxycarbonylation of ethylene studied in this project, the gaseous reagents must dissolve in the liquid solvent for the reaction to happen. Hence, it is essential to know and understand the vapour-liquid equilibrium (VLE) of the system, and so the saturation concentration of the solvent. In these reactions, mass transfer is a crucial process and might define the reaction performance. The driving force of mass transfer is the gradient of concentrations between the liquid interface (in contact with the gas phase) and the bulk liquid, and thus composition in equilibrium has a great effect since the liquid interface, formed between gas and liquid phases and representing the region of contact between phases, is at equilibrium condition.

The equilibrium compositions will depend on a number of variables, such as temperature and pressure, and on the chemical nature and concentrations of the substances in the mixture. Phase-equilibrium thermodynamics try to establish relations between the main physical properties of two or more phases in a state of equilibrium. This section of the thesis is of great importance since the concepts and equations explained will be widely applied throughout the following chapters.

1.3.1 Thermodynamics introduction

Thermodynamics had its origins in the middle of the nineteenth century,

but were only applied to a limited class of phenomena at that time, such as heat engines. As a result of developments over time, thermodynamics became applicable to a large number of problems in both physical and biological sciences. From its Greek root (*therme*, heat; *dynamics*, force) one might well wonder what "thermodynamics" have to do with the distribution of various components in different phases. Certainly, early thermodynamics were concerned only with systems of one component, and it was not until the great work of J. Willard Gibbs that thermodynamic methods were revealed to be useful in the study of multicomponent systems. Gibbs[37] was the first to see the generality of thermodynamics. He showed how a thermodynamic procedure was possible for a wide range of applications, including the behaviour of chemical systems.

Thermodynamic equilibrium is a condition in which no changes in the macroscopic properties of a system occur as a function of time, all potentials that can cause a change are equal. At equilibrium, an isolated system with fixed quantities of chemical species and two co-existing liquid and vapour phases does not change with time. The temperature, pressure and composition of the phases will all have constant values. However, the microscopic properties are not constant, molecules with high velocities, near the phase boundary, can pass from one phase to the other. But the overall flux of molecules is the same in both directions, so there is no net matter transfer between the different phases.

The basic thermodynamic relation of equilibrium is well known thanks to Gibbs. Thus, the equilibrium distribution of some component i between two phases α and β is initially defined by the relation:

$$\mu_i^{\alpha} = \mu_i^{\beta} \tag{1.1}$$

where μ is the chemical potential. Thermodynamics must now relate the chemical potential to system temperature, pressure, and composition, to properly define and understand the equilibrium condition. The chemical potential does not have an immediate physical significance and it is therefore desirable to express it in terms of some auxiliary functions, such as fugacity and activity, being more easily identified with physical reality.

For a pure component, the chemical potential is related to the temperature and the pressure by the differential equation:

$$d\mu_i = \overline{V}_i dP - \overline{S}_i dT \tag{1.2}$$

where s_i is the molar entropy and v_i the molar volume.

G. N. Lewis simplified the abstract equation of chemical equilibrium by considering first a pure ideal gas and then generalizing it to all systems the result obtained for the ideal case. From Eq. 1.2:

$$\left(\frac{\partial \mu_i}{\partial P}\right)_T = \overline{V}_i \tag{1.3}$$

Substituting the ideal-gas equation:

$$\overline{V}_i = \frac{RT}{P} \qquad 1.4$$

and integrating at constant temperature:

$$\mu_i - \mu_i^0 = RT \ln \frac{P}{P^0} \qquad 1.5$$

Hence, from Eq 1.5, the change in chemical potential for an ideal gas, in isothermally going from pressure a P^0 to a pressure P, equals the product RT and the logarithm of the pressure ratio P/P^0. Thus, an isothermic change in the chemical potential is a simple logarithmic function of the physical property pressure. However, Eq 1.5 can only be applied to pure ideal gases; it was generalized by Lewis by defining a function f, called *fugacity*. For an isothermal change for any component in any system, solid, liquid, or gas, pure or mixed:

$$\mu_i - \mu_i^0 = RT \ln\left(\frac{f_i}{f_i^0}\right) \qquad 1.6$$

Either μ_i^0 or f_i^0 is arbitrary, but both may not be chosen independently; when one is chosen the other is fixed.

For ideal gases, whether as pure components or in mixtures, each component fugacity, f_i, is equal to its partial pressure, $y_i P$. All pure or mixed systems approach ideal gas behaviour at very low pressures. Hence, the definition of fugacity is completed by the limit:

$$\frac{f_i}{y_i P} \to 1 \qquad \text{as} \qquad P \to 0 \tag{1.7}$$

where y_i is the mole fraction of *i*.

The ratio f/f^0 is called *a,* the *activity*. The activity of a substance shows how "active" it is relative to a standard state; it measures the difference between the chemical potential at a state of interest and that at a standard state.

The fugacity can be conceived of as a "corrected pressure", and the corrections are applied because of the presence of non-idealities, which can be explained by molecular considerations. The fugacity provides a transformation of the basic relation of equilibrium defined by the equality of chemical potentials. Hence, for phases α and β, respectively, Eq 1.6 is:

$$\mu_i^{\alpha} - \mu_i^{0\alpha} = RT \ln\left(\frac{f_i^{\alpha}}{f_i^{0\alpha}}\right) \tag{1.8}$$

and

$$\mu_i^{\beta} - \mu_i^{0\beta} = RT \ln\left(\frac{f_i^{\beta}}{f_i^{0\beta}}\right) \tag{1.9}$$

Substituting equations 1.8 and 1.9 in the equilibrium relation 1.1:

$$\mu_i^{0\alpha} + RT \ln\left(\frac{f_i^{\alpha}}{f_i^{0\alpha}}\right) = \mu_i^{0\beta} + RT \ln\left(\frac{f_i^{\beta}}{f_i^{0\beta}}\right) \tag{1.10}$$

Let's consider now two different cases, where the first one is that of equal standard states for both phases, i.e. suppose

$$\mu_i^{0\alpha} = \mu_i^{0\beta} \tag{1.11}$$

Hence, it follows that

$$f_i^{0\alpha} = f_i^{0\beta} \tag{1.12}$$

Equations 1.10, 1.11 and 1.12 give a new form of the fundamental relation of phase equilibrium:

$$f_i^{\alpha} = f_i^{\beta} \tag{1.13}$$

The second case would be that of the standard states of both phases are at the same temperature but not at the same pressure and composition. Using the exact relation between the two standard states:

$$\mu_i^{0\alpha} - \mu_i^{0\beta} = RT \ln\left(\frac{f_i^{0\alpha}}{f_i^{0\beta}}\right) \tag{1.14}$$

Substituting Eq. 1.14 into Eq. 1.10, again it is obtained:

$$f_i^{\alpha} = f_i^{\beta} \tag{1.13}$$

Equation 1.13 means that the equilibrium relation in terms of chemical potentials can be replaced without loss of generality by the relation of equality of fugacities for any species *i*. Equality between chemical potentials in equilibrium phases requires equality between the fugacities in

these same phases.

1.3.2 Thermodynamic model

In order to have more confidence in the experimental data, a theoretical model for phase equilibrium conditions calculation has been developed. The key factor of a thermodynamic model for theoretical calculations of equilibrium conditions is the accurate prediction of physical properties. In this section, the equilibrium relations used by the thermodynamic model are explained. For a more detailed development of the model and how calculations are performed see Appendix A.

The basic relationship for equilibrium is that for all components, in all phases of a system, the fugacities must be the same (Eq. 1.13). The physical properties are calculated using an activity coefficient method. In this method all vapour phase properties are derived from an equation of state and liquid phase properties are determined from excess terms from summation of pure component properties. In the activity coefficient method:[38]

$$f_i^v = \varphi_i^v y_i P \qquad 1.15$$

$$f_i^l = \gamma_i x_i f_i^{0l} \qquad 1.16$$

where:

P is the total pressure of the system,

$\varphi_i^v = f_i^v / p_i$ is the fugacity coefficient for component *i* in the vapour phase,

p_i is the partial pressure of component *i* in the gas phase,

$\gamma_i = \frac{a_i}{x_i} = \frac{f_i^l}{x_i f_i^{0l}}$ is the activity coefficient of component *i* (liquid phase),

f_i^{0l} is the fugacity of a pure liquid component *i* at the mixture temperature.

Fugacity coefficient

The vapour phase fugacity coefficient is defined by the following expression:

$$\ln \varphi_i^v = \frac{1}{RT} \int_V^\infty \left[\left(\frac{\partial P}{\partial n_i} \right)_{T,V,n_j} - \frac{RT}{V} \right] dV - \ln Z \qquad 1.17$$

For the resolution of this equation it is necessary to define an equation of state, which describes pressure, volume and temperature (P-V-T) behaviour of pure components and mixtures. An equation of state is usually explicit in pressure and has different terms to represent attractive and repulsive forces between molecules. Any thermodynamic property, such as fugacity coefficients can be calculated from the equation of state. Equation of state properties are calculated relative to the ideal gas properties of the same mixture at the same conditions.

The Redlich-Kwong[39] equation of state is used for all gas phase

calculations. This is a two-parameter cubic equation of state and is given in Reid et al.[40] as:

$$P = \frac{RT}{\overline{V} - b} - \frac{a}{\overline{V}\left(\overline{V} + b\right)} \qquad 1.18$$

where $\overline{V}$ is the molar volume.

Alternatively it can be given in terms of the compressibility factor Z:

$$Z = \frac{P\overline{V}}{RT} \qquad 1.19$$

$$Z = \frac{\overline{V}}{\overline{V} - b} - \frac{a\overline{V}}{RT(\overline{V}^2 + b\overline{V})} \qquad 1.20$$

The two parameters a and b are given by:

$$a = \frac{0.42748R^2T_c^{2.5}}{P_cT^{0.5}} \qquad 1.21$$

$$b = \frac{0.08664RT_c}{P_c} \qquad 1.22$$

where P_c and T_c are the critical pressure and temperature respectively. For multi-component systems mixing rules are used to determine the parameter values. The mixing rules used are:

$$\sqrt{a} = \sum_i y_i \sqrt{a_i} \qquad 1.23$$

$$b = \sum_i y_i b_i \qquad 1.24$$

In Appendix A it is shown the combination of the fugacity coefficient expression (Eq. 1.17) with the Redlich Kwong eqation of state.

Liquid phase activity coefficient

The liquid phase activity coefficient, γ_i, is determined from the UNIQUAC[41, 42, 43] model. This is a semi-empirical model and is based on the fact that intermolecular forces will cause a non-random arrangement of molecules in the mixture. The model is fitted to experimental binary vapour-liquid equilibrium data. Each binary pair requires two un-symmetrical adjustable parameters which are temperature dependent ($\tau_{ij} \neq \tau_{ji}$). The liquid phase activity coefficient is given by:

$$\ln \gamma_i = \ln\left(\frac{\Phi_i}{x_i}\right) + \frac{z}{2} q_i \ln\left(\frac{\theta_i}{\Phi_i}\right) + l_i - \frac{\Phi_i}{x_i}\sum_j x_j l_j + q_i\left[1 - \ln\left(\sum_j^{NC} \theta_j \tau_{ji}\right) - \sum_j^{NC} \frac{\theta_j \tau_{ij}}{\sum_k^{NC} \theta_k \tau_{kj}}\right] \qquad 1.25$$

where:

$$\Phi_i = r_i x_i / r_T \; ; \; r_T = \sum_k^{NC} r_k x_k$$

$$\theta_i = q_i x_i / q_T \; ; \; q_T = \sum_k^{NC} q_k x_k$$

$$l_i = \frac{z}{2}(r_i - q_i) + 1 - r_i$$

$$\tau_{ij} = \exp\left(a_{ij} + {}^{b_{ij}}\!/_{T} + C_{ij} \ln T + d_{ij} T + {}^{e_{ij}}\!/_{T^2} \right)$$

$z = 10$

r_i = pure component property, van der Waals volume parameter for molecule *i*

q_i = pure component property, van der Waals surface area parameter for molecule *i*

T = absolute temperature

NC = number of components

a_{ij}, b_{ij}, c_{ij}, and d_{ij} are unsymmetrical. That is a_{ij} might not be equal to a_{ji}, etc. Absolute temperature units are assumed for the binary parameters a_{ij}, b_{ij}, c_{ij}, d_{ij} and e_{ij}.

The values of the parameters used in the solubility calculations with the model are shown in Appendix A.

Liquid phase fugacity

The reference state for a solvent is usually defined as the pure component in the liquid state, at the temperature and pressure of the system. The liquid phase reference fugacity would be computed as:

$$f_i^{0l} = \varphi_i^v (T, p_i^0) p_i^0 \theta_l^0 \qquad 1.26$$

where θ_i^0 is called the Poynting factor[44] and is defined as:

$$\theta_i^0 = \exp\left(\frac{1}{RT}\int_{p_i^0}^{p}\bar{V}dp\right) \qquad 1.27$$

The Poynting factor is a correction that accounts for the change in fugacity with increase in pressure above saturation vapour pressure p_i^0. This means that the standard state fugacity is not exactly equal to the fugacity of pure species at saturation.

For light dissolved gases, as in the system under study in which the solubility values are very low, the pure component vapour pressure is not applicable as a reference fugacity as such gases are usually supercritical at the temperature and pressure of the solution. The reference state for a dissolved gas is redefined to be at infinite dilution and at the temperature and pressure of the mixtures. The liquid phase reference fugacity becomes the Henry's constant for that component in the mixture. Thus, the phase equilibrium relationship for a dissolved gas becomes:

$$\varphi_i^v y_i P = x_i \gamma_i^0 H_i \qquad 1.28$$

where

$$\gamma_i^0 = \frac{\gamma_i}{\gamma_i^\infty} \qquad 1.29$$

where γ_i^∞ is the activity coefficient of component *i* at infinite dilution.

Henry's constant

For an ideal mixture the partial pressure is linearly related to the mole fraction in the liquid by Raoult's law, where the proportionality factor is the pure vapour pressure of the component.[38] This law is usually found to be true for soluble gases. For sparingly soluble gases the proportionality factor is Henry's constant, H, viz:

$$p_i = H_i x_i \qquad 1.30$$

Henry's constant is a strong function of temperature. For most gases Henry's constant increases with temperature, but there are exceptions where the converse is true (e.g. carbon monoxide in MeP/MeOH).

Henry's constant is calculated for a dissolved gas component *i,* for one or more solvents (*A, B*), by the following:

$$\ln\left(H_i / \gamma_i^{\infty}\right) = \sum_A w_A \ln\left(H_{iA} / \gamma_{iA}^{\infty}\right) \qquad 1.31$$

where

$$w_A = \frac{x_A (V_{cA})^{2/3}}{\sum_B x_B (V_{cB})^{2/3}} \qquad 1.32$$

$$\ln H_{iA}\left(T, p_A^0\right) = a_{iA} + b_{iA}/T + c_{iA} \ln T + d_{iA} T + e_{iA}/T^2 \qquad 1.33$$

Where V_{ci} and p_i^0 are the critical volume and vapour pressure of the pure

component i, and the constants a_{iA}, …, e_{iA} are empiric parameters defined in the model.

Vapour pressure

The vapour pressure of a liquid is calculated using the extended Antoine equation:[45]

$$\ln p^0 = c_1 + \frac{c_2}{T + c_3} + c_4 T + c_5 \ln T + c_6 T^{c_7} \qquad 1.34$$

where c_i are experimentally determined constants.

Liquid density

The pure component liquid density is given by the DIPPR[46] equation:

$$\rho_l = \frac{c_1}{c_2^{\left(1+(1-T/c_3)^{c_4}\right)}} \qquad 1.35$$

Molar volume

The pure component saturated volume is given by the Rackett[45] equation:

$$\overline{V} = \frac{RT_c \left(Z^{RA}\right)^{\left[1+(1-T_r)^{2/7}\right]}}{P_c} \qquad 1.36$$

where Z^{RA} is the Rackett compressibility factor. Liquid mixture molar volumes are calculated by using the ideal mixing rules.

Heat capacity

The liquid pure component molar heat capacity and liquid mixture molar heat capacity are given by the differential of the liquid molar enthalpy:

$$c_p^l = \frac{dH^l}{dT} \tag{1.37}$$

$$c_{pm}^l = \frac{dH_m^l}{dT} \tag{1.38}$$

The vapour molar heat capacity is given by two ideal gas heat capacity models: a polynomial fit and the DIPPR[46] equation:

$$c_p^{ig} = c_1 + c_2 T + c_3 T^2 + c_4 T^3 + c_5 T^4 + c_6 T^5 \tag{1.39}$$

$$c_p^{ig} = c_1 + c_2 \left(\frac{c_3/T}{\sinh(c_3/T)} \right)^2 + c_4 \left(\frac{c_5/T}{\cosh(c_5/T)} \right)^2 \tag{1.40}$$

Heat of vapourization

Two models are used for calculating the heat of vaporization. Generally the DIPPR equation is used:

$$\Delta H_{vap} = c_1 (1 - T_r)^{\left(c_2 + c_3 T_r + c_4 T_r^2 + c_5 T_r^3\right)} \tag{1.41}$$

where c_x are experimentally fitted parameters and T_r is the reduced temperature. However, for components for which the parameters of the DIPPR equation are not available, the Watson[47] equation is used. This is given by:

$$\Delta H_{vap}(T) = c_1 \left(\frac{1 - T/T_c}{1 - c_2/T_c} \right)^{c_3 + c_4\left(1 - T/T_c\right)} \qquad 1.42$$

For examination of how these equations are combined to perform equilibrium calculations with the thermodynamic model see Appendix A.

1.3.3 Aspen Plus

ASPEN PLUS simulation package allows the creation of a bespoke process model, by defining a flow sheet and specifications of the chemical components and operating conditions. Following input of all specifications ASPEN PLUS is run to simulate the model. The process simulation is the action that executes all necessary calculations needed to solve the outcome of the system, predicting its behaviour. When the calculations are complete, ASPEN PLUS lists the results, stream by stream and unit by unit, so it can be observed what happened to the chemical species of the process model.

The equilibrium conditions are calculated in Aspen Plus by the application of a flash separation. Hence, a flash block with a gas and a liquid inlet, and a vapour and a liquid outlet, in equilibrium, is defined. The gas and liquid inlet conditions are fixed, except the mole flow of the gas feed, which is controlled by the desired temperature in the flash block. Then, by just defining the desired pressure and temperature within the flash block it is

possible to obtain the compositions of the liquid and the gas phases in equilibrium at those conditions of pressure and temperature.

In the flash block, pressure, temperature and L/V ratio are defined. The pressure in the flash block is defined by the quantity of gas present and vice versa. So specification of the vapour feed composition, with the pressure, temperature and L/V ratio defined, fixes the vapour quantity in relation of the total volume of the flash vessel. And so the amount of liquid (in relation with the total volume of the flash block) present is also fixed as long as the L/V ratio is defined. Hence by definition, a flash block is not affected by feed flows because are the conditions, pressure, temperature and L/V ratio, to define the quantities/volumes of liquid and vapour present.

For the simulation of the flash block in Aspen Plus, it is necessary to define two and only two of the following three variables: temperature, pressure, and L/V ratio. In our simulation, pressure and L/V ratio are defined in the flash block specification. The temperature is controlled by the flow of hot gas fed to the flash block. However, as it has been explained in the previous paragraph, changes in the vapour feed stream flow do not change the quantity of vapour present in the flash block, which is defined by the conditions of temperature, pressure and L/V ratio. This is just a tool employed to fix the temperature within the flash block.

On the other hand, the real system is a semi batch cell in which the liquid is static and the gas flow fixes the pressure. Hence in the real system the L/V ratio cannot be constantly fixed, but it does not change by much at different equilibrium conditions as experimentally observed. Checking in the simulation the results obtained with L/V ratio values ranging from 60 to 80 % of liquid volume in the vessel it has been observed that the results values change only by the 5% approximately, demonstrating that as long as the variation of the L/V ratio within the equilibrium cell is small the solubility results do not change dramatically. This possible difference between the experimental L/V ratio and that defined in the model is a reason for possible discrepancies between the experimental and simulated results. However, the simulation is considered to perform with a very low error in the range of conditions studied.

1.4. Gas solubilities

The definition of a vapour-liquid equilibrium (VLE) is equivalent to the determination of the solubilities of gaseous components in a particular solvent. Hence, the experimental determination of gas solubilities allows the study of the VLE, Henry's constants, and the validation of the thermodynamic model applied.

1.4.1 Previous experiments on gas solubility determination

The solubility of gases in liquids was one of the physical properties studied by the early chemists. Many well-known names appear in the literature, e.g. Henry in 1803, Berthelot, Bunsen, Carius, and Roscoe in 1855, Winkler in 1889, and other later workers.[48] In general, the solubility of gases in liquids has been studied by investigators who have wished to have these particular data for the investigation of the gas or, more infrequently, of the liquid or the solution. Few were interested in the phenomenon itself and in studying general behaviour in the solubility of gases in liquids. The literature cited shows the names of a large number of workers, scientists who studied the solubility of all gases in a wide variety of liquids, men who used all types of apparatus and experimental conditions, and men who exercised various degrees of experimental technique in producing their data.

Gas solubilities have always been of scientific interest, as they are the basis of the vapour-liquid equilibrium of any binary system with a gas phase of a different composition from the liquid phase. Obviously, there are different ways of performing solubilities measurement experiments and new methods have been developed over the years.

The experimental methods for measuring the solubility of a certain gas in a certain liquid have principally two different but very dependent parts. The first is bringing together the gas and the liquid and attainment of equilibrium. The second part is measuring the compositions of each phase for defining the solubilities and the vapour-liquid equilibrium.

The most usual method of mixing gas and liquid was in the past to shake the two phases together, as in the Ostwald[49] apparatus and its many modifications. An end-point is very rapidly obtained, but the possibility that this represents a condition of supersaturation rather than a true equilibrium, due to the violence with which the gas is forced into the liquid was pointed out by Cady, Elsey and Berger,[50] who made use of electromagnetic stirring in order to obviate this possibility. The use of gentle stirring results in conditions antithetical to those brought about by violent shaking. Solution was very slow, from 24 to 36 hours being required for reaching equilibrium, and as the final portions of gas are taken up by the liquid with extreme slowness the danger of undersaturation must

be present. These considerations led the authors in that moment to use a third method of mixing the gas and liquid phases, that of bubbling the gas through the liquid. This method is almost invariably chosen when the object sought is a saturated solution for investigation by analytical or other means. The procedure is also used for freeing liquids of gaseous impurities, so that it seems reasonable to expect that if at any time supersaturation should occur a continuation of the process would remove the excess gas and restore a condition of true equilibrium. It should be noted also that the time required in the 1930's, for a determination by bubbling through, fell between the extremes of the other methods, being between one and two hours.

In the first experiments the determination of the solubilities was performed by physical methods which were the most used and least complicated. These methods have been used until very recently, and even used nowadays. While analytical methods for determining gas solubilities are in general the most accurate, there are many systems to which they are not applicable, so the working out of a physical method as free as possible from the objections raised against such methods in the past, seemed desirable. Physical methods depend on the measurement of the change in volume or pressure of the system when measured quantities of gas and liquid are mixed together while the other variables are kept constant. However, the volume changes may not be followed with the desired degree

of accuracy.

Early experiments using physical methods are described in the very interesting work of Markham and Kobe, 1941.[48] The physical methods used are quite varied. Most of them are saturation methods, in which the measurement is that of the quantity of the gas necessary to saturate a quantity of initially gas-free solvent. Some are extraction methods, in which the measurement is that of the volume of gas that can be extracted from a quantity of saturated solution.

Physical methods evolved with the years and experience. Hence, in the 1960's[51] gas solubility experiments were usually carried out using physical methods measuring the volumes and quantities of liquid and gas before and after the equilibrium. A typical experimental system for these measurements is as follows. The apparatus consisted of a gas-measuring burette (C), an absorption cell (F), and a reservoir for solvent with suitable connections (M) (Figure 1.15). The burette was thermostated at the desired temperature, the same for the absorption cell F. The absorption cell (F) contained a glass-enclosed piece of iron to provide gentle, continuous magnetic stirring. Pure solvent was degassed applying vacuum and boiling the solvent for half an hour. The solvent was then allowed to flow into the absorption cell, where it was again boiled under low pressure for final degassing. Incomplete degassing was one of the most serious sources of error in measuring gas solubilities in this way. The liquid filled F, by

withdrawal of mercury into K, until the connecting system of glass tubing was filled with liquid solvent just through the bore of the stopcock at the top of F. After the desired amount of liquid had been passed into F, the stopcock at the top of F was closed while that between F and L was left open until thermal equilibrium between F and the thermostat R had been reached. L was then removed and weighed. From its increase in weight the volume of the liquid solvent was calculated. K was put in communication with F and the stopcock at the top of F opened to allow a little quantity of solvent to enter the capillary tube connecting F and C. The liquid meniscus was adjusted to a line near the stopcock on top of F. Closing the stopcock at the top of F, and opening both at the top of C, the pressure within the burette C was adjusted by letting mercury run in from A, or sucking it out, so the mercury level in the manometer was the same in both limbs. The mercury meniscus level in the gas burette C was read. Gas was then admitted to the absorption cell F. Its exact amount was determined by P-V measurements in the burette before and after introduction of gas into the absorption cell. The stirrer was then set in motion. While gas was being absorbed, the pressure was kept constant through frequent adjustments from A. Equilibrium was usually attained within 24 hours, then the gas was driven back into C by introducing mercury from K until the liquid reached the mark on the capillary near the stopcock F. The pressure was then finally adjusted and the volume of the remaining gas read.

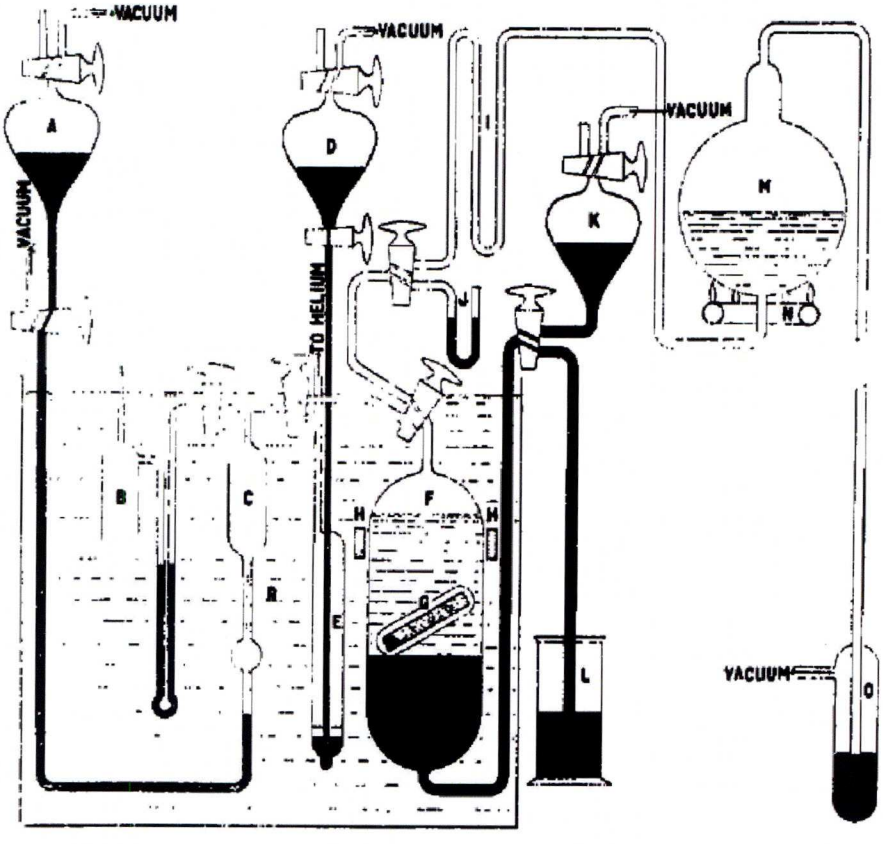

Figure 1.15. Gas solubility determination experimental system.[50] A, D, K: Mercury bulbs. B: Burette with atmospheric air. C: Sampling burette. R: Controlled temperature bath. G: Stirrer. H: Electromagnet. F: Absorption chamber. M: Solvent reservoir. E: Helium feed bulb.

There are of course many variations of this kind of systems.[52, 53, 54, 55] Most differences are in the method of mixing gas and liquid, but they are similar in the way of determining the solubilities, it is just measuring volumes differences.

Some experiments using chemical methods have been also described in many papers. A chromatographic method is described by Shoor, Walker and Gubblins,[56] 1968. In 1981, a new method was developed for the determination of gas solubilities in a liquid by saturating the liquid with a

bubbling stream of gas and analyzing the saturated liquid with a gas chromatograph. This simple method was applied to CO_2 dissolved in benzene, toluene, m-xylene, diphenyimethane, and l-methylnaphthalene for the purpose of checking with literature data, and the results were good.[57]

In 1994, Breman et al.[58] performed a new method for measuring solubilities of gases in liquids called the total pressure method. The experimental method is similar to that of Olsen[59], Cukor and Prausnitz[60], and Grad et al.[61] Known amounts of the two components were sealed in a vessel of known volume. The temperature was then increased stepwise, and the system was allowed to reach equilibrium. These equilibria were characterized by a set of primary measured values: the total pressure in the vessel, the temperature in the vessel, the vessel volume, the total number of moles of solute, and the total number of moles of solvent. The stainless steel autoclave was magnetically stirred by three six-bladed turbine stirrers placed on a common shaft and provided with four radial baffles, ensuring rapid physical equilibrium between the gas and liquid. The effective system volume was measured by filling the system with a known amount of pure nitrogen gas and subsequently measuring the pressure increase with a manometer. The system volume was calculated from the nitrogen mass balance. For measuring the gas-liquid equilibrium, the autoclave was filled with an amount of solvent accurately measured from the differential mass of the autoclave. While stirring, the solvent was degassed with a vacuum

pump. Gaseous solutes were fed from a supply cylinder. After stabilization of the pressure as indicated by manometer, the amount of solute fed to the autoclave could be accurately calculated from the differential mass of the supply cylinder applying a mass balance. Hence, it was a complicated and not very accurate method, but was fast, and it allowed for the measurement of liquid and gas compositions. This method has been used by many authors and investigators in recent years.

The use of the NMR technique, used in the present project, in gas solubility determination experiments is not very extensive. Searching in publications, only few papers have been found using NMR associated with the study of the solubility of CO and CO_2. [62, 63]

In the present project the experimental system consists of a gas flow system, where the gas is bubbled through the liquid solution, which is within a NMR sapphire tube, which is introduced within the NMR magnet. This system has the advantages of reaching the equilibrium point very quickly. And as the equilibrium cell is within the magnet, it is possible to record NMR spectra of the liquid sample at anytime, obtaining rapidly the composition in the liquid phase, and so knowing the mole fraction of the gases dissolved in the liquid. This method neither needs the determination of the amounts of gas and liquid in equilibrium, nor the volumes of the equilibrium cell and the consequent dead volumes, which makes it simpler,

but not less accurate or fast.

1.4.2 HP NMR for determination of gas solubilities

Application of NMR in gas-liquid systems has mainly focused on studies of the characterization of catalysts. In this project we apply NMR not only for characterization of a chemical system but also for the determination of the amount of gas components dissolved in a solvent in a reaction.

Several designs of NMR cells applied to studies of gas-liquid systems have been developed based on the idea of attaching a tube to a metallic valve and cap. The application of relative thin wall sapphire NMR tubes allowing high pressures and temperatures was firstly introduced by Roe in 1985.[64] Sapphire offers great tensile strength, is essentially chemically inert, and its coefficient of expansion is small enough to consider it negligible over the normal variable temperature range.[65] Variations and modifications of this sapphire NMR tube have been developed with time.[66] In 1991, Horvath and Ponce presented a modification of the tube allowing a higher sample volume (~ 1 mL) thus providing a better sensitivity. [67] In 1996, a system for the simultaneous measurement and control of the pressure and temperature of the sample was reported by Bai et al.[68] Further to the development of high pressure NMR cells which enable the measurement of the pressure inside the cell during reaction, Elsevier et al.[69] reported in 1999 a novel titanium sapphire HPNMR cell equipped with a pressure

sensor. In 2000, Wallen et al.[70] constructed a three piece high pressure NMR cell with capabilities of up to 400 bar, made of high performance polymers (PEEK, Victrex Plc.). However, these designs suffered from two major problems: the difficulty of changing the pressure of the sample *in situ* and the poor gas-liquid mixing in sealed or non-stirred tubes.

To overcome these problems new flow cells and bubble columns have been developed. Woelk and Bargon[71] reported in 1991 a number of different HPNMR instruments for the investigation of gas-liquid reactions at high pressures, they incorporated a flow system to overcome the problem of gas-liquid mixing. However, the limited maximum working pressure (20 bar) makes them unsuitable for the study of many homogeneously catalysed industrial reactions. In 1995, Yonker et al.[72] introduced a HPNMR cell and flow system, consisting of a folded silica capillary tube placed in a standard NMR tube, allowing the observation of pressure effects in chemical reactions and supercritical fluid systems. Baumann et al. reported in 1997 a flow gas bubble NMR cell designed to overcome the gas-liquid mixing problem. The cell consists of a 10 mm NMR tube equipped with a small PTFE tube as inlet for the gas and a second opening in a stopper for gas outlet.

An alternative approach to record NMR spectra under high pressures is the use of high pressure probes, in which a nonmagnetic autoclave of high mechanical strength and the rf circuit are placed in a wide bore magnet

instead of the standard probehead.[73, 74, 75, 76] A number of designs have addressed the gas-liquid problem, e.g. those of Jonas and Vander Velde,[77] and of Merbach[18] by utilizing a flip-flop stirrer design, and Rathke[78] circulating the solution via a conventional autoclave. However, these devices require great skill in design, manufacture, maintenance and operation. In 1998, Iggo and Shirley[16] reported a HPNMR probe combining good gas-liquid mixing with the ease of use of Roe's sapphire tube design.

In this project a novel HPNMR continuous flow bubble column (Figure 1.15) similar to that described by Baumann[79] has been used (detailed description in Chapter 2). It consists of a sapphire tube, containing the solvent, with a gas feed capillary tube bubbling the gas through the liquid solution. Gas bubbles exit from the holes perforated in the sides of a plugged-exit PTFE tube, dipped in the liquid solution, attached to the gas inlet. The gas flows continuously in a recirculation loop. The system allows easy control of pressure and temperature, good mixing, rapid equilibrium, no depletion of gas during reaction, big sample volume (4 mL), and good resolution. A condenser is introduced, by cooling down the bottom section of the gas outlet with cool running water to prevent liquid loss through evaporation. The introduction of a relaxation agent allows fast and continuous composition measurements in working catalytic reactions.

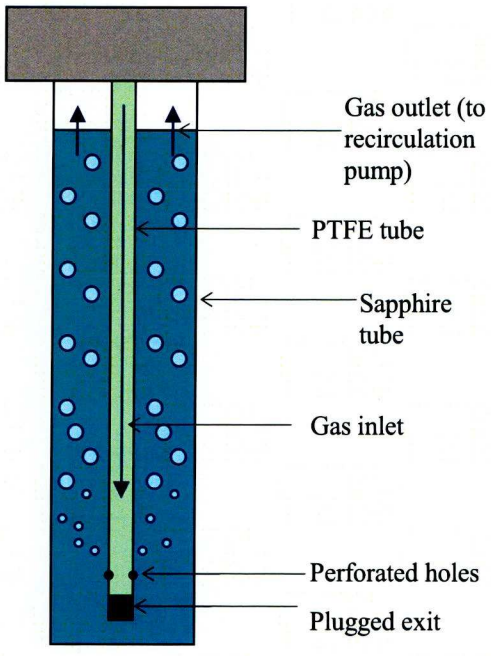

Figure 1.16. HPNMR bubble column scheme for experimental gas solubility determination.

1.5 Nuclear Magnetic Resonance (NMR)

Basics

Nuclear magnetic resonance spectroscopy, as its names implies, is a resonance spectroscopy where transitions between quantized energy levels are excited and the frequency dependence of the absorption (or emission) of energy is monitored to produce a spectrum. The number of these energy levels depends on interactions between spins (spin-spin coupling) whilst energy level separation is determined by the chemical environment (chemical shift). Hence, the NMR spectrum contains much chemical information about the system under study.

The energy levels involved in NMR spectroscopy arise from the interaction of the nuclear spin with the spectrometer magnetic field, with the magnetic fields set up by other nuclear spins; and with the magnetic fields set up by the electrons in the sample.

The spinning nucleus generates the *nuclear magnetic moment*, $\boldsymbol{\mu}$, which is a vector quantity proportional to the spin, $\boldsymbol{I}$. The constant of proportionality, γ, is called the *gyromagnetic ratio*. Every isotope has a different nuclear magnetic moment, $\boldsymbol{\mu}$, and hence its own and unique gyromagnetic ratio, γ.

Interaction with a magnetic field

The nuclear spin (strictly the nuclear spin angular momentum) is quantized and is given the quantum number I, $2I+1$ quantum levels are associated with the nuclear spin I. In the absence of an external magnetic field the nuclear spin states are degenerate, i.e. there is nothing with which the nuclear magnetic moment can interact so the orientation of the nuclear magnetic moment in space will not affect the energy of the system.

If the nucleus is placed in a magnetic field, different orientations of the nuclear magnetic moment will have different energies depending on the relative orientations of the nuclear magnetic moment and the applied field. Since the nuclear spin is quantized only certain orientations of the nuclear magnetic moment with respect to the applied field are allowed, each orientation corresponding to a different nuclear spin state, so $2I+1$ discrete energy levels are obtained (Zeeman splitting).

Larmour frequency

The energies of the allowed orientations of the nuclear magnetic moment depend on the strength of the applied field, on the size of the nuclear magnetic moment, and on the orientation of the nuclear magnetic moment to the applied field. Hence, for causing a nuclear spin transition between one energy level to another, the energy difference between levels, at a particular frequency, must be irradiated. This particular frequency is

known as the *resonance* or *Larmour frequency.* Since each isotope has a distinct gyromagnetic ratio (nuclear moment) the nuclear spins of each element will resonate at characteristic, distinct frequencies.

Rotating frame

The nuclear magnetic moments of the molecules in a liquid sample at any given time appear to be randomly oriented in all directions; however, there is an excess of nuclear magnetisation aligned with the applied field. There will therefore be a macroscopic nuclear magnetic moment associated with the sample. Like the individual nuclear moments, this macroscopic moment can be represented by a vector. Since the individual moments of which the macroscopic moment is comprised are required by quantization to be at an angle to the applied field, the macroscopic moment is also at an angle to the field and so it must precess about the field at the Larmour frequency. To simplify the physical picture of what happens to the macroscopic magnetisation during the NMR experiment, a rotating frame is used (*x', y', z'* axes), rotating at the Larmour frequency and with the z' axis inclined to the z axis at the same angle as the magnetisation instead of the laboratory frame (*x, y, z* axes), making the Larmour precession appear to "vanish".

Excitation pulse

In the Fourier transform method, the NMR experiment begins by

application of a pulse of radiation at the resonance frequency to induce transitions between the upper and lower nuclear spin energy levels. The transitions induced in the individual nuclear spins must change the macroscopic magnetisation of the sample and this change appears as a displacement of the magnetisation from the *z'* axis. The intensity of the excitation pulse determines the deviation of the magnetisation vector inclination from the *z'* axis, called the tip angle. The strength of the pulse, called the pulse length, is given in terms of the tip angle.

After the excitation pulse, the magnetisation vector precesses about the *z'* axis. The NMR signal observed is the projection of this precession on to the *x'y'* plane. Two important pulse lengths can be identified; a 90° pulse will bring the magnetisation vector into the *x'y'* plane and corresponds to the maximum intensity of the NMR signal; whilst a 180° pulse aligns the magnetisation along the minus *z'* axis, the magnetisation is said to be inverted and there is no observable magnetisation (the projection on the *x'y'* plane is zero).

Relaxation

In principal, the magnetisation should be allowed to return to its initial state, Boltzmann equilibrium, before the next excitation pulse is applied. This is very important because if the magnetization does not return to its initial state before the next pulse, this next pulse will modify the

magnetisation vector from a state different from the initial one, since the transition probabilities from the upper to the lower, and lower to upper energy levels are essentially equal. The intensity of the peak recorded after the Fourier transform gives an accurate measure of the number of spins present in the sample. So, if the spin does not relax completely, and it is excited before reaching its initially energy state, the amount of net emission would not be the correct, and the NMR experiment will no longer be quantitative; erroneous results would be obtained.

The processes which allow nuclear spins to lose energy and drop from the excited state to the ground state non-radiatively, i.e without emitting an NMR signal, is called relaxation. Nuclear spins can relax in several ways: by giving up energy non-radiatively to the surroundings (spin-lattice relaxation), when Boltzmann equilibrium will be re-established; or by giving up energy to other nuclear spins (spin-spin relaxation), without changing the total amount of excited spins in the system. These processes are normally exponential in nature and are characterized by the time constants T_1 and T_2 respectively. The reciprocal of the time constant equates to the rate constant for the relaxation. It is possible for magnetisation to be exchanged between spins faster than the Boltzmann equilibrium is re-established by dissipation of energy to the lattice, but clearly the reverse is impossible; hence $T_1 \geq T_2$. T_1 relaxation determines how frequently it is possible to sample the magnetisation; whereas T_2

relaxation tells us about the lifetime of the excited state and hence, via the uncertainty principle, the natural linewidth of the NMR line.

In the vector model, the NMR signal arises from the projection of the precessing nuclear magnetic moment on the $x'y'$ plane. In some samples this precession can last for hours but clearly the excitation must decay as energy is radiated to give the NMR spectrum, lost to the lattice, or exchanged with other spins present in the sample. Clearly the NMR signal will vanish if the projection of the moment on the $x'y'$ plane vanishes, this corresponds to spin-spin relaxation; the x' and y' components of the magnetisation dephase or lose coherence. This happens independently of relaxation of the z' component of the magnetisation, which corresponds to spin-lattice relaxation and re-establishment of Boltzmann equilibrium. A consideration of the geometry of the situation confirms that spin-spin relaxation must be at least as fast as spin-lattice relaxation, but that spin-lattice relaxation cannot be faster than spin-spin relaxation.

Advantages

NMR shows many advantages for the determination of gas solubilities. It has been already said that (1.4.1) contrary to other typical techniques for experimental determination of gas solubilities, the use of NMR excludes the requirement of determination of the amounts of gas and liquid in equilibrium, nor the volume of the equilibrium cell, and the consequent

dead volumes, which makes it simpler, but not less accurate or fast.

Some important advantages of the NMR technique are:

Linear response:

- The area under the peaks of all chemical components is linear and proportional to the amounts of the components present.
- Response is equal across the spectrum: equal amount of moles gives equal signal.

Resolution:

- Different chemical types have their own distinct and unique region of chemical shift, where peaks can be identified. The $^{13}C\{^{1}H\}$ resonances of each site are well separated – there is no need to deconvolute complex, overlapping spectra.
- Each kind of carbon has its own place in the spectrum. From the chemical shift (position) we can know which kind of carbon and so the observed molecule. All functional groups are clearly resolved and have unique and documented location.

Signal variance:

- The NMR spectrum shows a high signal variance with respect to the chemical property changes providing high reliability in determining the precision and accuracy of the property predictions.

- If the chemical properties are slightly changed, the effect on the NMR signal is big. Detection of slight chemical changes.

Absolute signal:

- The NMR signal is absolute and requires no frequency reference or zero like some other optical spectroscopic techniques. No calibration needed.

Structural information:

- Relative amplitude of the NMR signal is proportional to amount of nuclei in molecular structure.
- Signal split or broadness of the features gives information on neighboring nuclei in molecule.

NMR technique is usually used qualitatively, i.e. characterization of catalysts. But in this project we also use it quantitatively, i.e. liquid composition determination.

Dynamic range:

- Ratio of the minimum detectable peak area to the maximum peak area of 10^{-2}. Using ^{13}CO (99% pure) in a solvent with ^{13}C at natural abundance it is actually 10^{-4} (detection limit << 1%).

Hence, these advantages make NMR a very appropriate analytical technique for the experimental determination of gas solubilities. In next

chapter the NMR experimental system design used in this project is described.

1.6 Scope of the thesis

Based on the concepts presented above the aim of the present thesis is the determination of the four-component (carbon monoxide, ethylene, methanol and methyl propanoate) two-phase vapour-liquid equilibrium that takes place in the methoxycarbonylation of ethylene for the production of methyl propanoate (first stage of the Alpha Process for the production of MMA). Moreover, to monitor gas solubilities during reaction as well as to determine reaction rates. To achieve these goals a new NMR experimental system is designed allowing the determination of gas solubilities in working catalytic reactions.

1.7. References

(1) New MMA technology. *European Chemical News*, Oct 30-Nov 5 **2000**, *20*.

(2) Van Leeuwen, P. W. N. M. *Homogeneous catalysis. Understanding the art*; Kluwer Academic Publishers, Amsterdam, 2004.

(3) Moulijn, J. A.; van Leeuwen, P. W. N. M.; van Santen, R. A. Catalysis, an integrated approach to homogeneous, heterogeneous and industrial catalysis. *Stud. Surf. Sci. Catal.* **1993**, *79 (1)*, 45.

(4) Taylor, H. S. Catalysis and catalytic agents in chemical processes. *Journal of the Franklin Institute* **1922**, *194 (1)*.

(5) Natta, G. et al. Crystalline high polymers of α-olefins. *J. Am. Chem. Soc.* **1955**, *77 (6)*,1708–1710

(6) Darrell, D. D. *US Patent 3,282,981*, 1966.

(7) Von Kutepow, N.; Himmele, W.; Hohenschutz, H. *Chem. Ing.*

Technol. **1965**, *37, 297.*

(8) Smith, C. W. *US Pat. 3,456,017*, 1969.

(9) Kollar, J. *US Pat. 3,360,584,* 1967.

(10) Forster, D. Mechanism of rhodium complex-catalyzed carbonylation of methanol to acetic acid. Annals of the New York Academy of Sciences. **1977**, Vol. 295, No. The Place of Transition Metals in Organic Synthesis, 79.

(11) Pruett, R. L.; Smith, J. A. *US Pat. 3,527,809,* 1970.

(12) Freitas, E. R.; Gum, C. R. Shells higher olefins process. *Chem. Eng. Prog.* **1979**, *75 (1) 73.*

(13) Knowles, W. S.; Sabacky, M. J.; Vineyard, B. D. α-aminoacids by catalytic asymmetric hydrogenation. *J. Mol. Cat.* **1983**, *19, 159.*

(14) Kuepper, F. US Pat. 4,095,033, 1978.

(15) Roe, D. C.; Kating, P. M.; Krusic, P. J.; Smart, B. E. High resolution NMR techniques in catalysis. *Top. Catal.* **1998**, *5 (1-4)*.

(16) Iggo, J. A.; Shirley, D.; Tong, N. C. A high pressure NMR flow cell for the in situ study of homogeneous catalysis. *New J. Chem. Commun.* **1998**, *22*, 1043.

(17) Van der Slot, S. C.; Kamer, P. C. J.; van Leeuwen, P. W. N. M.; Iggo, J. A.; Heaton, B. T. Mechanistic studies of the hydroformylation of 1-alkenes using a monodentate phosphorus diamide ligand. *Organometallics*. **2001**, *20 (3)*, 430.

(18) Cusanelli, A.; Frey, U.; Marek, D.; Merbach, A. E. In situ high-gas pressure NMR spectroscopy. Synthesis and catalysis. *Spectrosc. Eur.* **1997**, *9 (3)*, 22.

(19) Cusanelli, A.; Sicula-Dadci, L.; Frey, U.; Merbach, A. E. Rhodium (III) and Iridium (III) solvates of the form $[(\eta^5\text{-}C_5Me_5)M(S)_3]^{2+}$ as models for the reactivity of half-sandwich compounds. *Inorg. Chem.* **1997**, *36 (10)*, 2211.

(20) Sen, A. Catalytic synthesis of alkene-carbon monoxide copolymers and cooligomers. Kluwer Academic Publishers, Amsterdam, 2003.

(21) Brubaker, M. M. *US Patent 2,495,286*, 1950.

(22) Reppe, W.; Magin, A. *US Patent 2,577,208*, 1951. Chem. Abstr. 1952, 46, 6143.

(23) Gough, A. *British Pat. 1,081,304*, 1967. Chem Abstr. 1967, 67, 100569.

(24) Fenton, D. M. *US Pat. 3,530,109*, 1970. Chem. Abstr. 1970, 73, 110466. *US Pat. 4,076,911*, 1978. Chem. Abstr. 1978, 88, 153263.

(25) Nozaki, K. *US Pat. 3,689,460*, 1972. Chem. Abstr. 1972, 77, 152860. *US Pat. 3,694,412*, 1972. Chem. Abstr. 1972, 77, 165324. *US Pat. 3,835,123*, 1974. Chem. Abstr. 1975, 83, 132273.

(26) Sen, A.; Lai, T. W. Novel palladium(II)-catalyzed copolymerization of carbon monoxide with olefins. *J. Am. Chem. Soc.* **1982**, *104 (12)*, 3520.

(27) Drent, E.; Budzelaar, P. H. M. Palladium-catalyzed alternating copolymerization of alkenes and carbon Monoxide. *Chem. Rev.* **1996**, *96 (2)*, 663-681.

(28) Drent, E. *Eur. Pat. Appl. 121,965 A2*. 1984. Chem. Abstr. 1985, 102, 46423.

(29) Drent, E.; Van Broekhoven, J. A. M.; Doyle, M. J. Efficient palladium catalysts for the copolymerization of carbon monoxide with olefins to produce perfectly alternating polyketones. *J. Organomet. Chem.* **1991**, *417 (1-2)*, 235.

(30) Clegg, W.; Eastham, G. R.; Elsegood, M. R.; Tooze, R. P.; Wang, X. L.; Whiston, K. Highly active and selective catalysts for the production of methyl propanoate via the methoxycarbonylation of ethene. *Chem. Commun.* **1999**, 1877-1878.

(31) Van Leeuwen, P. W. N. M.; Zuideveld, M. A.; Swennenhuis, B. H. G.; Freixa, Z.; Kamer, P. C. J.; Goubitz, K.; Fraanje, J.; Lutz, M.; Spek, A. L. Alcoholysis of acylpalladium(II) complexes relevant to the alternating copolymerization of ethene and carbon monoxide and the

alkoxycarbonylation of alkenes: the importance of cis-coordinating phosphines. *J. Am. Chem. Soc.* **2003**, *125 (18)*, 5523.

(32) Donald, S. M. A.; Macgregor, S. A.; Settels, V.; Cole-Hamilton, D. J.; Eastham, G. R. A computational study of the methanolysis of palladium-acyl bonds. *Chem. Commun.* **2007**, 562.

(33) Liu, J.; Heaton, B. T.; Iggo, J. A.; Whyman, R.; Bickley, J. F.; Steiner, A. The mechanism of the hydroalkoxycarbonylation of ethene and alkene-CO copolymerization catalyzed by Pd-II-diphosphine cations. *Chem. Eur. J.* **2006**, *12*, 4417.

(34) Zuidema, E.; Bo, C.; van Leeuwen, P. W. N. M. Ester versus polyketone formation in the palladium-diphosphine catalyzed carbonylation of ethene. *J. Am. Chem. Soc.* **2007**, *129 (13),* 3989.

(35) Eastham, G. R.; Heaton, B. T.; Iggo, J. A.; Tooze, R. P.; Whyman, R.; Zacchini, S. Synthesis and spectroscopic characterisation of all intermediates in the Pd-catalysed methoxycarbonylation of ethene. *Chem. Commun.* **2000**, 609.

(36) Nagai, K. New developments in the production of methyl methacrylate. *Appl. Catal., A.* **2001**, *221*, 367.

(37) Gibbs, J. *The Scientific Papers of J. Willard Gibbs.* Dover Publications, New York, 1961.

(38) Prausnitz, J. M. et al. *Molecular thermodynamics of fluid-phase equilibria.* 3rd Edition. Prentice Hall, Englewood Cliffs, NJ, 1999.

(39) Redlich, O.; Kwong, J. N. S. On the Thermodynamics of solutions V. An equation-of-state. Fugacities of gaseous solutions. *Chem. Rev.* **1979**. *44*, 223.

(40) Reid, R. C.; Prausnitz, J. M.; Poling, B. E. *The properties of gases and liquids.* 4th Edition. McGraw-Hill. 1987.

(41) Bondi, A. *Physical Properties of Molecular Crystals, Liquids and Gases.* John Wiley & Sons, New York, 1960.

(42) Abrams, D. S.; Prausnitz, J. M. Statistical thermodynamics of liquid

mixtures: A new expression for the excess Gibbs energy of partly or completely miscible systems. *AIChE J.* **1975**, *21*, 116.

(43) Prausnitz, J. M. et al. *Computer Calculations for Multicomponent Vapor-Liquid and Liquid-Liquid Equilibria.* Prentice Hall, Englewood Cliffs, 1980.

(44) Poynting. *Philos. Mag.* **1881**, *4 (12)*, 32.

(45) Rackett, H. G. Equation of state for saturated liquids. *J. Chem. Eng. Data.* **1970**, *15*, 514.

(46) Design Institute for Physical Property Data. http://dippr.byu.edu/

(47) Watson, K. M. Thermodynamics of the liquid state. Generalized prediction of properties. *Ind. Eng. Chem.* **1943**, *35*, 398.

(48) Markham, A. E.; Kobe, K. A. The solubility of gases in liquids. *Chem. Rev.* **1941**, *28 (3)*, 519.

(49) Morgan, J. L. R.; Pyne, H. R. Solubility relations in gas-liquid systems 1. *J. Phys. Chem.* **1930**, *34 (7)*, 1578.

(50) Cady, H. P.; Elsey, H. M.; Berger, E. V. The solubility of helium in water. *J. Am. Chem. Soc.* **1922**, *44 (7)*, 1456.

(51) Kobatake, Y.; Hildebrand, J. H. Solubility and entropy of solution of He, N_2, Ar, O_2, CH_4, C_2H_6, CO_2 and SF_6 in various solvents; regularity of gas solubilities. *J. Phys. Chem.* **1961**, *65 (2)*, 331.

(52) Sisi, J. C.; Dubeau, C.; Ozanne, N. Solubility of hydrogen selenide gas in water. *J. Chem. Eng. Data.* **1971**, *16 (1)*, 78.

(53) Sada, E.; Kito, S.; Ito, Y. Solubility of nitrous oxide in the mixtures of alcohols and water: comparison with Pierotti's gas solubility theory. *Ind. Eng. Chem. Fundam.* **1975**, *14 (3)*, 232.

(54) Chai, C.; Paulaitis, M. E. Gas solubilities of carbon dioxide in heavy hydrocarbons. *J. Chem. Eng. Data.* **1981**, *26 (3)*, 277.

(55) Miyano, Y.; Hayduk, W. Solubilities of n-butane gas and densities for acetone-methanol, acetone-ethanol, and acetone-propanol solvent solutions. *J. Chem. Eng. Data.* **1986**, *31 (1)*, 81.

(56) Shoor, S. K.; Walker, R. D.; Gubbins, K. E. Salting out of nonpolar gases in aqueous potassium hydroxide solutions. *J. Phys. Chem.* **1969**, *73 (2)*, 312.

(57) Horvath, M. J.; Sebastian, H. M.; Chao, K. Gas chromatograph method for the determination of gas solubility in liquids. *Ind. Eng. Chem. Fundam.* **1981**, *20 (4)*, 394.

(58) Breman, B. B.; Beenackers, A. A. C. M.; Rietjens, E. W. J.; Stege, R. J. H. Gas-liquid solubilities of carbon monoxide, carbon dioxide, hydrogen, water, 1-alcohols ($1 \leq n \leq 6$), and n-paraffins ($2 \leq n \leq 6$) in hexadecane, octacosane, hexadecanol, phenanthrene, and tetraethylene glycol at pressures up to 5.5 MPa and temperatures from 293 to 553 K. *J. Chem. Eng. Data.* **1994**, *39 (4)*, 647.

(59) Olsen, J. D. Solubility of nitrogen, argon, methane and ethane in ethylene oxide. *Ind. Eng. Chem. Fundam.* **1981**, *20 (4)*, 394.

(60) Cukor, P. M.; Prausnitz, J. M. Solubilities of gases in liquids at elevated temperatures. Henry's constants for hydrogen, methane and ethane in hexadecane, bicyclohexyl and diphenyl methane. *J. Phys. Chem.* **1972**, *76 (4)*, 598.

(61) Graaf, G. H.; Smit, H. J.; Stamhuis, E. J.; Beenackers, A. A. C. M. Gas-liquid solubilities of the methanol synthesis components in various solvents. *J. Chem. Eng. Data.* **1992**, *37 (2)*, 146.

(62) Park, J.-Y.; Yoon, S. J.; Lee, H. Effect of steric hindrance on carbon dioxide absorption into new amine solutions: thermodynamic and spectroscopic verification through solubility and NMR analysis. *Environ. Sci. Technol.* **2003**, *37 (8)*, 1670.

(63) Laurenczy, G.; Ohlin, C. A.; Dyson, P. J. Carbon monoxide solubility in ionic liquids: determination, prediction and relevance to hydroformylation. *Chem. Commun.* **2004**, 1070.

(64) Roe, D. C. Sapphire NMR tube for high-resolution studies at elevated pressure. *J. Magn. Res.* **1985**, *63 (2)*, 388.

(65) Tubes available from Tyco Saphikon, Milford, N. H.

(66) Kinrade, S. D.; Swaddle, T. W. A sample tube for NMR studies at elevated pressures and temperatures. *J. Magn. Res.* **1988**, *77 (3)*, 569.

(67) Horvath, I. T.; Ponce, E. C. New valve design for high-pressure sapphire tubes for NMR measurements. *Rev. Sci. Instrum.* **1991**, *62 (4)*, 1104.

(68) Bai, S.; Taylor, C. M. et al. A new high pressure sapphire nuclear magnetic resonance cell. *Rev. Sci. Instrum.* **1996**, *67 (1)*, 240.

(69) Gaemers, S.; Luyten, H.; Ernsting, J. M.; Elsevier, C. J. Multinuclear magnetic resonance studies under pressure of gases and in supercritical media employing a novel titanium-sapphire high-pressure cell with pressure sensor. *Magn. Reson. Chem.* **1999**, *37 (1)*, 25.

(70) Wallen, S. L.; Schoenbachler, L. K.; Dawson, E D.; Blatchford, M.A. *Anal. Chem.* **2000**, *72 (17)*, 4230.

(71) Niessen, H. G.; Trautner, P.; Wiemann, S.; Woelk, K.; Bargon, J. The toroid cavity autoclave for high-pressure and variable-temperature *in situ* nuclear magnetic resonance studies. *Rev. Sci. Instrum.* **2002**, *73 (3)*, 1259.

(72) Yonker, C. R.; Zemanian, T. S.; Wallen, S. L.; Linehan, J. C.; Franz, J. A. A new apparatus for the convenient measurement of NMR spectra in high-pressure liquids. *J. Magn. Res., A.* **1995**, *113*, 102.

(73) Heaton, B. T.; Strona, L.; Jonas, J.; Eguchi, T.; Hoffman, G. H. Carbon-13 nuclear magnetic resonance studies of rhodium carbonyl clusters on pressurization with CO/H_2. *J. Chem. Soc., Dalton Trans.* **1982**, 1159.

(74) Jonas, J.; Hasha, D. L.; Lamb, W. J.; Hoffman, G. A.; Eguchi, T. High-resolution probe for NMR measurements at high pressures and high fields. *J. Magn. Res.* **1981**, *42 (1)*, 169.

(75) Hoffmann, M. M., Conradi, M. S. Nuclear magnetic resonance probe for supercritical water and aqueous solutions. *Rev. Sci. Instrum.* **1997**, *68 (1)*, 159.

(76) Bonev, B. B.; Morrow, M. R. Simple probe for variable pressure deuterium nuclear magnetic resonance studies of soft materials. *Rev. Sci. Instrum.* **1997**, *68 (4)*, 1827.

(77) Vander Velde, D. G.; Jonas, J. A high-pressure probe for NMR studies of homogeneous catalysts. *J. Magn. Res.* **1987**, *71 (3)*, 480.

(78) Rathke, J. W. Toroid detectors in pressure probes. *J. Magn. Reson.* **1989**, *85 (1)*, 150.

(79) Selent, D.; Baumann, W.; Börner, A. Gaseinleitungs- und -zirkulationsvorrichtung zur Verfolgung von Reaktionen in flüssiger Phase unter Beteiligung gasförmiger Reaktanden unter Normal- und Hochdruck mittels Kernresonanzspektroskopie (Druck-NMR-Spektroskopie) unter stationären Bedingungen. *Patent IfOK, Rostock,* 17.07.**2003**.

Chapter 2

Experimental design

Chapter 2: Experimental design

2.1 Introduction

This chapter describes the different experimental system designs used for the determination of vapour-liquid equilibria and kinetic studies. These experimental systems are based on two analytical techniques; NMR and Gas Chromatography (GC), experimental determinations of liquid phase composition are always performed using NMR, whilst gas phase composition is determined by GC.

2.2 Sapphire tube static system

Preliminary gas solubility experiments were performed using an existing HP NMR sapphire tube system. These experiments afforded an initial estimate of the solubilities of carbon monoxide and ethylene separately in a mix of methyl propanoate and methanol.

2.2.1 Description

The system consists of a thin-walled (0.1 mm) NMR single-crystal sapphire tube (10 mm diameter) attached to a metallic valve assembly (Figure 2.1).[1, 2, 3] The sapphire tube is glued to a Ti alloy flange with

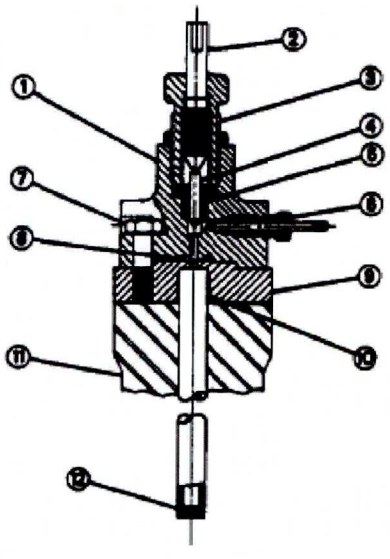

Figure 2.1. Schematic drawing of Roe's titanium alloy valve and sapphire tube assembly: (1) valve body, (2) valve stem drive handle, (3) stem drive and packing gland. (4) non-rotating stem, (5) packing assembly, (6) gas inlet port for 1/16-in tubing, (7) assembly screw (total of four), (8) Viton O-ring seal, (9) tube mounting flange, (10) epoxy sealant, (11) spinner turbine, (12) sapphire tube.

Aremcobond 565 adhesive. The Ti alloy valve assembly screwed into the flange allows pressurization and a large sample volume of about 0.3-0.4 mL. Through this valve the gas is fed into the sapphire tube containing the liquid solvent. The entire tube and valve assembly spins in a commercial magnet. The tube has a flat bottom surface, unlike a typical NMR tube, however, good NMR resolution is obtained. Hence, this design allows a large sample volume and so provides good NMR sensitivity.

2.2.2 Procedure

The sapphire tube was evacuated applying vacuum. The liquid solvent was introduced into the evacuated sapphire tube, and then the gas, from a pressurized bottle connected to the valve body, fed until the desired pressure was reached. The sapphire tube was then isolated from the gas bottle and placed in a thermal water bath at the desired temperature. A mechanical agitator was used to vigorously shake the tube to ensure equilibrium was reached. During the agitation the change in pressure in the tube was monitored until the pressure was stable, and so the equilibrium condition reached, which took approximately 15-20 minutes. The final pressure was noted, the tube sealed and disconnected from the gas feed line, in which the pressure transducer was placed. The tube was then taken to and introduced into the NMR probe, which had been previously heated to the desired temperature by the NMR spectrometer (*Bruker AMX2-200WB*) equipped with a *Bruker BVT2000* temperature control unit (T ±

0.1 K). Then the FID (free induction decay) acquired. The free induction decay is the observable NMR signal produced by the nuclear spin magnetization precession about the magnetic field. Recording an FID all resonances were measured in the time domain. The FID was converted from the time domain to the frequency domain by a Fourier transformation, and so, the NMR spectrum showing peaks at the characteristic resonances of the components present in the sample was obtained. Composition of the liquid solvent/dissolved gas filling the sapphire tube was determined from the areas under the peaks in the spectrum.

Solubility calculations from NMR spectra

The composition of the solution, and hence the gas solubilities were calculated from the spectra recorded by NMR. These spectra consist of separate peaks which represent different carbons and so different molecules present in the liquid contained in the NMR tube. The intensity of each peak is representative of the number of moles of the component it represents in the sample. Thus, from a spectrum it was possible to calculate the composition of the sample within the magnet (Figure 2.2).

Sample FID's were processed in two different ways: (i) applying a trapezoidal multiplication before Fourier transformation, and (ii) applying an exponential multiplication to the FID. Trapezoidal multiplication removed distortions at the base of the NMR peaks caused by truncation of the FID when using short acquisition times. Short acquisition times were of

interest for kinetic studies in which recording FID's as fast as possible was desirable. One aim of the project was to monitor liquid composition and gas solubilities during reaction. Exponential multiplication enhanced the signal to noise ratio in the spectra. The results of the two methods were compared to check for artifacts produced by trapezoidal multiplication. The relative intensities of the resonances due to the different carbons in the sample were similar for both processing methods.

Hence, integration of the peaks gave the relative amounts (moles) of each functional group present.

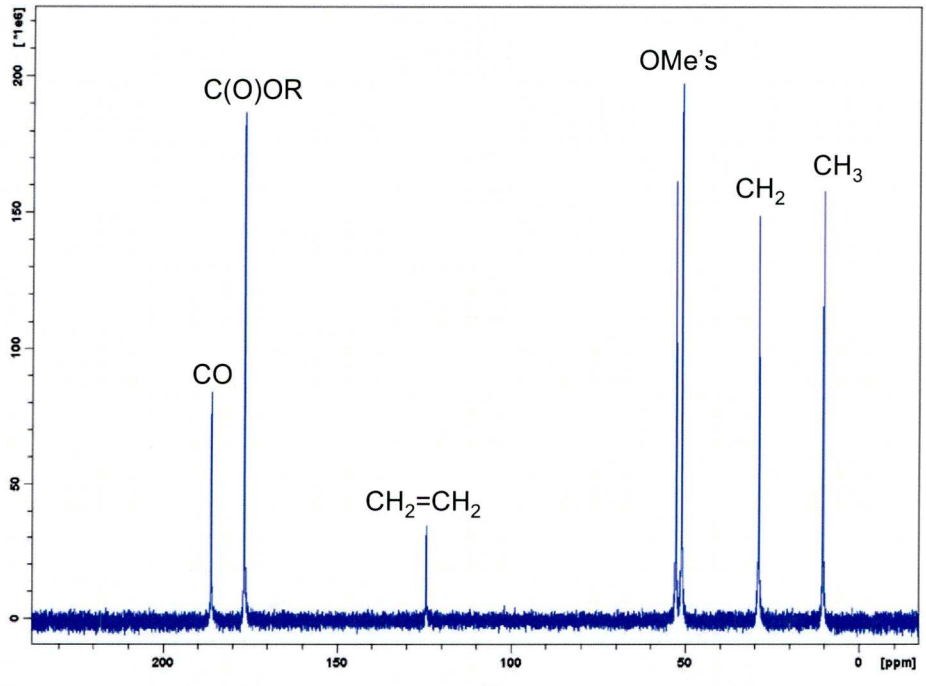

Figure 2.2. Typical spectrum for the system $^{13}CO:C_2H_4$ in MeOH/MeP (30/70 % wt).

The resonances in the $^{13}C\{^1H\}$ NMR spectrum (Figure 2.2) could be readily assigned based on literature data. The peak at approx. 185 ppm is due to carbon monoxide (**C**O), so its intensity is proportional to the number

of moles of CO in the liquid. The peak at 175 ppm is due to **C**(O)OR of MeP, and that at 124 ppm is due to ethylene. The resonances at 52 ppm are due to the (O**C**H_3) groups of MeP and MeOH; in some experiments these two resonances overlapped, so could not be integrated separately. The peak at approx. 28 ppm is due to **C**H_2 in MeP, and that at approx. 8 ppm represents the carbon of the **C**H_3 group in MeP.

Thus, the amounts of CO, C_2H_4, and MeOH present, are each represented by just one peak, whilst there are three peaks representing the moles of MeP. For calculating the mole fractions of each component in the mixture the first step was to average the peaks representing MeP. Then, knowing the molar quantity of MeP present and the combined intensity of the peak due to the (O**C**H_3) groups of MeP and MeOH, it is possible to derive the moles of MeOH present. Since the solubility of CO is very low in this solvent ^{13}CO >99 % enriched in ^{13}C was used to increase the intensity of the CO resonance so that the CO composition could be accurately determined. The intensity of the peak at ~185 ppm (CO), must, therefore, be divided by 0.99 when calculating the moles of CO present, while the intensities of the other peaks must be divided by 0.011 since the natural abundance of ^{13}C is 1.1 %. In the calculation of the moles of ethylene present it must also be remembered that the peak representing the C_2H_4 is generated by two carbons, so the area below this peak must be divided by *2 x 0.011*.

In Figure 2.2 can be observed that the different peaks representing MeP (CH_2, CH_3, and COOR peaks) are not the same height when they should represent the same amount of moles. This is explained by the time-energy uncertainty principle, that is, the excited states do not have a definite energy and each time they decay, the energy released is slightly different. The average energy has a peak at the theoretical energy of the state, but the distribution has a finite width called the natural line width. Hence, faster decaying states give broader line width. However, the area under the peaks, representing the number of moles, is the same for three different peaks representing MeP.

2.3 NMR bubble column flow system

This system was designed for the experimental determinations of gas solubilities in working catalytic reactions and is more appropriate for such measurements than the static sapphire tube because it allows for a continuous feed of gas, thus avoiding the possibility of gas starvation due to the reaction consuming dissolved gaseous reactants, and allowing easy control of the pressure in the equilibrium cell by the quantity of gas introduced. Furthermore, it allows the vapour-liquid equilibrium conditions to be changed without manipulation of the equilibrium cell, and provides very fast equilibration times, of ca. 3 minutes.

2.3.1 Description

The equilibrium cell used in this experimental design is a 10 mm diameter, 0.1 mm wall thickness sapphire tube,[1, 3, 4, 5] having a nominal burst pressure of ca. 600 bar. A modified version of Elsevier's HPNMR valve[6] is bonded to the tube using epoxy resin. This valve connects the sapphire tube with two concentric pipes which serve as inlet and outlet of gas. The internal pipe (~ 1 mm internal diameter) is terminated by a length of 1/16" PTFE tubing which is immersed in the solvent and feeds the gas to the bottom of the sapphire tube, bubbling it through the liquid. Bubbles produce agitation and good mixing of gas and liquid phases, and so the equilibrium condition is rapidly reached. The gas leaves the sapphire tube

from the valve at the top of it and through the external concentric pipe. The outlet gas is recirculated, passing through a reciprocating action syringe pump,[7] driving the gas again through the dip tube immersed in the solvent, contained in the equilibrium cell positioned in the NMR probe within the NMR magnet (Figure 2.3).

The concentric gas feed and exhaust lines are described by Selent[5] and were modified to incorporate a larger diameter section immediately above the HPNMR valve. Cooled water was passed through a copper tube wound around this wide diameter section to condense solvent contained in the exit gas. The HPNMR valve has also been modified to allow unimpeded drainage of condensed fluids back into the sample cell.

This gas circulation system allows for feeding the HPNMR cell with non-corrosive gases and gas recycling under anaerobic conditions. This system can be used at pressures up to 50 bar. The reciprocating pump allows an easy control of the pressurized gas stream flow, allowing a range of flow rates from 1 to 80 mL/min. The gas pressure within the gas feed and gas return capillary, respectively, is measured separately to within ±0.01 bar by two pressure transmitters (*Trafag*). The desired temperature in the equilibrium cell is controlled by the NMR spectrometer (*Bruker AMX2-200WB*) equipped with a *Bruker BVT2000* temperature control unit. The accuracy of the temperature control unit was determined by the water and nitrogen boiling point measurement, temperature control to within a ±0.1 K

was achieved. The pressure in the equilibrium cell is controlled by the action of a gas bottle head valve and an exhaust valve. Hence, it is easy to change and control the equilibrium condition and rapid dissolution of gas is achieved without the need for mechanical stirring or agitation of the HPNMR tube.

An additional advantage of this design with respect to the static sapphire tube is that the equilibrium is achieved within the NMR system so there is no thermal disturbance of the sample, as occurs in the static tube after agitation and sealing, while it is taken to the NMR spectrometer.

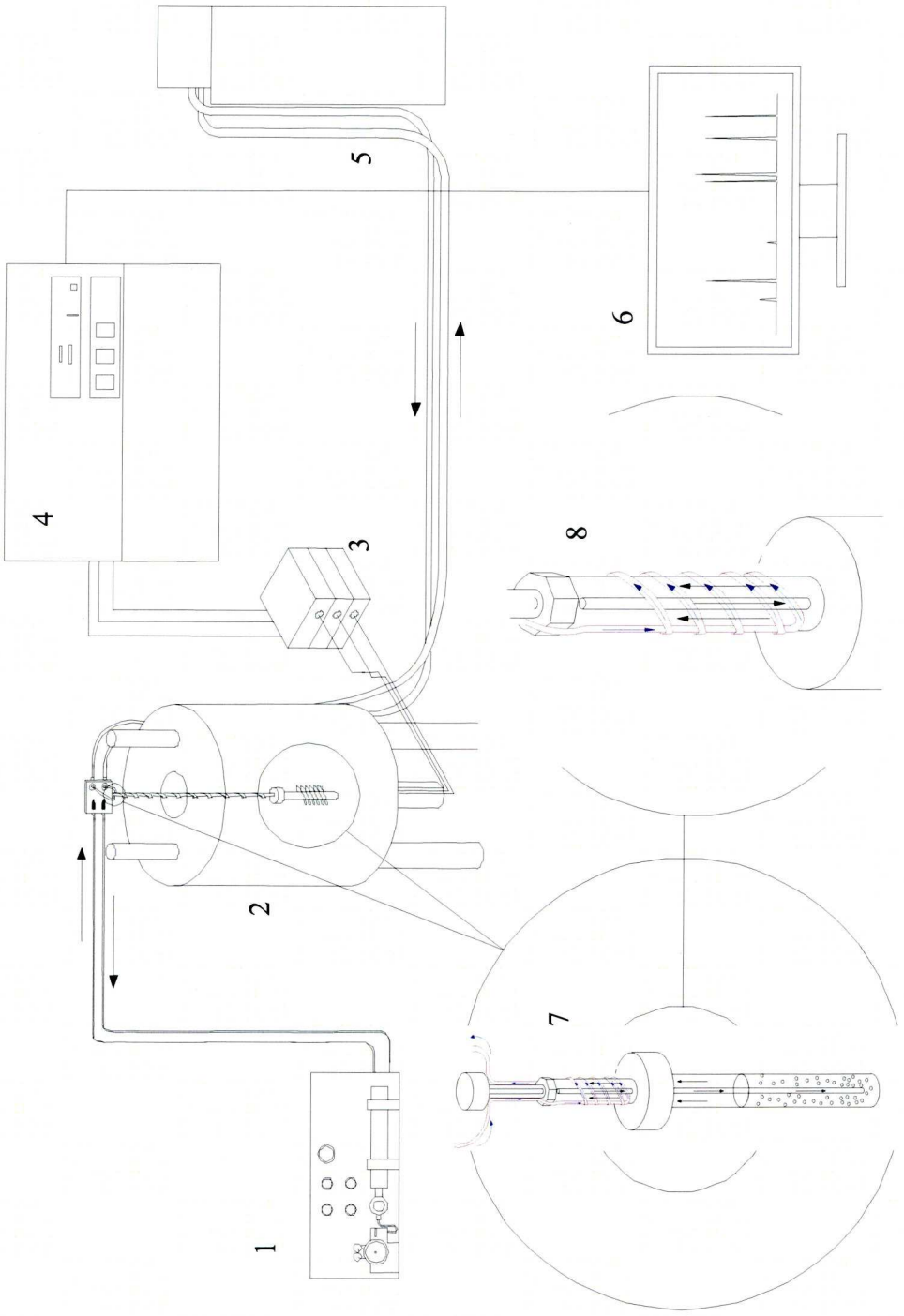

Figure 2.3. NMR bubble column flow system. Sapphire tube connected to a recirculating pump, with an inlet and outlet of gas, introduced in the NMR machine connected to the spectrometer. 1) Recirculating pump, gas feed cylinder, and valves for controlling the system pressure and gas flow. 2) NMR machine 200 MHz. 3) Preamplifier. 4) Spectrometer Bruker AMX2-200WB. 5) Cooler. Flow of cool water at -4ºC to the condenser. 6) User interface. 7) Gas inlet and outlet, and condenser. 8) Sapphire tube with capillary inlet and outlet lines with a solvent condensing section at the top of the valve.

2.3.2 Procedure

Every experiment using this experimental design started with the evacuation of gas lines and equilibrium cell so that no gaseous impurities were present in the system. During this evacuation, the sapphire tube containing the solvents was cooled, using liquid nitrogen, so that the solvents did not evaporate when applying vacuum. The system was then pressurized with feed gas, supplied from a gas cylinder attached to the pump lines. The pump was started and gas flowed continuously bubbling through the liquid solvent. The pressure was controlled by the quantity of gas introduced, once the pressure within the tube reached the desired value it was isolated from the gas bottle. The desired temperature within the NMR probe was set and the sapphire tube then introduced into the NMR magnet, and the system allowed to reach equilibrium (3 minutes). The equilibrium condition was achieved when pressure within the equilibrium cell was stabilized. The NMR spectrum was recorded, and the composition of the liquid phase at those pressure and temperature conditions could be obtained directly from the areas of the peaks of the spectrum recorded. The sample temperature was then changed to the next temperature, the system allowed to reach equilibrium, the pressure noted and a NMR spectrum at the new equilibrium condition recorded. The process was then repeated ultimately affording isotherms of P vs. x_i.

First experiments were used to determine the precision of the measurements. For this determination, the same experiment, at fixed compositions, pressure and temperature, was repeated four times, recording four different FID's. The latter were processed in two different ways, by a direct Fourier transformation, and applying an exponential multiplication to the FID before the Fourier transformation to enhance the signal to noise ratio in the spectrum. The peaks in the spectrum were integrated considering two different integration intervals, measuring the area under the peak taking more or less width of the baseline from the peak centre. Hence, recording four different FID's, processing them in two different ways, and integrating between two different intervals, sixteen experimental values of each peak area were obtained at the same equilibrium conditions. The random error, also called experimental uncertainty, of the area measured for each peak was calculated by the standard deviation:

$$\sigma = \sqrt{\frac{\sum_i (x_i - \bar{x})^2}{N-1}} \tag{2.1}$$

Where σ is the standard deviation, x_i is the measured value, $\bar{x}$ is the average value of the N measurements results.

Hence, the random error for each component composition was calculated at different concentration values (peak intensities), as areas under peaks of smaller intensities are resolved with less precision. Hence, for

measurements of low compositions of a component the random error was higher that the error in more concentrated solutions.

2.4 GC bubble column flow system

The gas chromatography (GC) flow system is designed with the purpose of determining the gas phase composition under conditions closely mimicing those of the NMR experiments. This would allow complete validation of the theoretical model described in Chapter 1, of the four-component two-phase system under study.

2.4.1 Description

This experimental system is independent of the NMR bubble column for the determination of the compositions of the liquid phase; only measurements of the gas phase are performed. Figure 2.4 shows a schematic diagram of the whole setup. It consists of an oven containing the equilibrium cell. This cell is essentially identical to that used in the NMR flow system. It consists of a sapphire tube, of the same dimensions as that used in the NMR bubble column, containing the liquid solvent. The inlet and the outlet gas lines have the same configuration as in the NMR flow system, two concentric pipes, the gas inlet is the inner tube, and the outer tube the outlet of gas. The inner tube is a 1/16" stainless steel tube that dips into the solvents and through which the gas is bubbled into the liquid phase. The exit gas from the equilibrium cell is recirculated by a magnetic pump through trace heated 1/8" stainless steel tubing and passes through GC injection valves, where it can be sampled, before re-entering the

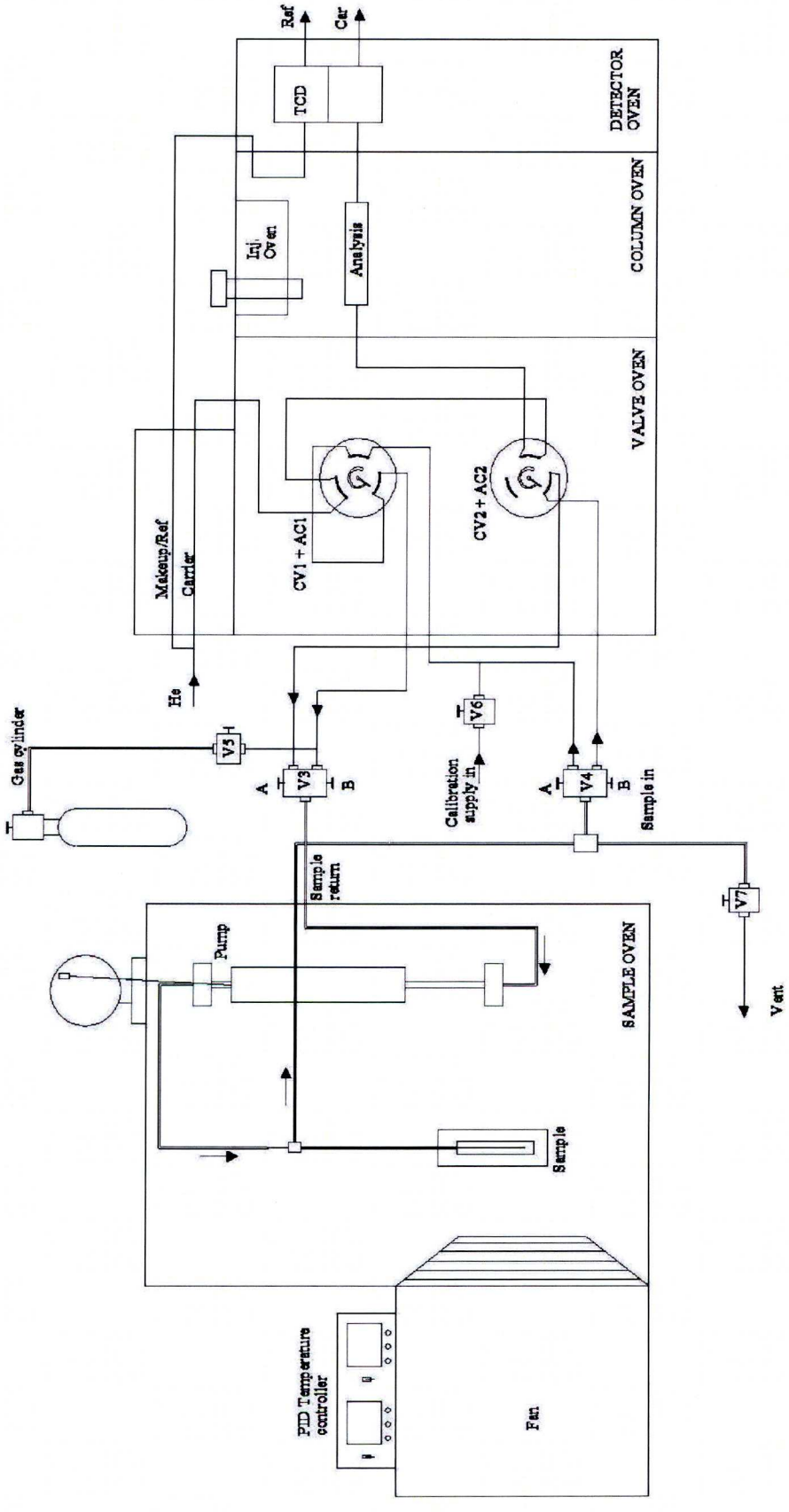

Figure 2.4. GC bubble column system.

equilibrium cell.

The bubble column equilibrium cell is placed in a thermostatically controlled oven. The pressure is controlled by the quantity of gas introduced in the system, and it is monitored by a pressure transmitter placed in the GC gas feed line connecting the equilibrium cell outlet and the GC injection valves. The pump allows the control of the gas flow in the recirculating loop.

The gas is supplied from a gas cylinder connected to the feed line. The system has an exhaust line through which the gas can be exhausted, and the system evacuated by the action of a vacuum pump.

2.4.2 Procedure

The GC column separates the components as a function of density and must be calibrated for the four components of interest. The calibration was done by the determination of the peak area of each component introduced onto the GC column as a function of its partial pressure, which is proportional to the number of moles of that component present. Hence, from the four peak spectra obtained during the experimental determinations, the partial pressure, and hence the molar fraction of each component in the gas phase in equilibrium at each condition of pressure and temperature can be calculated.

The experimental procedure started with the introduction of the solvents into the equilibrium cell. The system was then cooled with liquid nitrogen to prevent loss of solvents and the equilibrium cell evacuated. Once the system was evacuated, gas was introduced to give the desired pressure, and the oven (containing the equilibrium cell), the lines, and the GC injection valves and column were heated to the desired temperature. The magnetic pump was then started and the gas allowed to flow through the recirculation loop, entering the GC column only when the injection valves were opened. The gas was allowed to flow for 5 minutes to allow the system to reach equilibrium, then sampled and its composition measured. Three samplings were made for each composition determination. Then, the pressure condition was changed by changing the quantity of gas in the system. Once the range of pressures (1-20 bar) has been covered, the temperature condition was changed, and the procedure repeated. A typical spectrum and the operation conditions of the GC are shown in Appendix B.

2.5 NMR+GC bubble column flow system

Some modifications were made to the NMR bubble column flow system, described in section 2.3, for the determination of gas solubilities during reaction, where further issues are present, i.e. system pressure and gas phase composition are desired to be constant, even though dissolved gaseous components are consumed by reaction.

2.5.1 Description

As the gaseous components dissolved are being consumed by reaction, the pressure in a closed system decreases as the reaction proceeds. Therefore, to achieve a constant pressure during reaction, a gas reservoir equipped with a forward pressure regulator must be connected such that gas is automatically introduced in the system to replenish that consumed by reaction.

A second issue was the composition of the gas phase. Usually the gas phase during reaction is more concentrated in ethylene (~ 80 % mole) than in CO (~ 20 % mole). The reaction has a 1:1:1 stoichiometry in CO: C_2H_4: MeOH, so the gas phase composition changed as ethylene and carbon monoxide were consumed by reaction. To keep the gas phase composition unchanged two gas feed cylinders were used. A cylinder filled with the desired initial composition of ethylene and carbon monoxide for the reaction is used to pressurize the system initially, and a second cylinder

containing a 1: 1 molar composition of C_2H_4:CO is used to replenish the consumed ethylene and carbon monoxide.

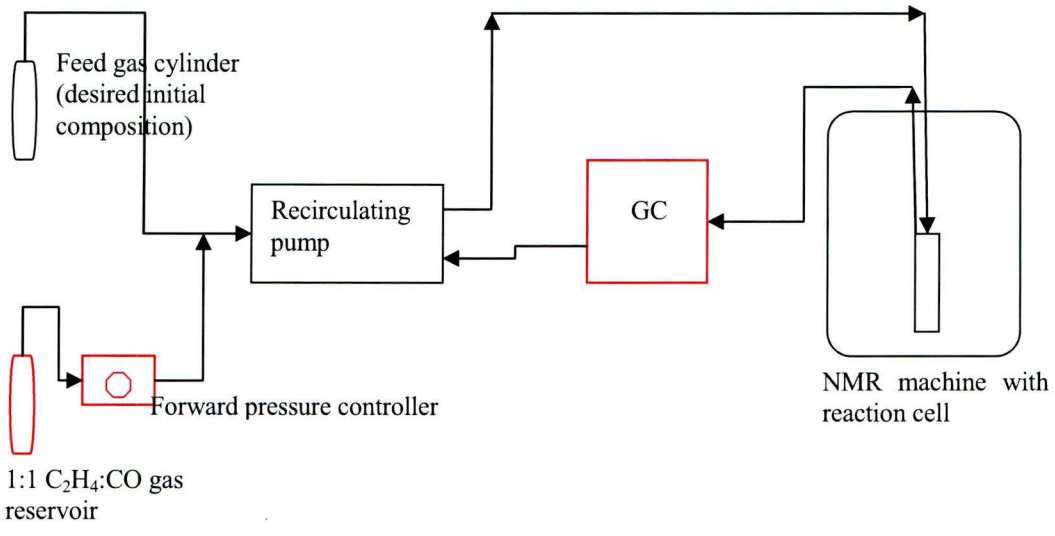

Figure 2.5. NMR + GC bubble column flow system.

A GC (section 2.4) is introduced in the gas return line so that the actual composition of the gas phase during reaction can be monitored. A schematic diagram of the NMR bubble column flow system modifications is shown in Figure 2.5.

2.5.2 Procedure

The procedure was analogous to that for the NMR bubble column VLE experiments, described in section 2.3.2 with the difference that two gas feed cylinders were used, and sampling of the return gas was performed. The pressure and temperature were kept constant during reaction (~ 15 bar;

373 K), and liquid composition measurements were performed continuously until the reaction stopped.

2.6 Conclusions

From the simple NMR sapphire tube system a new more complex NMR bubble column flow system was developed, allowing the determination of gas solubilities in working catalytic reactions, as well as the characterisation of the catalyst with the same sensitivity and accuracy as the sapphire tube, but avoiding the problems of gas starvation, equilibration time, and allowing an easy control of reaction conditions and determination of compositions.

The different systems described in this chapter were used in the experimental determinations showed in Chapters 4 and 5. In next chapter, the validation of the new bubble column NMR flow system experimental design is described.

2.7 References

(1) Horvath, I. T.; Millar, J. M. NMR under high gas pressure. *Chem. Rev.* **1991**, *91*, 1339.

(2) Horvath, I. T.; Ponce, E. C. New valve design for high-pressure sapphire tubes for NMR measurements. *Rev. Sci. Instrum.* **1991**, *62 (4)*, 1104.

(3) Roe, D. C.; Kating, P. M.; Krusic, P. J.; Smart, B. E. High resolution NMR techniques in catalysis. *Top. Catal.* **1998**, *5 (1-4)*.

(4) Sprengers, J. W.; Kluwer, A. M.; Gaemers, S.; Elsevier, C. J. High-pressure NMR spectroscopy: Some general aspects and applications. *Defect. Diffus. Forum.* **2002**, *208*, 283.

(5) Cusanelli, A.; Frey, U.; Marek, D.; Merbach, A. E. In situ high-gas pressure NMR spectroscopy. Synthesis and catalysis. *Spectrosc. Eur.* **1997**, *9 (3)*, 22.

(6) Elsevier, C. J. NMR at elevated gas pressures and its application to

homogeneous catalysis. *J. Mol Catal.* **1994**, *92 (3)*, 285.

(7) Selent, D.; Baumann, W.; Börner, A. Gaseinleitungs- und -zirkulationsvorrichtung zur Verfolgung von Reaktionen in flüssiger Phase unter Beteiligung gasförmiger Reaktanden unter Normal- und Hochdruck mittels Kernresonanzspektroskopie (Druck-NMR-Spektroskopie) unter stationären Bedingungen. *Patent IfOK, Rostock,* 17.07.**2003**.

Chapter 3

Experimental method validation

Chapter 3: Experimental method validation

3.1 Introduction

The reliability of the novel NMR bubble column experimental system described in Chapter 2 was first validated. The validation started with the design of the NMR experiment. The measured NMR spectra must be quantitative; to achieve this it is necessary to define properly the pulse program used during acquisition of the FID, the relaxation time constant T_1, and the number of scans performed for each composition determination These parameters will define the total FID recording time, and signal to noise ratio in the spectra.

Once the NMR parameters were correctly setup, compositions obtained using the new experimental system were validated by comparison with literature data for CO and C_2H_4 solubility in MeOH.

3.2 NMR experiment setup

3.2.1 Determination of T_1

Determination of the relaxation time constant T_1 is crucial for correct setting of the time delay between pulses. The spin-lattice relaxation process, described in Chapter 1, is mathematically defined by the exponential relaxation-time constant T_1. After a waiting period of $5 \times T_1$, after the application of the excitation pulse, the magnetization will have regained 99.3% of its equilibrium value; after $10 \times T_1$, it will have regained 99.9995%. In order for the measured NMR intensity to be quantitative for all resonances it is important to allow the system to return to equilibrium between each sequence. This time period between scans is called relaxation delay or pulse delay. It is critical when designing an NMR experiment to choose the relaxation delay carefully since different resonances will have different T_1's. If T_1 is too short, the spectra will not be quantitative; if T_1 is too long, the total experiment time is lengthened needlessly.

Two experimental methods were routinely used to determine the value of T_1: inversion recovery Fourier transform, and saturation recovery Fourier transform.

Inversion Recovery Fourier Transform (IRFT)

The IRFT method uses the following pulse sequence:

$$(180^\circ - \tau - 90^\circ - acquire - t)$$

Where τ is a variable delay and t is a recovery time chosen such that *(acquisition time + t)* $\geq 5T_1$. The measured line intensity is expressed as

$$I_t = I_\infty[1 - 2\exp(-\tau / T_1)] \qquad 3.1$$

Where I_∞ corresponds to $\tau = \infty$ (spin system in equilibrium), a condition practically met with $\tau_\infty = 5 \times T_1$.

Typically, the experiment is repeated using 10 different values for τ spanning the range $0.3T_1$ to $2T_1$.

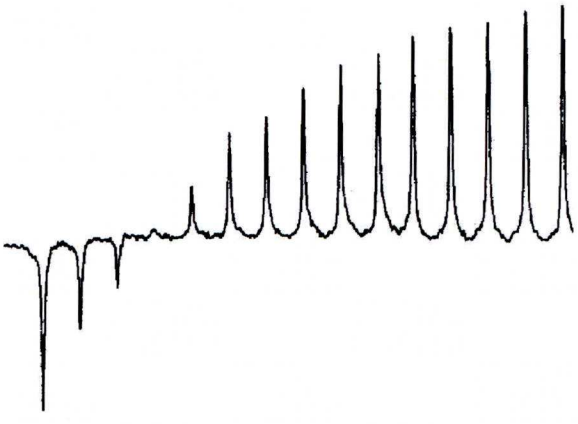

Figure 3.1.[1] IRFT-RFS method typical spectrum. The peak intensity increases with increasing delay between pulses, as the degree of relaxation of the magnetization increases.

This method is the most reliable, provided that the recovery delay is long enough to ensure complete relaxation of the nuclear spins. This can result in excessively long total experimental times.

Modifications and improvements:

Fast inversion recovery (FIRFT) is a method in which the long recovery time t between each sequence is replaced by a shorter delay t', thus

speeding up the measurement. A dynamic steady state, which requires the elimination of the first 10 scans, must be reached before each acquisition. This method is more sensitive to pulse value misseting and carrier offset position than the standard IRFT experiment.

Saturation Recovery Fourier Transform (SRFT).

In this method, the 180° pulse of the IRFT sequence is replaced by a saturating series of 90° pulses, that is:

$$[\ (90^{o}\text{ - }d)_i\text{ - }\tau\text{ - }90^{o}\text{ - }acquire\ ]$$

Where d is a variable delay. The line intensity then follows:

$$I_\tau = I_\infty\left[1-\exp\left(-\tau/T_1\right)\right] \qquad 3.2$$

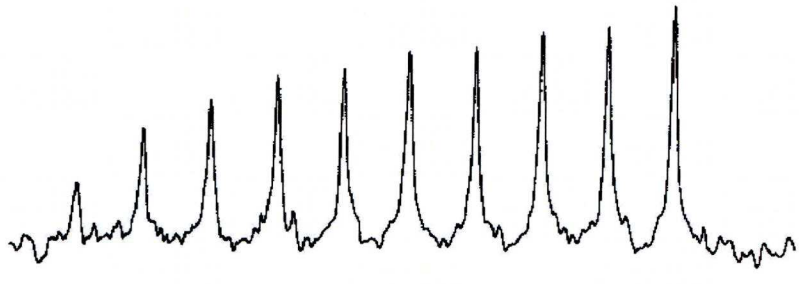

Figure 3.2.[1] SRFT-RFS method typical spectrum shape. The peak intensity increases with longer delays between pulses.

A homospoil pulse can be inserted between the 90° pulse train $(90^{o})_i$ and the variable delay τ, and again after FID acquisition to avoid echo build up or an "aperiodic pulse sequence", in which the delay between pulses in the saturating comb is varied.

This method is sensitive to pulse angle value missetting and has only half the total intensity change compared with the inversion recovery experiment. However, there is no need for a long recovery time between measurements, greatly reducing total experimental times.

3.2.2 Experimental determination of T_1's

An initial fast IRFT experiment suggested the longest T_1 in the sample was of the order of 25 seconds, the Saturation Recovery Fourier Transform method was, therefore, used for the accurate determination of T_1.

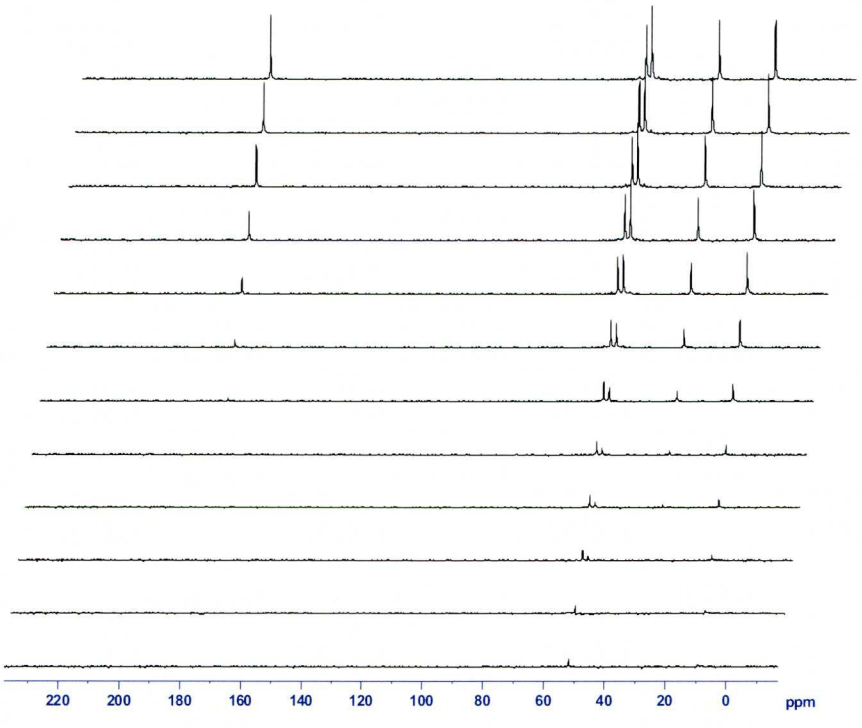

Figure 3.3. T_1 determination for solvents MeP/MeOH using the SRFT method.

A stack plot of the spectra recorded for the calculation of T_1's of the solvent species, employing the Saturation Recovery Fourier Transform method explained above, is given in Figure 3.3. The pulse delay was

changed from 0.1 to 48 seconds, taking the following values: 0.1; 0.5; 1; 2; 6; 15; 22; 30; and 48 seconds.

The intensities of the peaks increase with longer delays between pulses, when the spins are allowed to relax for longer. The exponential relation of the intensity of the carbonyl peak with time recorded during the experiment is shown in Figure 3.4.

Figure 3.4. Intensity of the C(O)OR peak as a function of relaxation time. T_1 calculation using the SRFT method.

The values of the T_1's of all the species present in the solvent mix MeP:MeOH [70:30 % wt.] are presented in Table 3.1.

	C(O)OR	OMe1	OMe2	CH_2	CH_3
T_1 (s)	35.3	5.7	10.8	8.8	4.9

Table 3.1. T_1 relaxation time constants for solvents species.

The carbonyl group in the methyl propanoate molecules had the longest T_1, 35.3 s, defining a pulse delay between pulses of approximately 3 minutes. For every liquid composition determination, 64 scans were recorded to ensure adequate signal to noise ratio. Hence, each composition measurement (64 scans with a delay between them of 3 minutes) would have taken approximately 3 hours, which is impractically long bearing in mind that measurements at least at 5 different pressures must be made for every equilibrium isotherm, which would have taken more than 15 hours. Furthermore, as the gas lines could not be left pressurized overnight, it would have been necessary to evacuate and fill the system several times for the determination of three solubility isotherms of each given gas composition in each given solvent mix. Furthermore, it was desirable to determine a complete equilibrium (3 isotherms) without manipulating the equilibrium cell.

Therefore, it was necessary to increase the relaxation rate to shorten the NMR experimental time. This can be achieved by the use of a relaxation agent, which must be sufficiently dilute in the solvent mix not to affect the solubilities of the gaseous components.

Relaxation agents are usually compounds of a paramagnetic transition metal or lanthanide ion. When unpaired electron spins are present in the sample, the nuclear spins can transfer energy to the electron spins. Since the electronic magnetic moment is about 1000 times larger than the nuclear magnetic moment, electron-nuclear dipole-dipole relaxation will be the dominant relaxation mechanism when paramagnetic species are present, making the relaxation much faster.

In this phase of the project, the standard NMR relaxation agent, $Cr(acac)_3$, was chosen. Relaxation time constants were measured using $Cr(acac)_3$ in MeP:MeOH [70:30 % wt.], pressurized with carbon monoxide and ethylene.

In a preliminary experiment using a very low concentration of $Cr(acac)_3$, 1 mg/mL, T_1*'s* for the carbons with protons bonded were found to be much longer than that of the CO carbon. Satisfactory T_1 values were obtained with a concentration of 6 g/L of $Cr(acac)_3$. The measured T_1*'s* were then in the range 1.1 to 2.1 seconds, Table 3.2. Thus, addition of 6 g/L of $Cr(acac)_3$ to the solvent mix levelled the relaxation times for all resonances to < ca. 2 s. A time delay of only 15 seconds was then necessary to ensure complete relaxation of all the spins, giving an experimental time of approximately 16 minutes for each liquid phase composition determination by NMR spectroscopy.

	CO	C(O)OR	C_2H_4	OMe1	OMe2	CH_2	CH_3
T_1 (s)	1.1	1.81	2.07	1.4	1.23	1.58	1.55

Table 3.2. T_1 relaxation time constants for solvents species with 6 g/L of $Cr(acac)_3$.

Surprisingly, the relaxation time of dissolved CO is less than that of the protonated carbons, indicating a "non-ideal" interaction between the dissolved gas and the relaxation agent. However, this interaction must be transient since neither line broadening of the resonance nor a coordination shift is observed. We have assumed this interaction does not affect the solubility of CO. The validation of the experimental system reliability, by replication of experimental solubility results obtained in other investigations (section 3.4) without the addition of any extra chemical substance (i.e. relaxation agent) to the chemical system under study justified this assumption.

3.3 The nuclear Overhauser effect- nOe

Spin-lattice relaxation rate is not the only factor that can affect the relative intensities of the NMR resonances of different sites in a molecule/system. In addition to T_1, the signal intensity is also affected by the use of proton decoupling. This affects the intensity of different ^{13}C NMR signals differently as a result of the nuclear Overhauser effect (nOe).

A description of the nOe effect can be found in most NMR texts. That given here follows that of "Modern NMR Techniques for Chemistry Research".[1].

The nOe is the change in the intensity of an NMR resonance that results when the transitions of another one are perturbed, as the total system attempts to stay at equilibrium, i.e. when the population differences of one part are forceably changed, other parts change in compensation.

Suppose the normal intensity of a resonance (i.e. that observed at thermal equilibrium and without perturbing the system) is I_0. Then if the intensity observed while saturating some other related resonance (and waiting for the new equilibrium to be established) is I, the nOe is defined as:

$$\eta_i(s) = {(I - I_0)}/{I_0} \qquad 3.3$$

where $\eta_i(s)$, the fractional increase in signal intensity at nucleus i when nucleus s is saturated, is the nOe.

Consider two spin 1/2 nuclei *i* and *s* with the same gyromagnetic ratio but different chemical shifts. This system has four energy levels: $\alpha\alpha$, $\alpha\beta$, $\beta\alpha$ and $\beta\beta$ (Figure 3.5).

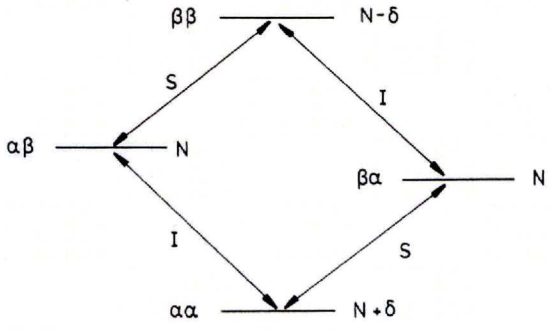

Figure 3.5. Energy levels and populations of a homonuclear AX system.[1]

Chemical shifts are generally very small in comparison with Larmour frequencies, so the transitions of each nucleus are nearly equal in energy, making the states $\alpha\beta$ and $\beta\alpha$ nearly degenerated; for clarity the energy difference between them has been greatly exaggerated in the figure. Assuming there is no J-coupling, the two transitions of nucleus *i* have equal energy, as do those of nucleus *s*; the unperturbed spectrum consists of two singlets of equal intensity.

Now suppose the total number of nuclei in the system is *4N*. If the four levels were of equal energy, they would all be equally populated and each would contain *N* nuclei. However, at equilibrium a Boltzmann distribution will be set up. For simplicity it is assumed that the difference in energy between states $\alpha\beta$ and $\beta\alpha$ is negligible, so that the states have equal

populations. The state $\alpha\alpha$, being of lower energy, will then contain an excess of nuclei, while $\beta\beta$ will be deficient by an equal amount. If the excess is called δ, the populations of the levels will be as shown in Figure 3.5. The quantities of most interest here are the population differences between states, which can be summarised as follows:

$\Delta M = 1$ *transition:* *i transitions:* $\left.\begin{matrix}\alpha\alpha - \alpha\beta \\ \beta\alpha - \beta\beta\end{matrix}\right\}....\delta$

s transitions: $\left.\begin{matrix}\alpha\alpha - \beta\alpha \\ \alpha\beta - \beta\beta\end{matrix}\right\}....\delta$

$\Delta M = 0$ *transition:* $\left.\begin{matrix}\beta\alpha - \alpha\beta\end{matrix}\right\}....0$

$\Delta M = 2$ *transition:* $\left.\begin{matrix}\alpha\alpha - \beta\beta\end{matrix}\right\}....2\delta$

The first four differences are across the normal transitions which give rise to the NMR lines, while the other two involve changes in the quantum number M (i.e. the total of the individual quantum numbers m for the two nuclei) of 0 *($\beta\alpha$–$\alpha\beta$)* or 2 *($\alpha\alpha$–$\beta\beta$)*. While transitions of this type are not observed under normal conditions (because of quantum mechanical selection rules), it cannot be safely assumed that they will not be involved in the relaxation of the system. Instead, it should be considered that if these population differences are disturbed, the system will try to restore them by any available means. This leads to several possible pathways by which the system could relax (Figure 3.6).

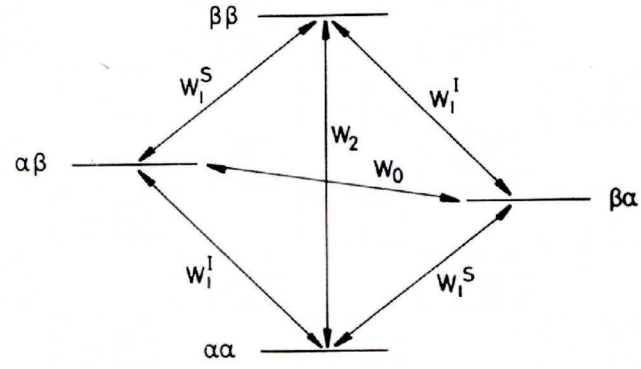

Figure 3.6. Connections between the energy levels of an AX system, which may be involved in relaxation.[1]

Now assume that the relaxation across a single transition is a first order process, it is proportional to the extent to which the population difference across the transition differs from its equilibrium value. The rate constants for the various processes are designated *W*, with a subscript to indicate the change in *M* involved, and where necessary a superscript to indicate which nucleus the transition belongs to. In the most general case (where there might be J-coupling) there is no reason to assume that the two transitions of a given nucleus relax at equal rates, but here for simplicity it is done so.

In the nOe experiment, the population differences across some transitions are forced to change, and then the signals from others are observed. Invariably the aim is to affect all the transitions of a nucleus equally, so for instance we might saturate both transitions of *s* and then observe the signals due to *i* after the new equilibrium has been established. To analyse this experiment, the possible effect of each relaxation pathway can be

estimated by considering the circumstances immediately after the saturation of *s* (Figure 3.7).

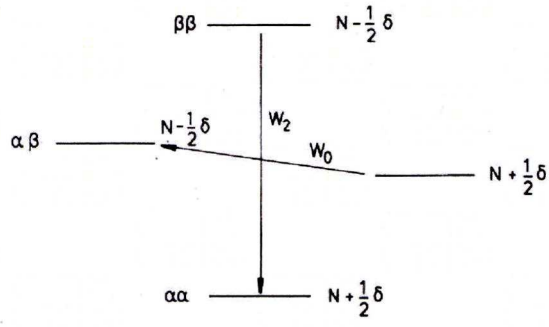

Figure 3.7. The initial direction of cross-relaxation after saturation of the *s* transitions.[1]

The new population differences are:

$\Delta M = 1$ *transitions:* *i transitions:* $\left.\begin{matrix} \alpha\alpha - \alpha\beta \\ \beta\alpha - \beta\beta \end{matrix}\right\}....\delta$

s transitions: $\left.\begin{matrix} \alpha\alpha - \beta\alpha \\ \alpha\beta - \beta\beta \end{matrix}\right\}....0$

$\Delta M = 0$ *transition:* $\beta\alpha - \alpha\beta\}....\delta$

$\Delta M = 2$ *transition:* $\alpha\alpha - \beta\beta\}....\delta$

The system as a whole is no longer at equilibrium, and the hypothesis is that it will try to adjust itself closer to that state. Consider this from the perspective of each possible relaxation pathway in turn. W_1^s, is of course,

irrelevant, because the population differences across those transitions are fixed by the saturating irradiation. The population difference across each *i* transition at equilibrium was δ, and that is still the case, so from the point of view of W_1^i no change is necessary. *If only single quantum transitions are active as relaxation pathways, saturating s does not affect the intensity of i,* or in other words there is no nOe at *i* due to irradiation of *s*.

The real interest begins when considering W_2 and W_0. The population difference between $\alpha\beta$ and $\beta\alpha$ is now δ, whereas at equilibrium it was 0. Thus W_0 acts so as to transfer population from the state $\beta\alpha$ to the state $\alpha\beta$, to try to restore a population difference of 0. This in turn increases the population of the top of one *i* transition, and decreases the population of the bottom of the other one, thereby decreasing the total intensity of signals due to *i*. This tendency is counteracted by W_1^i, since from its point of view the *i* transitions were already at equilibrium, so the net result will depend on the balance of W_1^i and W_0. *If W_0 is the dominant relaxation pathway, saturating s decreases the intensity of signals due to i*, or in other words there is a negative nOe at *i* due to irradiation at *s*.

Consider now W_2. The population difference $\alpha\alpha$–$\beta\beta$ is now δ, whereas at equilibrium it was 2δ. Thus, W_2 acts so as to transfer population from the state $\beta\beta$ to the state $\alpha\alpha$ to try to restore a population difference of 2δ. This in turn decreases the population of the top of one of the *i* transitions and increases the population of the bottom of the other one, thereby increasing

the intensity of signals due to *i*. This tendency is counteracted by W_1^i, etc. *If W_2 is the dominant relaxation pathway, then saturating s increases the intensities of signals due to i,* or in other words there is a positive nOe at *i* due to irradiation at *s*.

In our experiment, proton decoupling is used to collapse the multiplets in the ^{13}C NMR spectrum that would otherwise arise. Whenever there are groups of different active nuclei present in a molecule (i.e. CH_2), scalar coupling between them occurs. Scalar coupling arises because the nuclear magnetic moments of other NMR active nuclei (^1H) surrounding the nucleus under observation (^{13}C) produce small magnetic fields in addition to the fields due to the spectrometer and the chemical shift (variation in frequency resonance due to chemical shielding). Thus, the observed nucleus sees several fields depending on surrounding NMR active nuclei. This effect causes the peak of the observed nucleus in the spectrum to split. The effect of scalar coupling can be removed by irradiating the coupling nucleus (^1H) at its resonance frequency to induce rapid transitions between the possible orientations of the spin. Neighbouring nuclei then see a single, averaged field, rather than distinct fields, for the different possible orientations of the nuclear magnetic moment of the coupling nucleus. This is called decoupling, and simplifies the NMR spectral analysis and increases the signal to noise ratio.

However, decoupling also results in rapid reorientation of the dipolar interaction between the ^1H and ^{13}C spins and proves to be a suitable source

of fluctuating fields to stimulate longitudinal relaxation. Hence, dipolar coupling causes cross-relaxation (i.e. W_0 and W_2 processes), resulting in a nOe between the two nuclei. Now dipolar coupling is a through space effect falling off as r^6. It follows that different carbon sites will experience different nOe's due to differences in the number of, and distance to, the surrounding protons. As a result, the $^{13}C\{^1H\}$ NMR spectrum will no longer be quantitative since the intensity of the resonances is now modulated by the local proton environment. The effect of nOe on transition intensity in MeP/MeOH/CO is shown in the spectra shown in Figure 3.8, in which very different relative intensities are present depending on the detailed experimental setup as a result of nOe effects.

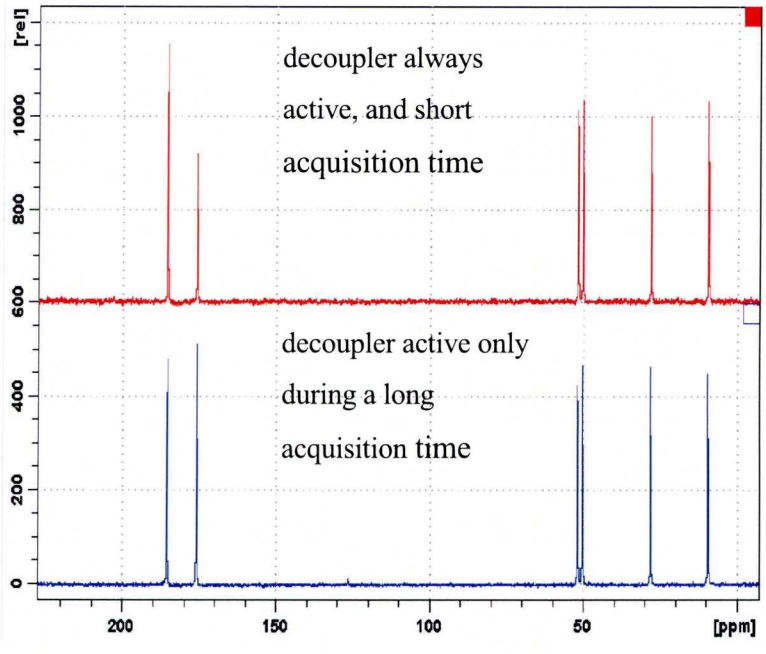

Figure 3.8. nOe on transition intensity in MeP/MeOH/CO.

Fortunately n.O.e is a dynamic effect requiring long proton irradiation times to reach maximum levels (Figure 3.8 top), its effect can, therefore, be minimized by turning the decoupler off during the recovery delay – the *inverse gated decoupling experiment* (Figure 3.8 lower trace). Thus, it is very important for these experiments using NMR to define a very good setup of the experiment and FID recording (correct parameters, appropriate pulse program, etc.), as the results can be very different from the correct values. The inverse gated decoupling scheme has been used throughout this thesis.

3.4 Solubilities of CO and ethylene in methanol

With the experimental design established, and the NMR experiment setup well defined, the experimental methodology can be validated by replicating some solubility measurements previously reported in the literature.

The literature data chosen to validate the experimental system are: the solubility of C_2H_4 in MeOH;[2] and the solubility of CO in MeOH.[3, 4] The choice of the literature data was based on the chemical resemblance to the system under study, the solubilities of carbon monoxide and ethylene in methanol were the most similar chemical systems found in the literature. The accuracy of the solubility results quoted in the literature was based on previous experimental determinations by other authors; results were reproduced within a 5% deviation.

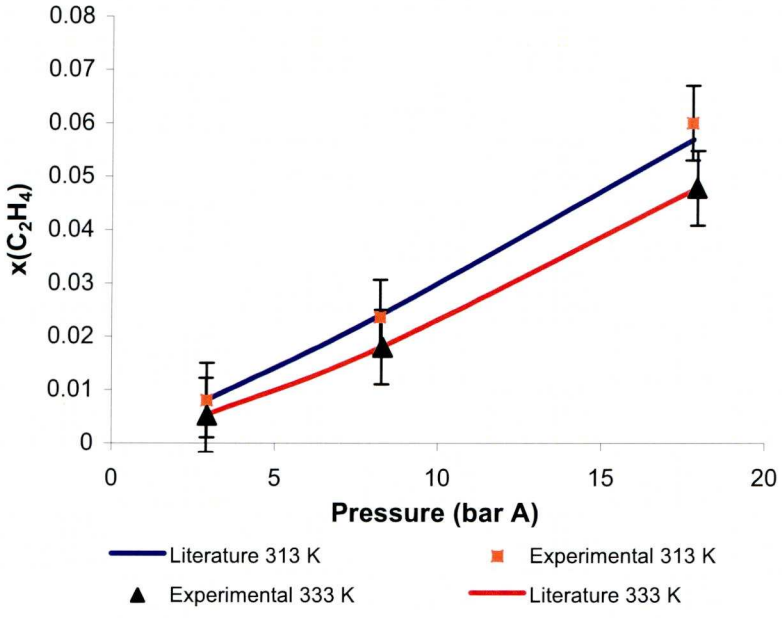

Figure 3.9. Experimentally determined C_2H_4 solubiltiy in MeOH compared with literature reported values.

The comparison between the literature results and those obtained experimentally in our experimental system for the solubility of ethylene in methanol are presented in Figure 3.9 as two isotherms. The error bars represent the random error calculated with the standard deviation as explained in Chapter 2. This random error arises from possible slight variations in the equilibrium condition during measurements, FID processing methods applied, and peak integration intervals chosen.

A very good fit of the experimental values compared with the literature is obtained. This good comparison proves the system reliability for the ethylene solubility determination.

Experimental data for the solubility of CO in MeOH have been found in the literature, data for different conditions of pressure and temperature are reported, but not as composition vs. pressure isotherms. Because of this, the comparison is presented as the literature composition versus the experimental composition at individual (P, T) data points, Figure 3.10.

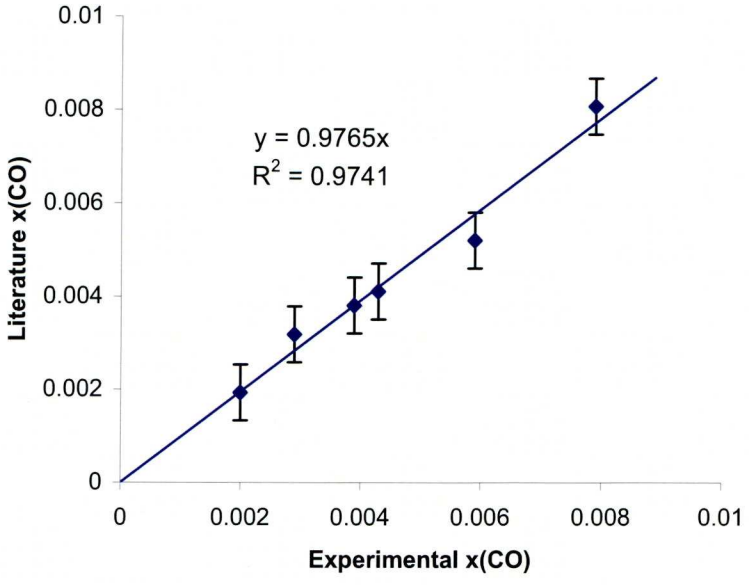

Figure 3.10. Experimentally determined CO solubilty in MeOH compared with literature reported values.

A linear relationship is found with the slope of the line, 0.98, very close to 1, i.e. the result obtained is again satisfactory, validating the experimental design proposed.

Thus, the new experimental NMR system for the determination of solution composition has been validated by comparison with experimental data from the literature. The solubility of CO in dichloromethane[5] has also been

replicated within a 10% deviation from literature data, further validating the good performance of the experimental design for measuring solubilities of gases in liquid solvents.

3.5. Conclusion

A novel experimental system for the determination of gas solubilities using HPNMR has been accurately designed and setup. The use of a concentration of 6 mg/mL of $Cr(acac)_3$ dissolved in the solvent mix as relaxation agent is needed to shorten the NMR experimental time. The inverse gated decoupling scheme is used in the NMR measurements to reduce the nOe. The HPNMR experimental system reliability has been checked by comparison with results previously reported in the literature. The validation results obtained are successful, demonstrating the reliability of the new NMR bubble column gas flow system designed.

3.6 References

(1) Derome, A. E. Modern *NMR Techniques for Chemistry Research.* Pergamon Press, Oxford, 1987.

(2) Konobeev, B. I.; Lyapin, V. V. Solubility of ethylene and propylene in organic solvents. *Khim. Prom. Ukr.* **1967**, *43*, 144.

(3) Liu, Q.; Takemura, F.; Yabe, A. Solubility and diffusivity of carbon monoxide in liquid methanol. *J. Chem. Eng. Data.* **1996**, *41 (3)*, 589.

(4) Tonner, S. P.; Wainwright, M. S.; Trimm, D. L. Solubility of carbon monoxide in alcohols. *J. Chem. Eng. Data.* **1983**, *28*, 59.

(5) Jonasson, A.; Persson, O.; Rasmussen, P. Vapor-liquid equilibria of systems containing dichloromethane and gaseous components. *J. Chem. Eng. Data.* **2000**, *45 (4)*, 642.

Chapter 4

Gas solubilities determination

Chapter 4: Gas Solubilities Determination

4.1 Introduction

Gas solubilities have been determined experimentally for many years because of the interest and importance in chemical processes ruled by a vapour-liquid equilibrium such as extraction, absorption, reactions under compressed gas, etc. It has been shown in Chapter 1 how the solubilities of gases in liquids are defined and understood from vapour-liquid equilibrium thermodynamics. The solubilities of the single gaseous components of interest in this work, carbon monoxide (CO) and ethylene (C_2H_4), have been previously determined in various solvents[1, 2, 3, 4, 7] but not in a mixture of methanol (MeOH) and methyl propanoate (MeP), nor have the solubilities of mixtures of these gases in single or mixed solvent been measured. These experimental measurements are crucial for the validation of the thermodynamic model previously described (Chapter 1). From what is known, thermodynamic models are very good and reliable in many cases but not always, because even though they can predict intermolecular interactions between different components in each phase, in some cases these interactions are far from ideal and the model does not include their effects on thermodynamic properties and vapour-liquid equilibrium calculations.

Previous experiments[5] measuring the solubility of carbon monoxide in a mixture of MeOH/MeP were performed using a '*static system*' consisting of a closed sapphire tube described in Chapter 2. In this system the solvents are charged in a sapphire tube, which is then evacuated at liquid nitrogen temperature, pressurized with ^{13}CO to the desired pressure, and finally allowed to equilibrate in a thermostatic heating water bath to the desired temperature while mechanical agitation is applied. Once the equilibrium condition is reached, 15 minutes, the sapphire tube is introduced in the NMR magnet, and the $^{13}C\{^{1}H\}$ NMR spectrum is recorded.

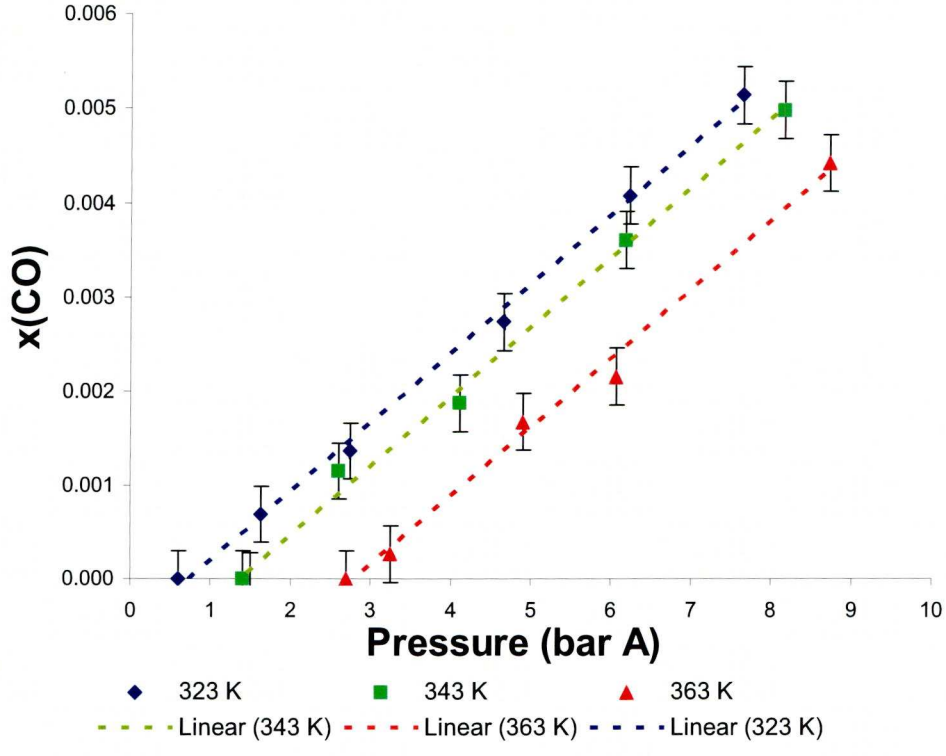

Figure 4.1. Solubility of CO in liquid solvent MeP/MeOH [70:30 % wt.] experimentally measured in the sapphire tube 'static' experimental system.

Figure 4.1 shows the solubility of CO at temperatures 323 K, 343 K, and 363 K, and total system pressure (due to CO gas and the solvent vapour pressure) ranging from 0 to 10 barA. Carbon monoxide solubility shows linear behaviour with pressure, following Henry's law. All three solubility lines cross the system pressure axis (zero composition of CO in the liquid phase) close to the vapour pressure values of the solvent MeP:MeOH [70:30% wt.] at the three different temperatures (0.62 ± 0.01 bar at 323 K; 1.35 ± 0.02 bar at 343 K; 2.68 ± 0.04 bar at 363 K). These vapour pressures have been experimentally determined, thermodynamically calculated using Antoine's equation in Aspen Plus, and checked with literature values.[6, 7]

However, given the limitations of this experimental system (Chapter 2), a more reliable experimental system for the purpose of the determination of gas solubilities in equilibrium as well as in working catalytic reactions, was developed as described in Chapter 2. This new design has been applied to the determination of single and mixed carbon monoxide and ethylene gas solubilities in a liquid mixture of MeP:MeOH (70:30 % wt.), and the results obtained are described in this chapter.

The specific solvent composition of MeP:MeOH (70:30 % wt.) is studied because it is the composition of the feed stream to the reactor for the methoxycarbonylation of ethylene in the first stage of the Alpha Process. This feed stream to the homogeneous catalytic reactor is the head product

stream from a distillation column in which the reactor product stream, concentrated in MeP, is split in a light stream formed by the azeotrope [MeP:MeOH (70:30 % wt.)] which is recirculated to the reactor, and heavy stream of pure MeP.

4.2 Experimental: Procedures and materials

The experimental methods used in this chapter are the same as those described in Chapter 2. The 'continuous recirculation bubbling gas flow system' is used for the determination of the solubilities of single gas and mixed carbon monoxide/ethylene in a mixture of methyl propanoate and methanol MeP:MeOH [70:30% wt.]. A mixture of methyl propanoate (Aldrich, >99% pure) and methanol (Aldrich >99% pure) is used as liquid solvent. A cylinder containing ^{13}CO (CKGas, >99% pure), and another one filled with ethylene (BOC gases, >99% pure) are used as feed gases. Depending on the gas solubility to be determined, one of them is attached to the feed line so that the system can be filled and pressurized with the gas of interest at any time.

For the determination of the solubility of mixtures of these gases, a feed gas cylinder of the desired composition was made up. For that, three cylinders, one containing ^{13}CO, another containing C_2H_4, and one empty, are attached to a high pressure line. This line is designed so that one end is connected to a vacuum pump, so the line can be evacuated before mixing the gases of interest in the empty cylinder, and the lines from the carbon monoxide and ethylene cylinders mix in a "T" connection, leading the gas to the empty cylinder where finally the desired gas mixture will be contained (Figure 4.2). Because the pressure in the cylinder must be measured and controlled, a valve (HiP) is introduced between the "T"

connection and a pressure transducer (Druck) situated close to the empty/gas mixture cylinder head. It is thus possible to monitor and control (allowing or not the gas to pass through the valve) the pressure in the cylinder and so control the quantity/composition of each gaseous component. The molar composition of the mixture is considered to be proportional to the partial pressure of each gas in the cylinder, assuming

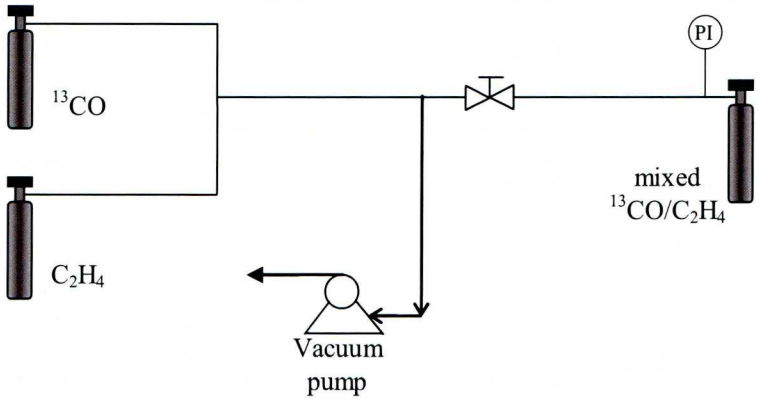

Figure 4.2: Mixed gas ($^{13}CO/C_2H_4$) cylinder making.

both gases are ideal. For example, if a desired mixture of molar composition of 80% in C_2H_4 and 20% in ^{13}CO, and a total pressure in the cylinder of 40 bar is required, the procedure would be: 1) evacuate the lines and empty gas mixture cylinder; 2) introduce ^{13}CO and pressurize the cylinder to 8 bar (this is the partial pressure of ^{13}CO in the cylinder, so that the partial pressure of ethylene should be four times this, that is 32 bar, and the sum of them is the total 40 bar pressure desired in the cylinder); 3) close the valve allowing the gas to be introduced into the empty/gas

mixture cylinder, and evacuate the lines from the "T" connection to the feed cylinders; 4) open the C_2H_4 cylinder and allow a small flow, to avoid temperature rise, of gas through the valve until the pressure in the gas mixture cylinder reaches the desired final pressure, 40 bar; and finally, 5) close the cylinders and evacuate the lines. The final composition of the gas mixture in the cylinder is then measured by Gas Chromatography (GC) so the exact composition of the feed gas introduced in the system is known.

The experimental procedure for the solubility (vapour-liquid equilibrium) determination by NMR was that explained in Chapter 2, which is basically to introduce the solvent mixture MeP:MeOH (70:30% wt.) into the sapphire equilibrium cell; evacuate all the lines of the system cooling down the equilibrium cell with liquid nitrogen so that the solvents were not evaporated; introduce 1-2 bar of the desired gas to be dissolved in the solvents; remove the cooling liquid nitrogen so the equilibrium cell returned to room temperature. Once all the chemical components were in the system, solvent in the cell and gas filling the lines, the equilibrium cell was placed in the NMR magnet (Bruker AMX II-200WB MHz), the magnetic field shimmed, and then the desired condition of pressure and temperature achieved by introducing feed gas and heating the equilibrium cell with a hot air current. The pump was started so that the gas flowed (at 12 mL/min) through the recirculation loop and bubbled in the liquid continuously. The equilibrium condition was usually reached in 2-3

minutes; equilibrium was known to be achieved by pressure stabilization. Then the $^{13}C\{^{1}H\}$ NMR spectrum was recorded, taking 18 minutes for each measurement, and the composition of the liquid phase calculated directly from the peak areas in the NMR spectrum. After one equilibrium condition has been measured, this condition was changed, usually starting from a low pressure (3-4 bar), and changing the temperature from high to low and recording the actual pressure in the system. Once the equilibrium condition at each temperature in the desired range have been measured, additional feed gas was introduced into the equilibrium cell increasing the pressure keeping the temperature constant at that of the last experiment (low in this case). A second series of measurements was then made, raising the temperature and recording the system pressure that resulted. In this way a series of composition vs. pressure isotherms could be obtained. It was important that at the usual starting condition of high temperature and low pressure, the low pressure was higher than the vapour pressure of the solvents at that temperature, to ensure that the solvent did not evaporate. In order to obtain a good resolution in the NMR spectrum it was essential to have the maximum quantity of solvent in the equilibrium cell, i.e. evaporation must be avoided at all times. A condenser was designed with this purpose as explained in Chapter 2.

From the spectra recorded the composition of each component in the liquid phase was calculated directly from the area under the peak representing

each kind of carbon atom present. The composition in the liquid phase of the gaseous components defined the solubility of each gas in the solvent. This solubility was represented as a function of total pressure of the system or partial pressure of the gaseous component and system (equilibrium cell) temperature.

Henry's law should provide an excellent approximation of the equilibrium composition in the liquid phase of the gaseous components of interest, CO and C_2H_4, as these components were dilute (low composition) in the liquid solvent and the system temperature was well below the critical temperature of the solvent. Recalling the equation for defining the Henry's coefficient of a component in a vapour-liquid equilibrium:

$$p_i = H_i x_i \qquad 4.1$$

Where, H_i is the Henry's coefficient for component i present in both gas and liquid phases in equilibrium. Henry's coefficient, which depends only on temperature, defines the solubility of a component in a liquid phase as a function of partial pressure and can be calculated from the slope of the line representing the partial pressure of the component of interest versus its mole fraction in the liquid phase. The partial pressures of carbon monoxide and ethylene can be obtained from Eq. 4.2, which defines the equilibrium from the equality of the fugacity of a component in the gas phase with the fugacity of the component in the liquid phase.

$$p_i = y_i P = x_i p_i^o \gamma_i \qquad 4.2$$

This equation is an approximation of the combination of equations 1.15 and 1.16 because it neglects corrections in the gas phase and the Poynting factor; however, it is common practice to apply it for the calculation of partial pressures.[8] Hence, the partial pressures of MeOH and MeP in the gas phase can be obtained measuring the composition of the liquid phase by NMR, and calculating the vapour pressures and activity coefficients of methanol and methyl propanoate in the range of temperatures under study (323 K to 373 K). These properties have been calculated using the thermodynamic model defined in Aspen Plus, using the UNIQUAC[9, 10] equation for the calculation of the liquid phase activity coefficients and Antoine's equation for the vapour pressure prediction for a liquid mixture with an initial composition of 70% wt. in methyl propanoate and 30% wt. in methanol.

The total pressure of the system is experimentally measured by calibrated pressure transducers. So the difference between the total pressure and the partial pressure of the solvent components, MeOH and MeP, is the partial pressure of the gaseous component.

Values obtained applying equation 4.2 are an approximation of the real values of the partial pressures as the activity coefficients (Table 4.1) are a function not only of temperature, but also of composition (Eq 1.25). The

Methanol		
Temperature	*Vapour Pressure*	*Activity Coefficient*
323 K	0.55	1.30
343 K	1.25	1.28
363 K	2.54	1.26
373 K	3.53	1.25
Methyl Propanoate		
Temperature	*Vapour Pressure*	*Activity Coefficient*
323 K	0.35	1.34
343 K	0.73	1.31
363 K	1.41	1.27
373 K	1.89	1.26

Table 4.1: Vapour pressures and activity coefficients, calculated with Aspen Plus, of MeOH and MeP at the solvent composition (MeP:MeOH) in equilibrium at 10 bar and each temperature studied. (Vapour pressures are only function of temperature).

composition in the liquid phase is always close to 70% wt. of MeP and 30% wt. of MeOH, but deviations occur in experiments because of changes in pressure, temperature, and solubility of gases. Even without the presence of gaseous components (CO, C_2H_4), the composition of liquid (x_{MeOH}, x_{MeP}) and gas (y_{MeOH}, y_{MeP}) phases in equilibrium changes with pressure and temperature conditions. The compositions used for the calculation of the activity coefficients of mixed MeOH and MeP at each temperature, are those of equilibrium of the solvent (MeP:MeOH) at the average pressure in the range of working pressures (0-20 bar), 10 bar.

The purpose of these experiments is to validate the thermodynamic model applied, so that once it is validated it can be used with more accurate and complex thermodynamic relations for the determination of Henry's coefficients. Thus, the validation of the thermodynamic model is made by evaluation of theoretical equilibrium compositions obtained with the model compared with experimental solubility results.

		γ_{MeOH}		γ_{MeP}		γ_{CO}		γ_{C2H4}	
P (bar A)	**Feed gas**	**323 K**	**373 K**	**323 K**	**373 K**	**323 K**	**373 K**	**323 K**	**373 K**
20	**CO**	1.304	1.262	1.338	1.242	0.64	0.66	-	-
	C_2H_4	1.532	1.356	1.125	1.15	-	-	1.808	1.809
4	**CO**	1.308	1.295	1.333	1.21	0.632	0.652	-	-
	C_2H_4	1.344	1.298	1.292	1.207	-	-	1.914	1.753
20	**C_2H_4:CO 4:1**	1.465	1.333	1.177	1.17	0.619	0.653	1.846	1.823
4	**C_2H_4:CO 4:1**	1.337	1.297	1.301	1.207	0.629	0.652	1.92	1.753

Table 4.2: Activity coefficients in MeP:MeOH [70:30 % wt,] calculated in Aspen Plus at different conditions of composition, temperature, and pressure.

The activity coefficients of MeP and MeOH were considered constant with temperature for the calculations of the partial pressures from experimental compositions of the liquid phase; however, inspection of the values given in Table 4.2 reveals that these coefficients are not precisely constant at different pressures and compositions of the liquid phase; at higher pressures there is an increase in the composition of gaseous components dissolved. Thus, by definition of Henry's law (for supercritical components

at infinite dilution, page 38) it is expected that solubilities deviate from Henry's law when the dissolved gas in the liquid phase is not dilute. Similarly the thermodynamic model, which calculates the activity coefficient of each component at any given condition of temperature, pressure and composition, calculates equilibrium compositions of the liquid phase with deviations from Henry's law at higher pressures. Differences between the experimentally determined Henry's coefficients and the modelled values are expected because the experimental values were calculated considering the MeOH and MeP activity coefficients to be constant with temperature, meanwhile the thermodynamic model accounts for deviations in MeOH and MeP compositions at different equilibrium conditions, and furthermore it applies the correction of the activity coefficient at infinite dilution as shown in equations 1.28 and 1.29. However, as said before, comparison of Henry's coefficients obtained with the less complex procedure using equation 4.2 and experimentally determined compositions, with the model results, will allow for the validation of the more accurate calculation performed with the thermodynamic model as far as they agree within a 15% deviation.

It is interesting to note that the activity coefficient is less than unity for carbon monoxide, but it is greater than unity for ethylene. From the definition of activity coefficient (Eq. 4.3) it is known that it describes deviations from ideality in liquid solutions. If it is higher than unity, as

happens for ethylene, the fugacity of the component in solution is higher than it would be in an ideal solution; otherwise the fugacity of the component in the real solution is lower than that for the ideal case.

$$\gamma_i = \frac{f_i}{x_i f_{i,pure}} \qquad 4.3$$

The fugacity can be interpreted as the tendency to vaporize. If compounds vaporize more than in an ideal solution, as happens for ethylene, then the average distance between different molecules in solution increases with respect to an ideal solution, indicating repulsion between unlike molecules. Hence, an activity coefficient higher than unity physically means repulsion forces between molecules, and therefore, solubility decreases with deviations from ideality; meanwhile for values lower than unity, attractive forces occur, and the less ideal is the solution the more attractive are the forces, and the component becomes more soluble.

The equilibrium between phases is defined by the equality of the fugacity of a component in each phase, so the fugacity for each component must be the same in both the liquid and gas phases. Deviations from ideality in the gas phase for ethylene and carbon monoxide are much less than in the liquid phase, so the fugacity in the gas phase can be considered equal to the partial pressure of each component (fugacity coefficient = 1). Now, ethylene shows positive deviations ($\gamma > 1$) from ideality in the liquid phase

and consequently its solubility is lower than it would be in an ideal solution.

$$f_i^g = p_i = f_i^l = \gamma_i f_i^{pure} x_i \qquad 4.4$$

Carbon monoxide shows the opposite deviation from ideality, the activity coefficient is lower than unity, hence its solubility is higher than it would be in an ideal solution of MeP:MeOH.

An interesting point to note is that the fugacity of the pure component in the liquid phase will affect the solubility, as seen in Eq. 4.4, hence for components of high fugacity, low solubility should be observed. This gives an initial indication of the low solubility of carbon monoxide, for which the fugacity at 10 bar total pressure and 323 K is 591.7, meanwhile for ethylene under the same conditions fugacity is 38.6 (values computed using the thermodynamic model).

For the validation of the thermodynamic model calculations of the gas phase, a set of experimental determinations of compositions of the gas phase in equilibrium were performed using the experimental system and analysing the composition of the recirculating gas phase by Gas Chromatography, as described in Chapter2. The experimental system is basically the same as that used for the determination of the composition of the liquid phase, but the analytical method is changed. These experiments

provide data for checking that the thermodynamic model applied accurately predicts the gas phase in equilibrium with the solvent.

4.3. Single gas solubility results

The separate solubilities of carbon monoxide, and ethylene, were determined in the solvent mixture MeP:MeOH (70:30% wt.) at temperatures 323 K, 343 K, and 373 K and in the pressure range 0 - 20 barA (absolute pressure of the system).

4.3.1. Carbon monoxide solubility in Methyl Propanoate/Methanol

In this vapour-liquid equilibrium experimental determination, the gas phase was initially formed of pure carbon monoxide (^{13}C labelled due to NMR detection requirements), and the liquid phase was a mixture of MeP:MeOH (70:30% wt.). The amount of carbon monoxide dissolved in the solvent mix increases with the total pressure (barA) of system, as expected since the system is pressurized by the addition of carbon monoxide gas. The quantity of carbon monoxide dissolved also increases at lower temperatures at constant total pressure of the system (the behaviour of gas solubility with temperature must be evaluated at constant partial pressure of the gaseous component in the gas phase, as shown later). This difference in solubility with temperature is greater at low total pressures, while as the total pressure increases the solubility becomes less affected by temperature. This effect is evidenced by a difference in the slopes of the solubility isotherms, the slope of the isotherm increasing with temperature, see Figure 4.3. As the amount of dissolved carbon monoxide decreases, the

solubility lines tend to the value of the vapour pressure of the pure mixed solvent at each different temperature.

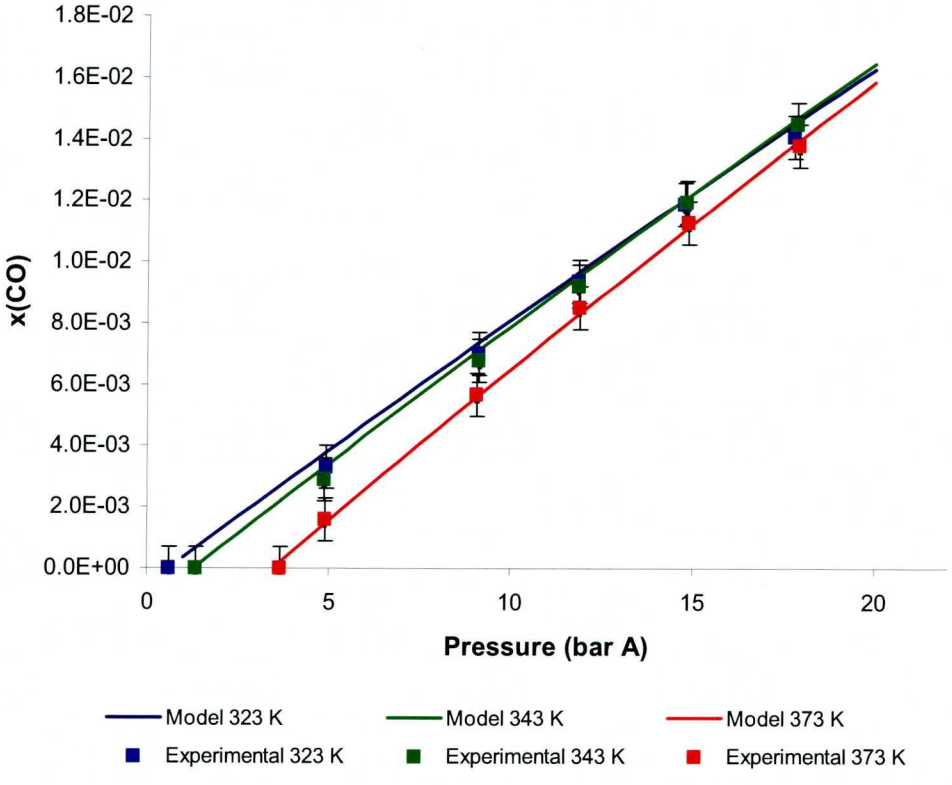

Figure 4.3: Solubility of CO in MeP:MeOH (70:30% wt.) as a function of total pressure of the system (barA).

The solubilities of each gas have also been modelled using the thermodynamic model. The model reproduces the experimental results well, indicating that the thermodynamic model used (explained in detail in Appendix A) is capable of accurately predicting the solubilities of carbon monoxide in the mixed solvent MeP:MeOH (70:30 % wt.).

Comparing these results with those obtained with the sapphire tube 'static' system (Figure 4.4), in which a much smaller quantity of isotopically

enriched gas is fed into the system and neither flowing nor bubbling of gas into the liquid phase is used to improve mixing, reveals that the quantity of carbon monoxide dissolved is much greater using the new system. This could be due to equilibrium not being reached even after 15 minutes of vigorous agitation. By contrast, equilibrium is reached rapidly on bubbling the gas through the solution, and maintained during the NMR measurement.

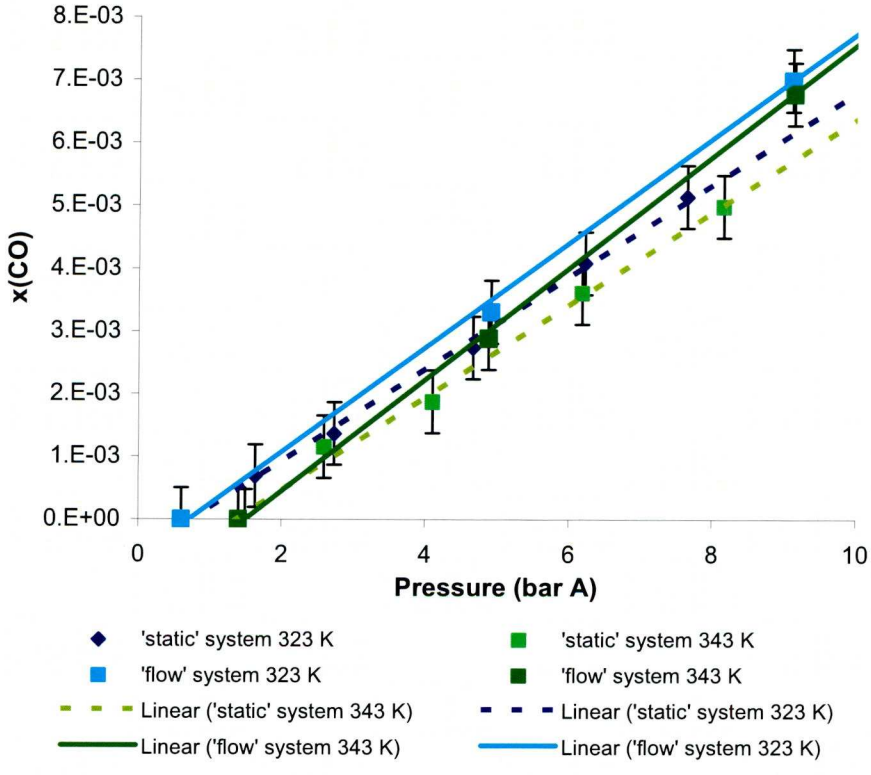

Figure 4.4: Comparison of 'gas flowing and bubbling' system with 'static' sapphire tube system.

Lines in Figure 4.4 are linear trend lines fitted to the scatter experimental points.

Determination of CO Henry's coefficient

The increase in the slopes of the solubility lines noted above reflects how the solubility of carbon monoxide increases with temperature. In principle, Henry's coefficients for each temperature can be determined from the inverse slopes of plots of x(CO) vs. partial pressure of CO, (Eq 1.30) shown in Figure 4.5. Partial pressures of CO were calculated according to procedure explained in pages 142-145. Note that equation 4.2, for the calculation of partial pressures of MeOH and MeP, does not apply for supercritical light dissolved gases (page 38), as is CO in this case.

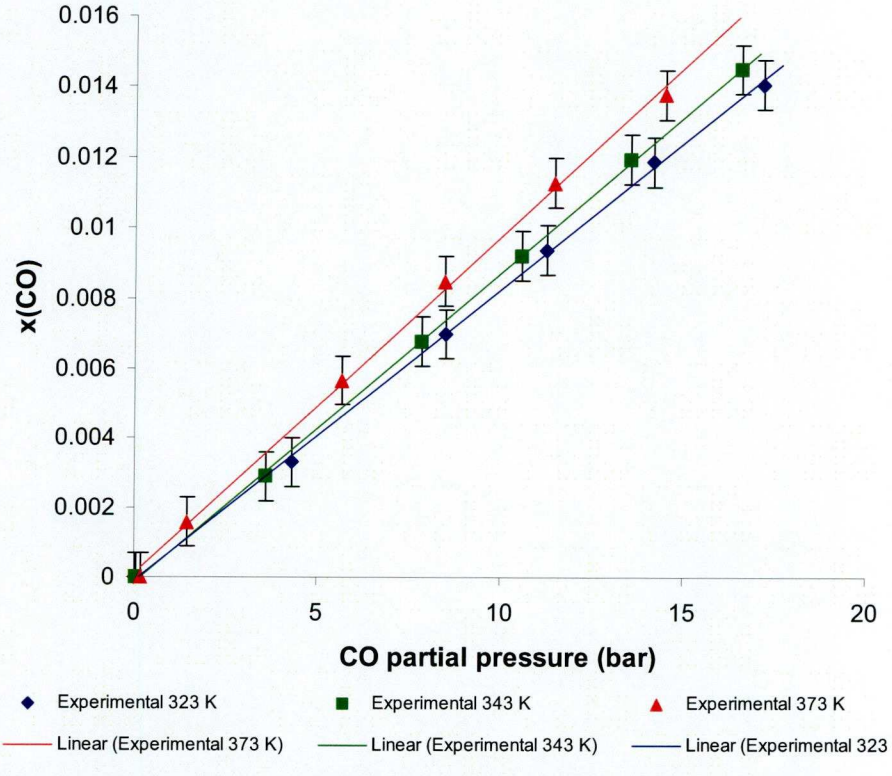

Figure 4.5: CO solubility in MeP:MeOH (70:30% wt.) as a function of its partial pressure.

The solubility of carbon monoxide in a mixture of methyl propanoate (70%wt.) and methanol (30% wt.) has been shown to increase with temperature, i.e. the Henry's coefficient of carbon monoxide in this system is higher at low temperatures, Table 4.3.

T (K)	Experimental H_{CO}	Model H_{CO}
323	1212 ± 121	1122.3
343	1145 ± 114	1049.3
373	1003 ± 100	934.6

Table 4.3: Henry's coefficient of CO in solvent MeP:MeOH (70:30% wt.) at different temperatures.

Table 4.3 shows that the values for the Henry's constant calculated from experimental data are always higher, ca. 10%, than those calculated by the thermodynamic model. This consistent deviation is explained by the fact that the calculation of partial pressures, used for the estimation of the experimental Henry's constants, neglects the correction of the activity coefficient at infinite dilution, and considers constant activity coefficients at each temperature as explained in page 146.

4.3.2 Ethylene solubility in Methyl Propanoate/Methanol

The solubility of ethylene (C_2H_4) in a mixture of MeP:MeOH (70:30% wt.) was next experimentally determined and thermodynamically modelled in

the range of absolute system pressures 0 - 20 bar, at temperatures 323 K, 343 K, and 373 K, and the Henry's coefficients calculated.

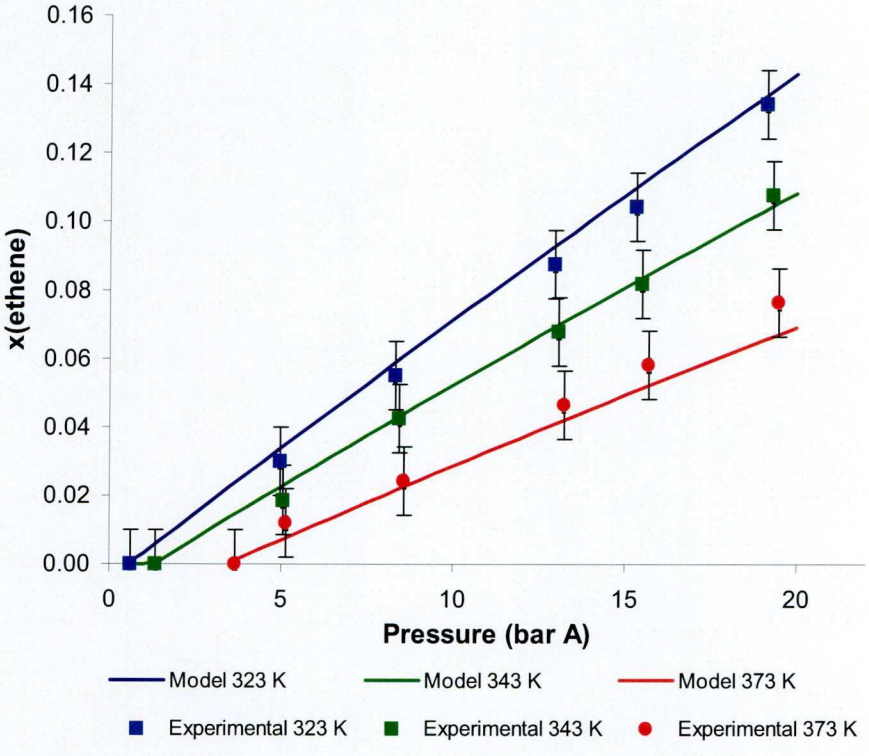

Figure 4.6: Solubility of C_2H_4 in MeP:MeOH (70:30% wt.) as a function of total pressure of the system (barA).

The solubility of ethylene, Figure 4.6, clearly decreases with increasing temperature; the temperature effect is more marked at higher pressures (difference in slopes). The points at zero solubility correspond with the vapour pressure of the liquid solvents at each temperature. The thermodynamic model calculations reproduced quite well the experimental observations. The experimental error is higher for the ethylene data than for the carbon monoxide because the former is not enriched in ^{13}C, so even

though the absolute values of its solubility are higher, the NMR spectrum peak intensity is much lower than that for the CO (which is amplified 100 times because of enrichment), which means that deviations in the peak intensity values have greater impact on composition.

Determination of C_2H_4 Henry's coefficient

Inspection of the solubility lines versus the ethylene partial pressure in the gas phase shows how the slope of the solubility line increases with decreasing temperature, so the Henry's constant increases, and the solubility decreases. This behaviour is the reverse of that observed for carbon monoxide, being that more usual for the solubility of a gas in a liquid.

The value for the Henry's constant of ethylene in MeP:MeOH (70:30 % wt.) (Table 4.4) is of the order of nine times smaller than that for carbon monoxide at 323 K; about seven times smaller at 343 K; and approximately five times at 373 K. This means that ethylene is nine times more soluble than carbon monoxide at 323 K, and this difference gets smaller with increasing temperature because the ethylene solubility decreases with temperature while that of carbon monoxide increases.

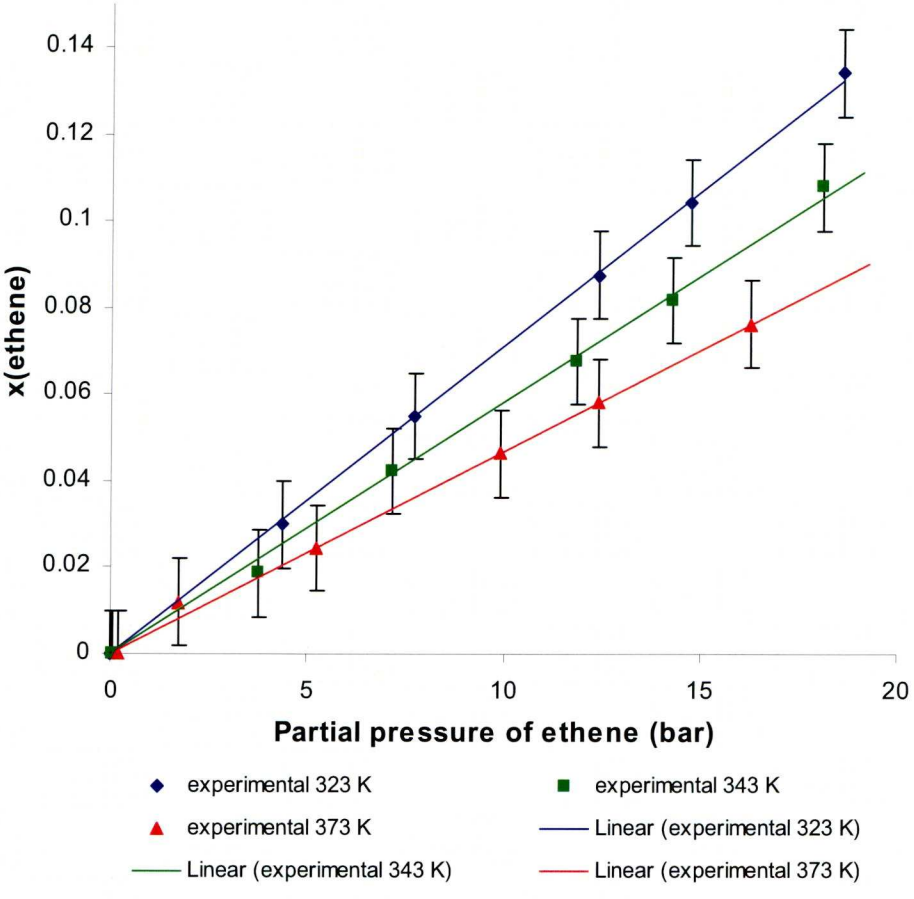

Figure 4.7: Solubility of C2H4 in MeP:MeOH (70:30% wt.) as a function of partial pressure of ethylene (bar).

T (K)	Experimental $H_{ethylene}$	Model $H_{ethylene}$
323	140.3 ± 10	127.4
343	171.7 ± 12	157.5
373	213 ± 15	211.4

Table 4.4: Henry's coefficient of ethylene in solvent MeP:MeOH (70:30% wt.) at different temperatures.

Comparing the experimental values of solubility with those calculated by the thermodynamic model, it can be concluded that the model reproduces

the solubility of single gases in mixed solvents well. There is again consistency in the deviation of the experimentally calculated Henry's constants with respect to the modelled values due to the calculation method of the partial pressure used for the determination of the experimental Henry's constant.

4.3.3. Discussion: Temperature effect on solubility

It is experimentally observed that temperature has a different effect on the solubilities of CO and ethylene.

Carbon monoxide shows atypical behaviour for the solubility of a gas with temperature, which is usually expected to decrease on increasing the temperature as stated in many elementary textbooks on chemistry. However, this is not a valid generalisation about the behaviour of gas solubility with temperature. As shown elsewhere[8], Henry's coefficients change differently with temperature in different binary systems; these changes depend not only on the temperature but also on the particular chemical properties of the system. Thus, using the Gibbs-Helmholtz equation and applying some thermodynamic relations[11], the temperature derivative of the solubility can be obtained as a function of either the partial molar entropy or the partial molar enthalpy of the gaseous solute in the liquid solvent.[12] Assuming that the solvent is essentially non-volatile

and the activity coefficient of the solute is independent of the composition due to its low solubility, we obtain:

$$\left(\frac{\partial \ln x_2}{\partial \ln T}\right)_P = \frac{\Delta \bar{s}_2}{R} \tag{4.5}$$

$$\left(\frac{\partial \ln x_2}{\partial 1/T}\right)_P = -\frac{\Delta \bar{h}_2}{R} \tag{4.6}$$

The derivation of equations 4.5 and 4.6 is shown in Appendix C.

Where x_2 is the mole fraction of the gas solute in the liquid phase and

$$\Delta \bar{s}_2 \equiv \bar{s}_2^L - s_2^G = \left(s_2^L - s_2^G\right) + \left(\bar{s}_2^L - s_2^L\right) \tag{4.7}$$

$$\Delta \bar{h}_2 \equiv \bar{h}_2^L - h_2^G = \left(h_2^L - h_2^G\right) + \left(\bar{h}_2^L - h_2^L\right) \tag{4.8}$$

Where, s_2^G and h_2^G are the partial molar entropy and enthalpy of pure gas component 2; s_2^L and h_2^L are the partial molar entropy and enthalpy of pure liquid component 2; $\bar{s}_2^L$ and $\bar{h}_2^L$ are the partial molar entropy and partial molar enthalpy of component 2 dissolved in the liquid phase; all of them at system temperature and pressure.

Considering first Eq. 4.5 it can be seen that when the variation of the partial molar entropy of solution of the solute is positive the solubility of gaseous component 2 increases with temperature; otherwise, it decreases.

This variation in partial molar entropy can be expressed by Eq. 4.7, where the first term represents the entropy of change of state of pure component 2; and the second term the partial molar entropy of mixing the condensed solute with the solvent. The first term, entropy of change of state, is expected to be negative because the entropy of a gas phase component is higher than that of the same material in liquid state at the same temperature. For carbon monoxide the variation in entropy due to change of state, from gas to liquid, at 223 K (p^0 = 96.73 bar) is -0.5804 kJ/kg·K, whilst for ethylene it is -1.694 kJ/kg·K at 223 K (p^0 = 10.61 bar) (values calculated applying the thermodynamic model in Aspen Plus). Considering ideal entropy of mixing of the two liquids (the solvent 1, and the condensed solute 2) the entropy of mixing both liquids using excess functions relations (Chapter 2) can be expressed as:

$$\bar{s}_2^L - s_2^L = -R \ln x_2 \qquad 4.9$$

The value for this entropy change is always positive since $x_2 < 1$, and the smaller the solubility the greater its value. Therefore, for very low solubility gases, the second term of Eq. 4.7 is large and positive; when the magnitude of this term is larger than that of the first term (negative value) the overall entropy change on dissolution $\Delta\bar{s}_2$ is positive and the solubility will increase with the temperature, as happens for carbon monoxide in the liquid mixture MeP:MeOH (70:30% wt.). Thus the solubility of carbon

monoxide has been shown to be very low, x_{CO} in MeP:MeOH (70:30 % wt.) under the conditions at which the entropy of change of state has been evaluated (223 K, and 96.73 bar) is 0.056. Calculating the entropy of mixing applying Eq. 4.9 the value obtained for this entropy change is 0.8541 kJ/kg·K, which is greater in magnitude than the negative value of the entropy of condensation of pure carbon monoxide at those conditions (-0.5804 kJ/kg·K) (Table 4.5). Hence, the change in entropy of carbon monoxide due to the solution of the gas into the liquid solvents under study is positive, and so the solubility increases with temperature as experimentally observed. These calculations were done at the temperature condition of 223 K because the temperatures of work (323 – 373 K) are too high for the model to properly resolve the vapour pressure of carbon monoxide. Wilhelm and Battino[13] report relations of enthalpies and entropies of solution with solubilities of different gases in different solvents, including that of carbon monoxide in pure methanol, and report a positive value for the total change of entropy of solution (0.15 kJ K^{-1} kg^{-1}), i.e. the solubility of carbon monoxide in methanol exhibits the same behaviour as observed here in a mixture MeP:MeOH (70:30% wt.).

The solubility of ethylene in MeP:MeOH is much higher than that of carbon monoxide, $x_{C_2H_4}$ = 0.464 at 223 K and 10.61 bar; the value for the entropy change of mixing the condensed ethylene with the liquid solvents (Eq. 4.9), is positive but lower than for the carbon monoxide, -R$\ln x_2$ =

0.228 kJ/kg·K. The entropy of mixing of ethylene is lower in magnitude than the (negative value) entropy of change of state of pure ethylene (-1.694 kJ/kg·K), making the total entropy change for the dissolution of ethylene gas in the liquid solvents negative (Table 4.5). From Eq. 4.5 this negative value leads to the conclusion that the solubility of ethylene should decrease at higher temperatures as is observed experimentally.

Consideration of the partial molar enthalpy change of solution, Eq. 4.6, leads to additional understanding of the temperature effect on gas solubility. When the change in the partial molar enthalpy of solution of gaseous solute 2 is positive, the solubility of gas 2 in the solvent 1 increases with temperature; otherwise it decreases. The partial molar enthalpy change is expressed by two terms in Eq. 4.8, where the first term corresponds to the enthalpy of change of state of pure gaseous component 2, and the second term corresponds to the variation of partial molar enthalpy of mixing of condensed solute 2 with liquid solvent 1. The enthalpy of change of state of the solute (first term in Eq. 4.8) is expected to be negative, because the enthalpy of a liquid is generally higher than that of a gas at the same temperature. The value for the enthalpy of condensation of pure carbon monoxide calculated applying the thermodynamic model in Aspen Plus is -129.51 kJ/kg at 223 K (p^0 =96.73 bar), whilst for ethylene a more exothermic enthalpy of -377.91 kJ/kg at 223 K (p^0 = 10.61 bar) is obtained. Values for the enthalpy of change of

state of carbon monoxide, calculated with the thermodynamic model in Aspen Plus, agree with experimental measurements[14, 15] confirming that the model is reliable for these calculations. Now the magnitude of the enthalpy of condensation of pure ethylene is higher than for carbon monoxide and so the process is more exothermic.

The partial molar enthalpy of mixing the condensed solute and the liquid (second term of Eq. 4.8) depends on intermolecular forces and therefore on the chemical properties of the components present in the vapour-liquid equilibrium. The more cohesive the intermolecular forces between the dissolved solute and solvent, the easier the mixing and the enthalpy of mixing is negative (exothermic). Conversely, in the absence of solvation between the solute and the solvent, this quantity tends to be positive (endothermic), and the less cohesive the intermolecular forces the more endothermic the enthalpy of mixing. These intermolecular forces can be of different kinds, for example when ions or permanent dipoles are present electrostatic forces occur; induction forces happen between permanent dipoles and induced dipoles with polarizable electrons; chemical forces can lead to association and solvation or the formation of loose chemical bonds, e.g. hydrogen bonding.

Studies of how chemical forces affect the solubility of gases in liquids are not common given the difficulty of characterizing these chemical forces in a quantitative way; the chemical affinity of a solvent depends on the nature

of the solute to be dissolved, and the chemical effects in solution must be studied relatively rather than absolutely. However, there are some studies of the importance of chemical effects on gas solubility, e.g. Gutmann discusses the definition of a method for characterizing specific solute-solvent interactions and defines donor-acceptor numbers[16]; Zellhoefer et al. describe the importance of chemical effects in the solubility of Freon-21 in different solvents[17]; Demyanovich and Lynn present a correlation providing Henry's constants in terms of chemical thermodynamic parameters[18]; Brown and Brady[19] reduced their solubility data via dissociation equilibrium constants; and Edwards et al. have studied the ionization effect on solubility[20]. When chemical forces affecting the solubility are not significant, physical forces between solute and solvent can then play a key role; some correlations have been developed based on the consideration of these forces[21].

In the chemical system under study the chemical forces will be dominant with respect to the physical forces (electrostatic and induction forces) because the dipole moment of MeOH and MeP are the same (1,7 Debye)[22, 23], while carbon monoxide is almost nonpolar, having a very low dipole moment (0,1 Debye).[6, 7]

Hence, methanol molecules in the liquid phase can solvate via hydrogen bonds; a hydrogen atom attached to an oxygen (electronegative atom) forms a loose bond with electronegative oxygen of another methanol

molecule. The molecule providing polar hydrogen for a hydrogen bond is called a donor; meanwhile the molecule that provides the electron rich site to which the hydrogen is attracted is called an acceptor. Hence, methanol may serve as both donor and acceptor, whereas methyl propanoate (ester) can only function as acceptor (Figure 4.8).

From this it might be considered that methanol would be less volatile than methyl propanoate, because of the chemical interactions between molecules. But it is necessary to consider van der Waals forces, which are caused by continuous movement of electrons in molecules, inducing fluctuating polarizations of nearby particles and reorienting them in such a way that the electropositive end of one molecule is attracted to the electronegative end of another, hence producing attraction forces between molecules. Large molecules have more electrons and nuclei that can create van der Waals attractive forces, so their compounds usually have higher boiling points than similar compounds made up of smaller molecules. This effect explains why methyl propanoate has a higher boiling point than methanol, the MeP molecule is larger than the MeOH one and so more van der Waals attractive forces occur. Hence, methanol has a higher vapour pressure than methyl propanoate (at 343 K; 1.25 bar > 0.73 bar). When the components are mixed, the vapour pressure (at 343 K; 1.35 bar) is even higher than that of pure methanol, the mixture MeP:MeOH (70:30% wt.) is more volatile than either single compound (this is because of the

formation of an azeotrope). The increase in volatility can be understood as follows: when MeP and MeOH are mixed, it is difficult for a molecule of MeP to find another identical molecule, so the van der Waals attractive forces are not as strong as when only MeP molecules are present in a liquid phase. Furthermore, the hydrogen bond formed between molecules of MeOH is stronger than that formed between MeOH and MeP molecules,

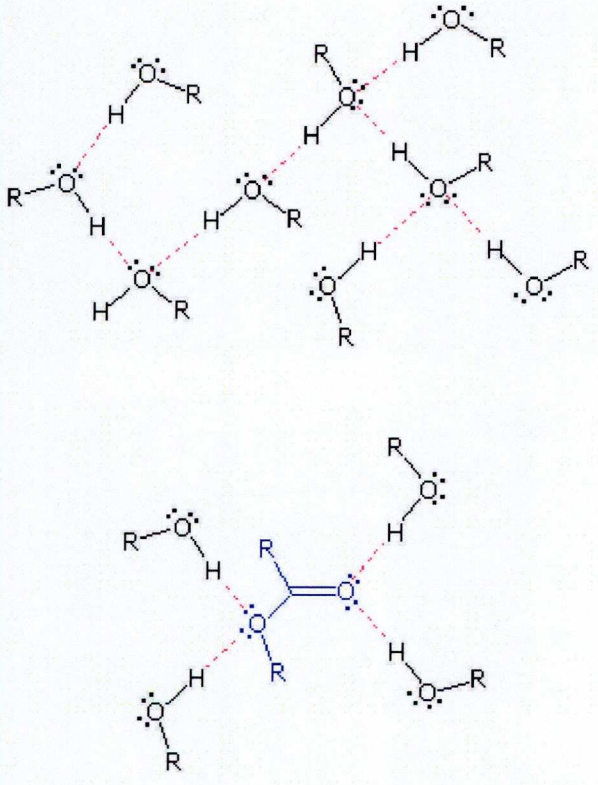

Figure 4.8: Solvation effects in MeOH/MeP

as the oxygen of the alcohol group is more electronegative than those of a carbonyl or ester groups. As it is more difficult for two molecules of methanol to find each other in the mixture than in the pure component, a large quantity of weak hydrogen bonds between MeOH and MeP

molecules will be present, thus the solvation forces are weaker than when only MeOH molecules are present in the liquid phase.

When carbon monoxide is dissolved in the solvent system, it does not interact chemically with the solvent since it has a very low dipole moment and it has no hydrogen atoms which could link with solvent molecules via hydrogen bonds. Consequently the solubility of CO is low. Moreover it is necessary to break hydrogen bonds between solvent molecules to dissolve carbon monoxide in the liquid, which makes the enthalpy of mixing endothermic. In conjunction with the fact that the enthalpy of change of state of carbon monoxide is not very exothermic (-129.51 kJ/kg at 223 K), the total enthalpy of solution of CO in MeP:MeOH might be positive, and from Eq. 4.6 its solubility is expected to increase with temperature, as is observed experimentally, i.e. the enthalpy of mixing is greater (i.e. more endothermic) in magnitude than that of change of state (Table 4.5). From a molecular point of view, when temperature increases the motion of the molecules becomes faster, and it is easier to break the hydrogen and Van der Waals bonds between molecules making more space available for the molecules of the solute to be placed in the matrix of the liquid.

Ethylene is non polar so electrostatic forces do not occur, and as it is dissolving in polar solvents dispersion forces do not occur either. Ethylene contains four hydrogen atoms linked to two carbons bonded by an electron rich double bond, so the hydrogen atoms may well form hydrogen bonds

with the electronegative oxygen atoms of methanol and methyl propanoate (proton acceptors). These intermolecular interactions would lead to solvation effects which can explain the higher solubility of ethylene and would make the mixing process easier and more exothermic. Hence, the total enthalpy change for the dissolution of ethylene gas in the solvent MeOH:MeP (70:30 % wt.) is exothermic (Table 4.5). As shown in Eq. 4.6, a negative enthalpy change means that the solubility of ethylene will increase at lower temperatures, as is experimentally observed. This is typical behaviour for the solubility of a gas in a liquid.

	ΔS (kJ/kg·K)			**ΔH** (kJ/kg)		
	Change of State (G-L)	*Mixing*	*Total*	*Change of State (G-L)*	*Mixing*	*Total*
CO T = 223 K; $P^s(CO)$ = 96.73 bar;	-0.5804	0.8541	**> 0**	-129.51	> 0	**> 0**
C2H4 T = 223 K; $P^s(C_2H_4)$ = 10.61 bar	-1.694	0.228	**< 0**	-377.91	< 0	**< 0**

Table 4.5. Entropies and enthalpies for the dissolution of carbon monoxide and ethylene in MeP:MeOH (70:30 % wt.).

In conclusion, the statement that the solubility o gases in liquids decreases at higher temperatures is usually wrongly generalised. It has been shown by experiment that this is not always true, and can be explained theoretically using thermodynamics.

4.4. Mixed gases results

4.4.1. Mixed gases solubility determination

The solubility of carbon monoxide and ethylene mixtures has been determined experimentally in the solvent mixture MeOH:MeP (70:30 % wt.) at six different initial gas mixtures compositions. The experimental results have been used to validate a thermodynamic model of the four component system, which has been used to calculate the Henry's constants of the gaseous components when mixed at different molar compositions.

Henry's constants have not been calculated from the experimental data because the gas phase composition has not been experimentally measured simultaneously with the experimental determination of the liquid compositions at any specific equilibrium condition, so is difficult and inaccurate to determine the partial pressures of the four component gas phase. In principle, this could be done assuming the molar ratio of C_2H_4:CO in the gas phase to be constant, and then proceeding as was done for the single gases determinations, with the activity coefficients and vapour pressures of the liquid solvents, methanol and methyl propanoate, the partial pressures of the four components could be calculated. However, since the carbon monoxide composition is low in both phases in many cases, a small change in the ratio of C_2H_4:CO in the gas phase due to

dissolution will lead to large errors in the partial pressure of carbon monoxide, and thus in the calculated Henry's constants.

However, the thermodynamic model was validated, by agreement with experimental results, for the resolution of liquid phase compositions in section 4.3. Validation for the resolution of composition of the gas phase at equilibrium, and so for the calculation of partial pressures of CO and C_2H_4, is shown later in section 4.5. Hence, partial pressures, necessary for the calculation of Henry's coefficients, were resolved with the thermodynamic model (as shown in Appendix A).

Six different molar compositions of the feed gas, covering the range of molar ratio ethylene to carbon monoxide from 0.5 to 25 were studied. The experimental results for the solubility of mixed carbon monoxide and ethylene in the solvent mixture at different temperatures and gas phase composition are shown graphically in Figs. 4.9 – 4.14, which also show comparison with the calculated solubility using the thermodynamic model.

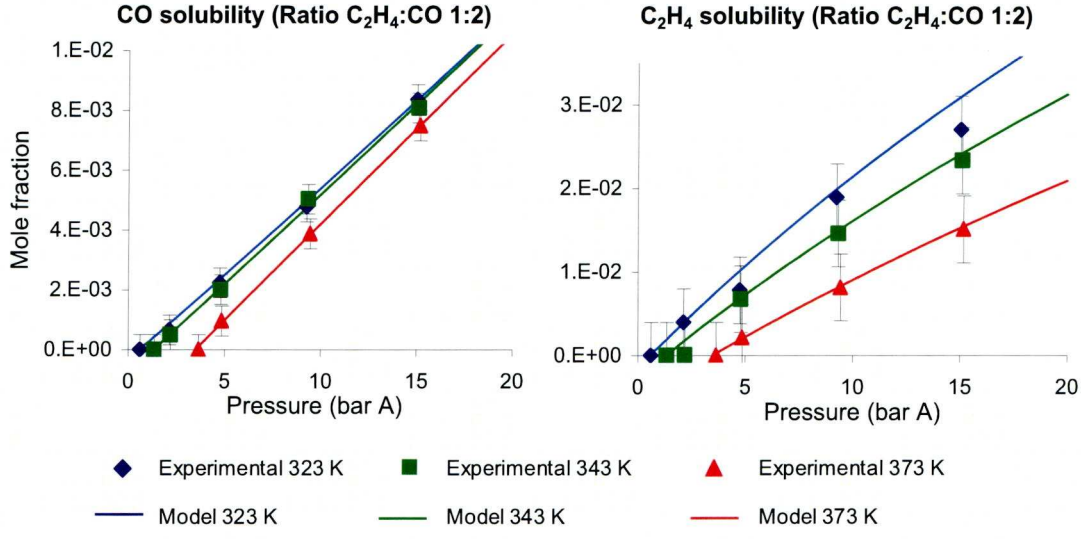

Figure 4.9: Solubility of ethylene and carbon monoxide mixed in a molar ratio **1:2**, respectively, in solvent MeP:MeOH (70:30% wt.) at different temperatures.

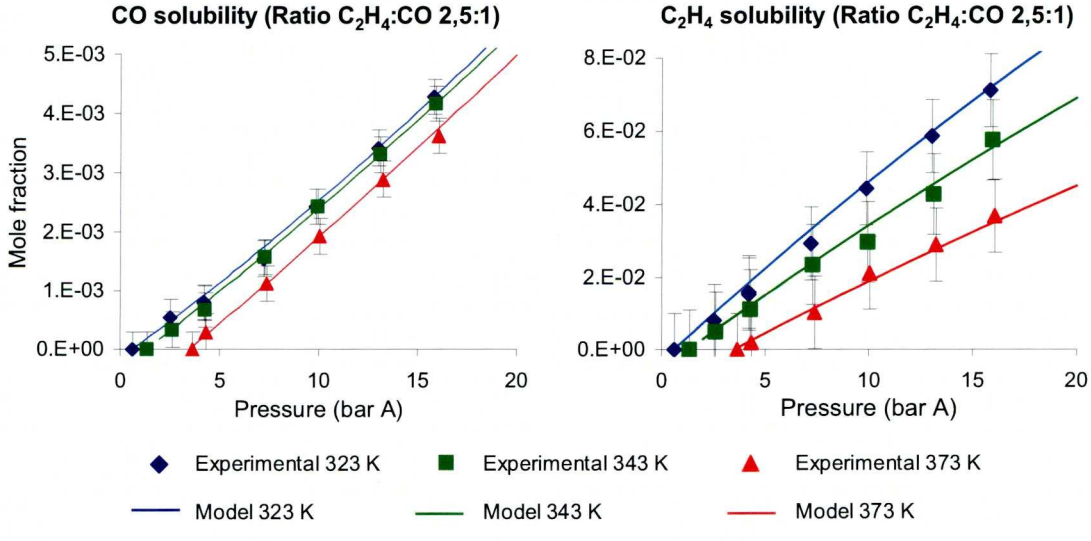

Figure 4.10: Solubility of ethylene and carbon monoxide mixed in a molar ratio **2,5:1**, respectively, in solvent MeP:MeOH (70:30% wt.) at different temperatures.

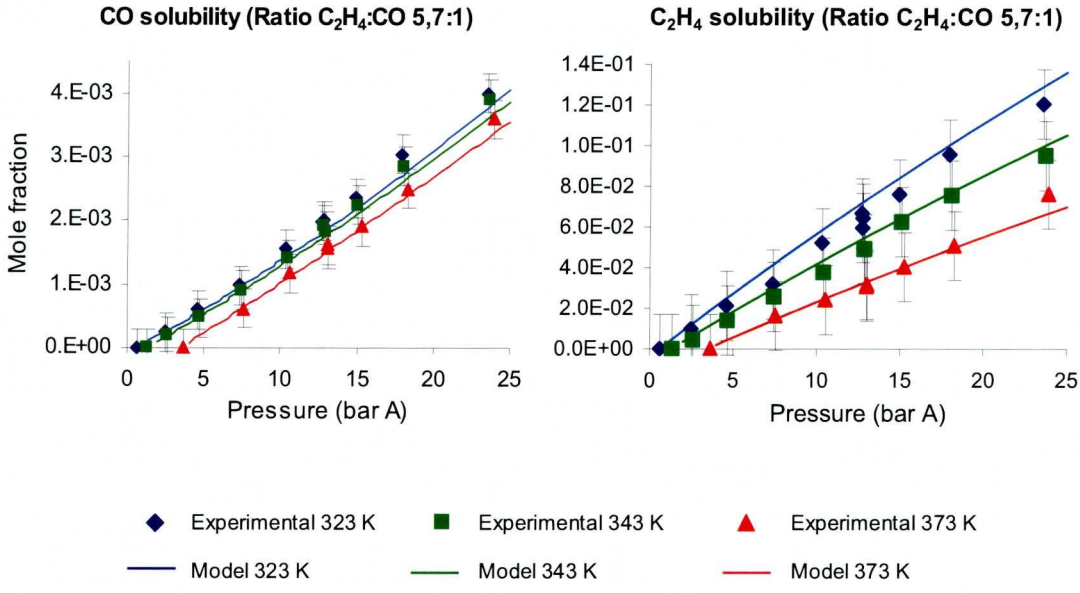

Figure 4.11: Solubility of ethylene and carbon monoxide mixed in a molar ratio **5,7:1**, respectively, in solvent MeP:MeOH (70:30% wt.) at different temperatures.

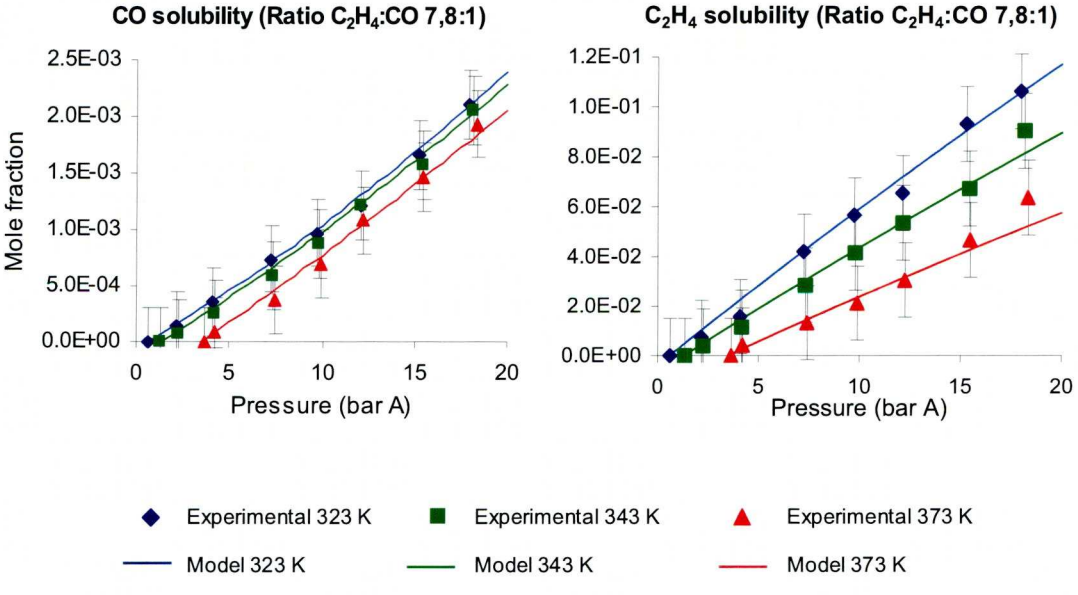

Figure 4.12: Solubility of ethylene and carbon monoxide mixed in a molar ratio **7,8:1**, respectively, in solvent MeP:MeOH (70:30% wt.) at different temperatures.

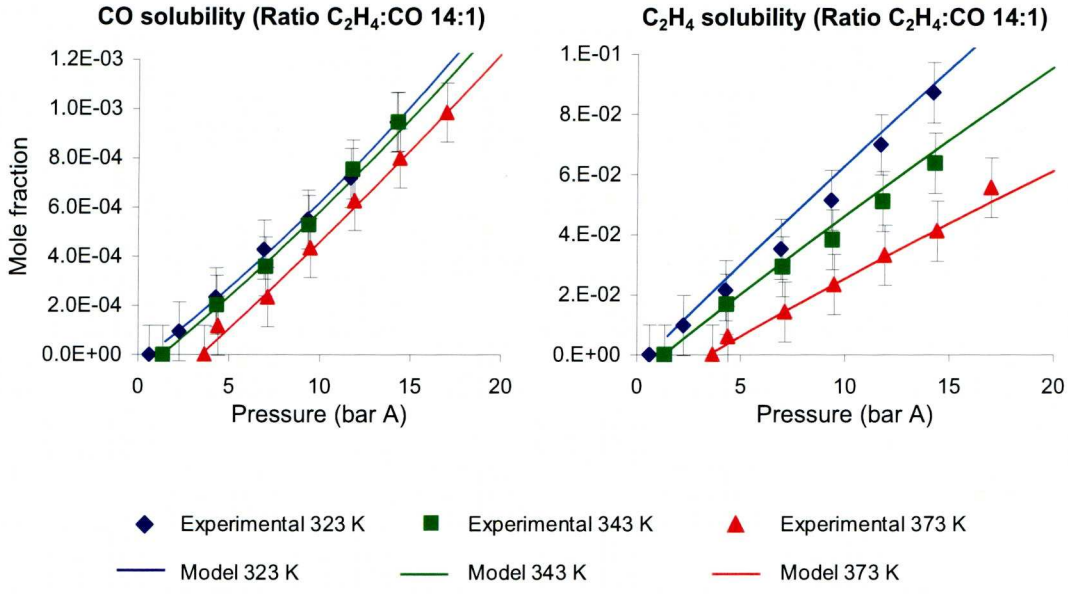

Figure 4.13: Solubility of ethylene and carbon monoxide mixed in a molar ratio **14:1**, respectively, in solvent MeP:MeOH (70:30% wt.) at different temperatures.

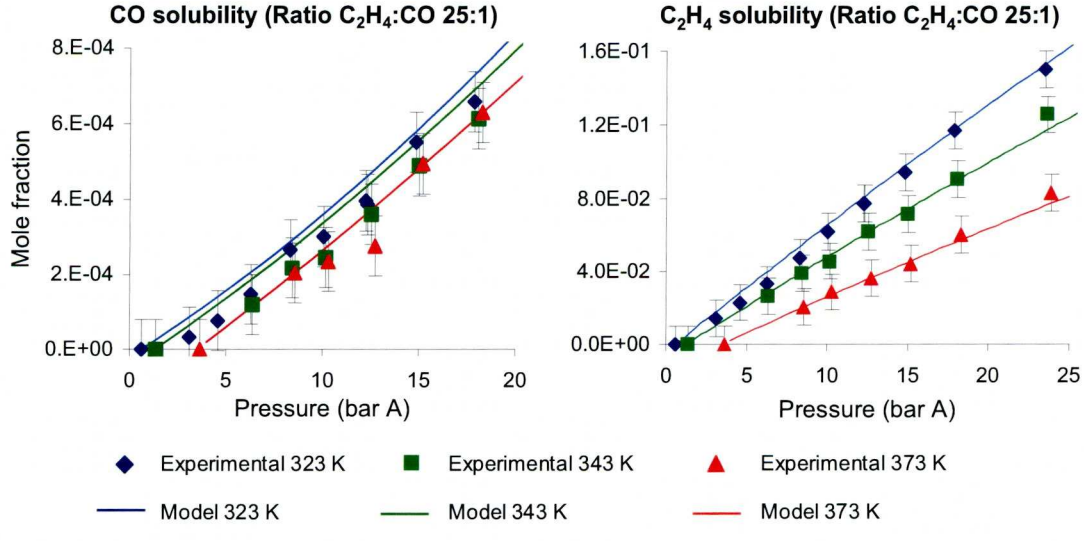

Figure 4.14: Solubility of ethylene and carbon monoxide mixed in a molar ratio **25:1**, respectively, in solvent MeP:MeOH (70:30% wt.) at different temperatures.

Since the quantity of gaseous component present, and so its partial pressure, is less at lower compositions, the amount of the gaseous component dissolved decreases when its composition is lower in the gas phase, e.g. at low C_2H_4:CO ratios the solubility of ethylene is lower than at higher ratios. The experimental results for the solubility of carbon monoxide are well reproduced by the thermodynamic model, except for lowest composition (highest ratio C_2H_4:CO of 25:1) studied where the experimental results are usually lower than the results calculated by the model. This is attributed to the increasing experimental error (determined as explained in Chapter 2 page 95) for the CO data under these conditions resulting from the very low NMR peak intensity; a slight error in quantitation of this intensity results in a high percentage error in the value of the solubility. The same effect is observed in the ethylene data, although the effect is not so marked because the lowest composition of ethylene in the gas phase measured is much higher than the lowest composition for carbon monoxide. Furthermore, as has been shown previously (4.3.1 and 4.3.2), the solubility of ethylene is one order of magnitude greater than that of the carbon monoxide. Nevertheless, the model reproduces the experimental results well with less than 5 % deviation between experimental and modelled compositions. Even in the two worst cases, very low compositions of carbon monoxide or ethylene in the gas phase, the greatest difference between the experimental and modelled solubility results is less than 25 % for CO, and less than 10 % for ethylene.

4.4.2 Discussion: Deviations from ideality

It is interesting to note in the experimental results that when a gaseous component composition in the gas phase is low, the solubility lines are less linear and have curved shapes, indicating deviation from linear behaviour of solubility defined by Henry's law. Deviations from Henry's law are more easily observed by representing the solubility of the dissolved component as a function of the partial pressure, calculated using the thermodynamic model (Appendix A) and using Henry's law (Figs. 4.15, 4.16).

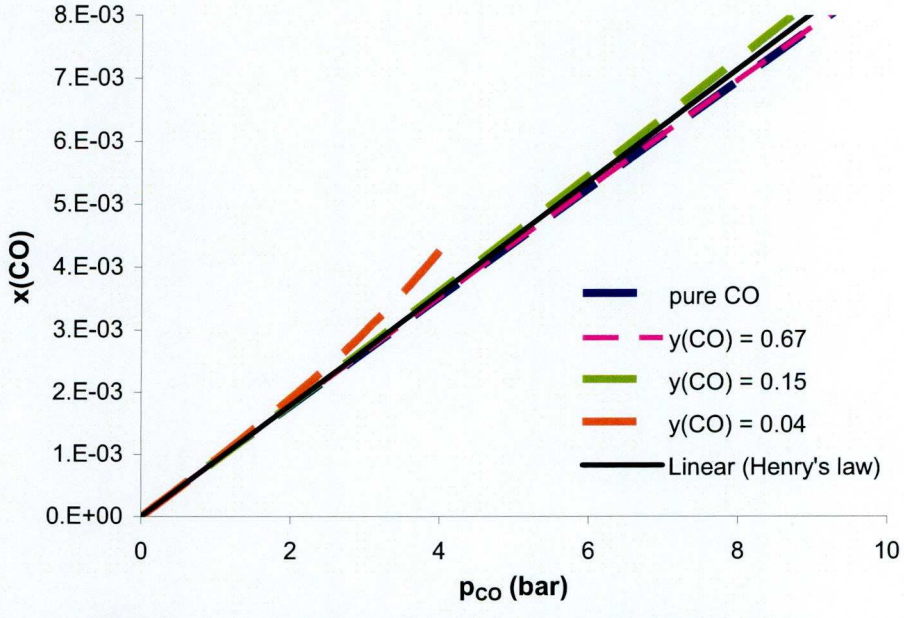

Figure 4.15: Deviations from ideality of CO solubility in MeP:MeOH (70:30% wt.) at 323 K calculated by the thermodynamic model.

Inspection of Fig. 4.15 reveals that the CO solubility lines predicted by the model are not completely linear, but show deviations from Henry's law linear behaviour.

Thus, at high pressures the deviations from Henry's law are more pronounced. As explained in Chapter 1, these deviations at higher pressures come from the definition of Henry's law, looking at equations 1.28 and 1.29 in Chapter 1 it can be seen that linear behaviour characterizing Henry's law will only occur when the liquid phase activity coefficient is constant and evaluated at infinite dilution. Hence, as a component gets more concentrated in the solution the linear behaviour vanishes. When these deviations make the solubility lower than the ideal predicted by Henry's law, we define it as positive deviations from Henry's law, as the real values would correspond with higher Henry's constants (lower solubility). Otherwise, negative deviations from Henry's law occur.

When there is a high composition of CO (low C_2H_4:CO ratio) in the gas phase (*67-100 %* moles), the CO solubility is lower than that predicted by Henry's law. Therefore, positive deviations from Henry's law for carbon monoxide occur. As the CO composition in the gas phase is decreased (higher C_2H_4:CO ratios), the solubility show less positive deviations from Henry's law. Hence, at low compositions of CO in the gas phase (0-*15 %* moles), deviations change from positive deviations to negative deviations from Henry's law, i.e. solubility values are higher than those predicted by

Henry's law, which would mean a lower Henry's coefficient for carbon monoxide at that temperature.

In conclusion, for carbon monoxide solubility, more positive deviations from Henry's law are observed as the gas phase is more concentrated in CO (lower C_2H_4:CO ratios).

Inspection of Figure 4.16 reveals that ethylene solubility calculated by the model as a function of the partial pressure shows positive deviations from Henry's law at high pressures. Large positive deviations from Henry's law are observed at low composition of ethylene (low C_2H_4:CO ratio) in the gas phase (*33 %* moles). When the composition of ethylene in

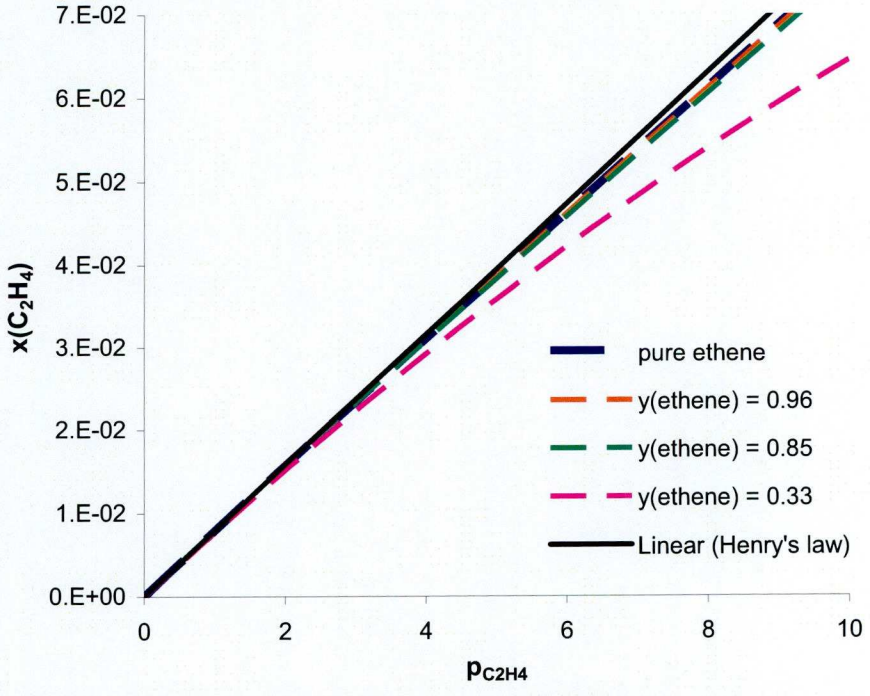

Figure 4.16: Deviations from ideality of C_2H_4 solubility in MeP:MeOH (70:30% wt.) at 323 K calculated by the thermodynamic model.

the gas phase is increased (higher C_2H_4:CO ratio) (*85* -100 % moles), Henry's law reproduces better the experimental results than for lower compositions of ethylene in the gas phase.

In conclusion, ethylene solubility shows more positive deviations from Henry's law as the gas phase becomes less concentrated in ethylene (lower C_2H_4:CO ratios).

In summary, ethylene and carbon monoxide show different solubility behaviours from the point of view of deviations from Henry's law. Ethylene solubility shows more positive deviations from Henry's law, i.e. lower solubilities, at lower C_2H_4:CO ratios, whereas carbon monoxide shows less positive, or even negative, deviations at higher gas phase C_2H_4:CO composition ratios. In other words, the solubility of carbon monoxide is greater than the solubility predicted by Henry's law as its composition in the gas phase decreases (higher ratios C_2H_4:CO); while for ethylene the reverse behaviour is observed.

This can be explained by the difference in the activity coefficients values of ethylene and carbon monoxide, being greater and lower than unity respectively (Table 4.2). Ideality implies an activity coefficient equal to unity, but when components are mixed deviations from ideality occur. Now, the activity coefficient of carbon monoxide is less than unity, and when mixed with ethylene non idealities occur and it deviates even more

from unity, i.e. it becomes lower still. Inspection of equation 4.3 reveals that solubility is inversely proportional to the activity coefficient. Hence, for carbon monoxide the activity coefficient decreases when mixed with ethylene, and as it gets less concentrated (higher C_2H_4:CO ratios), the solubility increases showing more negative deviations from Henry's law. Conversely, the activity coefficient of ethylene is greater than unity (Table 4.2), so it increases deviating more from unity when non idealities occur, as when mixed with carbon monoxide. Hence, at lower concentrations of ethylene in the gas phase (lower C_2H_4:CO ratios) the activity coefficient gets higher values, and so the solubility decreases showing more positive deviations from Henry's law.

These deviations of activity coefficients caused by the mixing of carbon monoxide with ethylene affecting their solubilities can be clearly observed in the Henry's constants, calculated using the thermodynamic model for the solubility experiments performed (Table 4.5).

Ratio ethylene:CO	323 K		343 K		373 K	
	H(CO)	H(ethylene)	H(CO)	H(ethylene)	H(CO)	H(ethylene)
Pure CO	1122.3		1049.3		934.6	
0,5	1128.7	130.2	1061.6	161.0	925.9	219.8
2,5	1119.8	129.5	1052.6	160.3	917.4	217.0
5,7	1116.1	129.2	1049.3	160.0	917.4	215.3
7,8	1114.8	129.2	1048.2	159.7	917.4	214.8
14	1113.6	129.0	1047.1	159.7	917.4	214.3
25	1112.3	128.9	1046.0	159.7	917.4	213.8
Pure ethylene		127.4		157.5		211.4

Table 4.5: Henry's coefficient of carbon monoxide and ethylene in solvent MeP:MeOH (70:30% wt.) at different gas phase composition and temperatures.

Thus, carbon monoxide becomes more soluble as its composition in the gas phase decreases (lower activity coefficient); meanwhile ethylene gets more soluble at higher compositions in the gas phase (lower activity coefficient).

4.5 Determination of the gas phase equilibrium composition

The basic aim of the experiments described in this section was to validate the thermodynamic model (Appendix A) for the gas phase in equilibrium. Hence, the determination of the composition of the gas phase formed using an initial molar ratio C_2H_4:CO of 3.5:1 in equilibrium with the liquid solvent mixture MeP:MeOH [70:30 % wt.] was determined for the temperatures 323, 343, and 373 K, and in the range of pressures 0-20 bar using the experimental system described in Chapter 2. The equilibrium cell used is essentially similar to that used in the NMR determination of the liquid phase equilibrium compositions, but the analytical method used is now Gas Chromatography.

The experimental results compared to the predictions using the thermodynamic model are shown in Figs. 4.17-4.19 and show good agreement between the experimental and calculation data for the range of temperatures, pressures and components studied with the exception of methanol composition at low temperatures, where the experimental results are lower than those calculated by the model. This difference is attributed to the fact that the experimental temperature is below, or very close, to the boiling point (65 °C for MeOH; and 79 °C for MeP) and some condensation may have occurred in the transfer lines connecting the equilibrium cell and the GC apparatus. This deviation in methanol composition makes the CO and C_2H_4 compositions also to slightly deviate

from the thermodynamic model values. Alternative experimental data are available for these conditions, Blanco and Ortega[6] have also studied the vapour-liquid equilibrium of methanol and methyl propanoate for a liquid of composition MeP:MeOH [70:30 % wt.] and report that the gas phase in equilibrium at 1.4 bar is richer in MeOH (0.62 mole fraction) than in MeP (0.38 mole fraction), as predicted by our thermodynamic model.

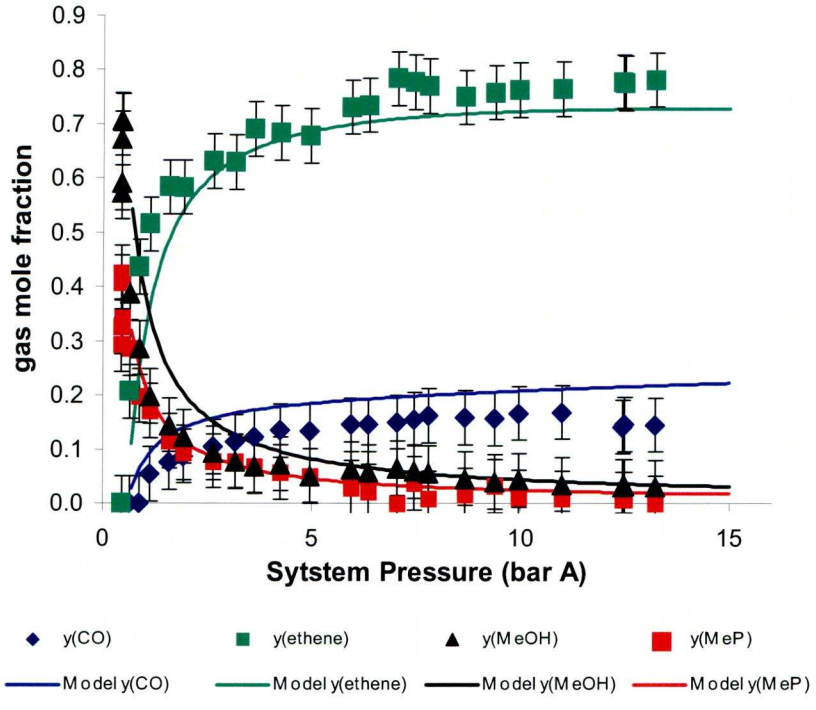

Figure 4.17: Compositions of the gas phase initially formed by a molar ratio C_2H_4:CO 5:1 in solvent MeP:MeOH (70:30% wt.) at **323 K.**

At higher temperatures the amount of MeOH and MeP increases in the gas phase, and also at lower pressures, when it is easier to evaporate the solvents. As the pressure of the gas phase increases, more CO and C_2H_4 are

present in the gas phase and the solvents' compositions get lower. Hence, at high pressures the compositions of methanol and methyl propanoate tend to zero, and those of ethylene and carbon monoxide to the ratio 3.5:1 (corresponding compositions (0.78:0.22)).

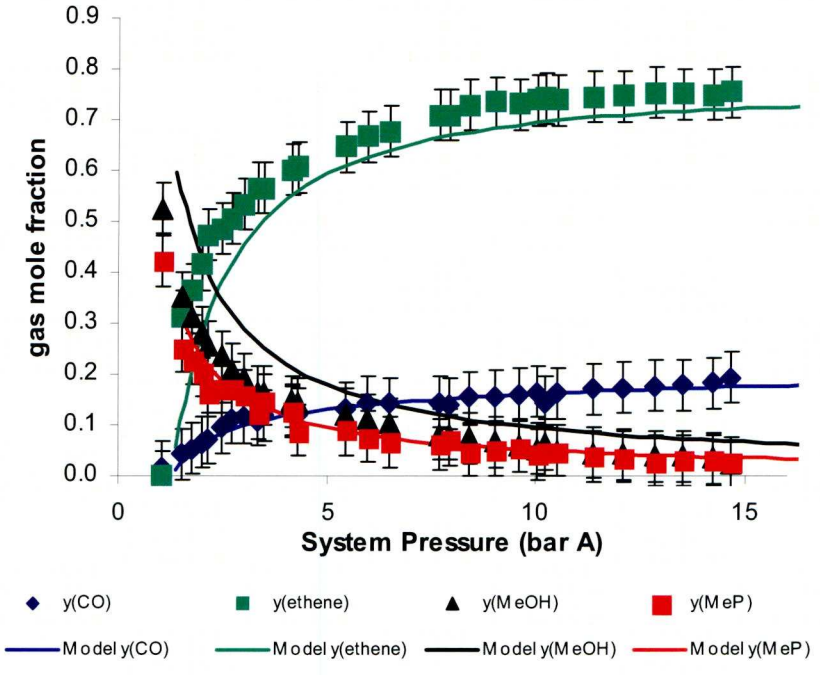

Figure 4.18: Compositions of the gas phase initially formed by a molar ratio C_2H_4:CO 5:1 in solvent MeP:MeOH (70:30% wt.) at **343 K.**

The composition of methanol in the vapour phase is higher than that of methyl propanoate, and this difference gets greater at higher temperatures. This is because of the temperature dependence of the vapour-liquid equilibrium curves and the azeotrope composition. Hence, at higher temperatures the azeotrope composition gets richer in methanol.

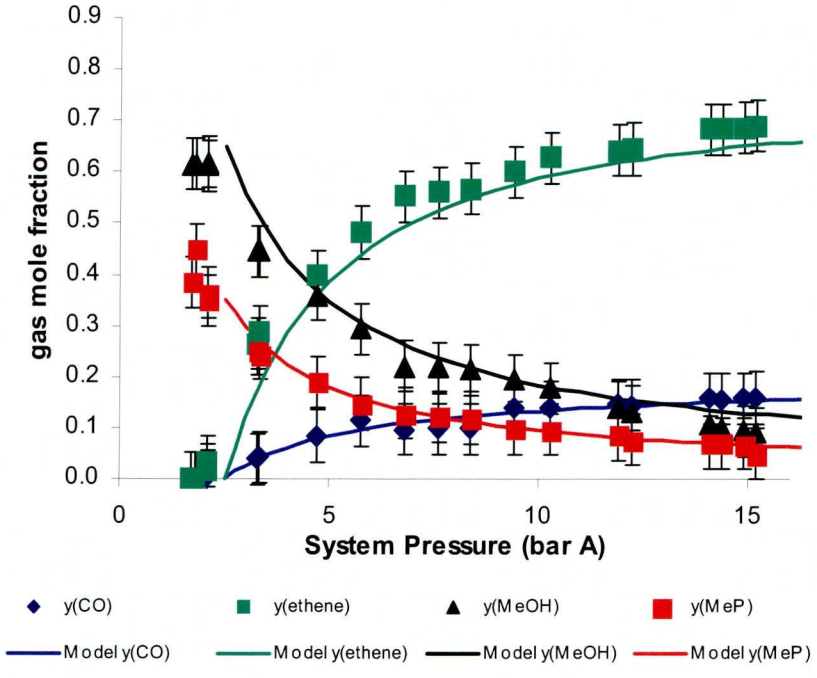

Figure 4.19: Compositions of the gas phase initially formed by a molar ratio C_2H_4:CO 5:1 in solvent MeP:MeOH (70:30% wt.) at **363 K.**

In summary, the experimentally determined behaviour of the gas phase is reproduced well by the thermodynamic model, validating its performance for resolution of the gas phase compositions in the vapour-liquid equilibria described in this thesis.

4.6 Conclusions

The solubility of carbon monoxide and ethylene, both as single gases and mixtures, in the solvent mixture methyl propanoate-methanol [70:30 % wt.] have been successfully determined and compared with predictions made by a thermodynamic model. The agreement between the experimental and theoretically calculated results validates the thermodynamic model. The model performs well for the resolution of vapour-liquid equilibrium calculations in a wide range of pressures, temperatures and compositions.

Figures 4.20 and 4.21 show three-dimensional surfaces representing the solubilities of carbon monoxide and ethylene at constant temperature (i.e. 373 K) as a function of the total pressure of the system and the composition of the gas phase. The solubilities of CO and C_2H_4 increase with the total pressure of the system and with composition in the gas phase, so CO solubility increases at lower C_2H_4:CO ratios, meanwhile C_2H_4 solubility increases at higher C_2H_4:CO ratios. The increase in solubility with pressure is much more apparent at high concentration in the gas mixture (low C_2H_4:CO ratios for CO and high C_2H_4:CO ratios for C_2H_4), and the effect of the C_2H_4:CO composition ratio of the gas is emphasized at high system pressures.

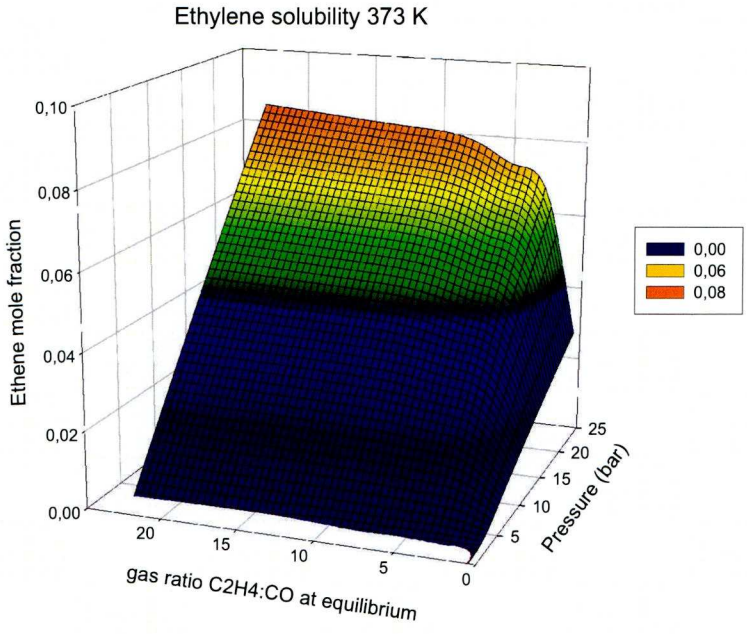

Figure 4.20: Ethylene solubility in solvent MeP:MeOH (70:30% wt.) at **373 K** at different pressures and gas phase compositions.

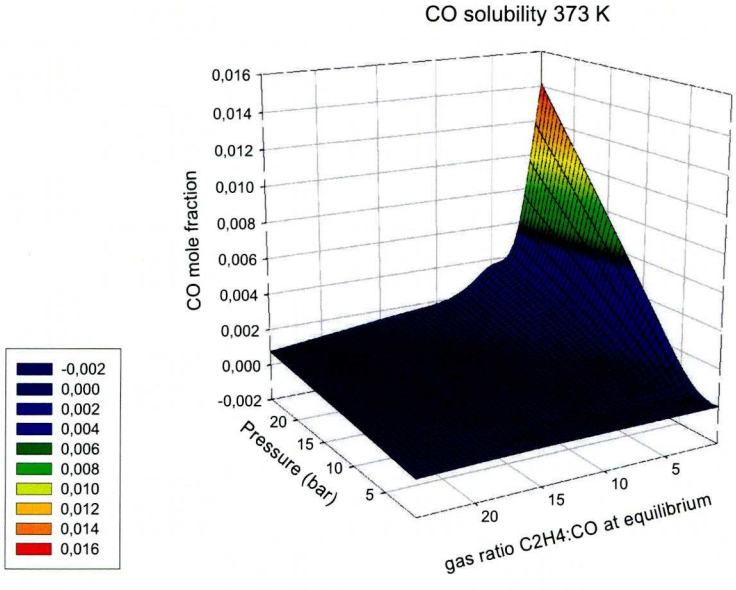

Figure 4.21: Carbon monoxide solubility in solvent MeP:MeOH (70:30% wt.) at **373 K** at different pressures and gas phase compositions.

The solubility of carbon monoxide is shown to be much lower than that of ethylene as expected given the values of the fugacities of the pure components. The solubilities of CO and C_2H_4 show different behaviour with temperature; the solubility of carbon monoxide increases with increasing temperature, whilst C_2H_4 shows the opposite behaviour. This difference can be explained by the changes in entropy and enthalpy occurring during the process of dissolution of a gas in a liquid phase. Hence, for carbon monoxide this is an endothermic process with a positive change in entropy; whereas it is exothermic, and a negative entropy change for ethylene.

Meaningful comparisons of the solubilities of components in a mixture require knowledge of the Henry's coefficients, as they define the solubility as a function of partial pressure of a component in the gas phase. Comparison of the Henry's constants of different gaseous components for the same solvent gives an evaluation of solubilities at the same partial pressure in the gas phase, whereas using solubility values at total system pressure requires the consideration of the gas phase composition. Henry's coefficients have been determined for carbon monoxide and ethylene in MeP:MeOH.

When carbon monoxide and ethylene are mixed in the gas phase their solubilities change slightly. However, these variations in solubility are not the same for both components. Hence, the solubility of carbon monoxide

decreases at high composition in the gas phase (low C_2H_4:CO ratio), but ethylene becomes more soluble when concentrated (high C_2H_4:CO ratio). This is so because of different deviations from ideality of carbon monoxide and ethylene due to the different values of the activity coefficients, being lower than unity for carbon monoxide, and larger for ethylene.

In conclusion, a good understanding of the vapour-liquid equilibrium between ethylene-carbon monoxide gas phase with methanol-methyl propanoate liquid phase has been achieved, which is vital for the design of catalytic homogeneous reactions where gaseous reactants dissolve in a reacting liquid phase.

4.7 References

(1) Liu, Q.; Takemura, F.; Yabe, A. Solubility and diffusivity of carbon monoxide in liquid methanol. *J. Chem. Eng. Data.* **1996**, *41 (3)*, 589.

(2) Purwanto; Deshpande, R. M.; Chaudhari, R. V.; Delmas, H. Solubility of hydrogen, carbon monoxide, and 1-octene in various solvents and solvent mixtures. *J. Chem. Eng. Data.* **1996**, *41 (6)*, 1414.

(3) Boyer, F. L.; Bircher, L. J. The solubility of nitrogen, argon, methane, ethylene and ethane in normal primary alcohols. *J. Phys. Chem.* **1960**, *64 (9)*, 1330.

(4) Lee, L.; Shih, R.; Ou, H.; Lee, T. Solubility of ethylene in mixtures of toluene, norbornene, and cyclic olefin copolymer at various temperatures and pressures. *Ind. Eng. Chem. Res.* **2003**, *42 (26)*, 6977.

(5) Pepin, A. H. A. Spectroscopic studies on catalytic intermediates involved in the methoxycarbonylation of ethene. *PhD Thesis, University of Liverpool.* **2005**.

(6) Blanco, A. M.; Ortega, J. Isobaric vapor-liquid equilibria of metanol + methyl ethanoate, + methyl propanoate, and + butanoate at 141.3 kPa. *J. Chem. Eng. Data.* **1996**, *41 (3)*, 566.

(7) Hahn, J.; Mueller, G.; Stoeck, S. Determination of the vapour-liquid equilibria in binary systems formed by methanol, ethanol, water, methyl propionate, and methyl butyrate. *FIZ Report.* **1988**, 9301.

(8) Prausnitz, J. M. et al. *Molecular thermodynamics of fluid-phase equilibria.* 3rd Edition. Prentice Hall, Englewood Cliffs, NJ, 1999. p.597.

(9) Bondi, A. *Physical Properties of Molecular Crystals, Liquids and Gases*. John Wiley & Sons, New York, 1960.

(10) Abrams, D. S.; Prausnitz, J. M. Statistical thermodynamics of liquid mixtures: A new expression for the excess Gibbs energy of partly or completely miscible systems. *AIChE J.* **1975**, *21*, 116.

(11) Hildebrand, J. H. et al. *Regular and Related Solutions.* Van Nostrand Reinhold, New York, 1970.

(12) Sherwood, A. E. and Prausitz, J. M. The heat of solution of gases at high pressure. *AIChE J.* **1962**. *8 (4),* 519.

(13) Wilhelm, E.; Battino, R. Thermodynamic functions of the solubilities of gases in liquids at 25°C. *Chem. Rev.* **1973**, *73 (1)*, 1.

(14) Liessmann,G.; Schmidt,W.; Reiffarth,S. *Recommended Thermophysical Data. Data compilation of the Saechsische Olefinwerke Boehlen*, Germany, 1995.

(15) Tonner, S P.; Wainwright, D.L.; Trimm, N. W. C. Solubility of carbon monoxide in alcohols. J. *Chem. Eng. Data.* **1983**, *28 (1)*, 59.

(16) Gutmann, V, *The donor-acceptor approach to molecular interactions.* Plenum Press, New York, 1978.

(17) Zellhoefer, G. F.; Copley, M. J.; Marvel, C. S. Hydrogen bonds involving the C-H link. The solubility of haloforms in donor solvents. *J. Am. Chem. Soc.* **1938**, *60 (6)*, 1337.

(18) Demyanovich, R. J.; Lynn, S. Prediction of infinite dilution activity coefficients of sulfur dioxide in organic solvents. *J. Soution Chem.* **1991**, *20 (7)*, 693.

(19) Brown, H. C. and Brady, J. D. Solubility of hydrogen chloride at low temperatures. A measure of the basic properties of aromatic nuclei; π- and σ- complexes and their role in aromatic substitution. *J. Am. Chem. Soc.* **1952**, *74 (14)*, 3570.

(20) Edwards, T.J.; Maurer, G.; Newman, J.; Prausnitz, J. M. Vapor-liquid equilibria in multicomponent aqueous solutions of volatile weak electrolytes. *AIChE J.* **1978**, *24*, 966.

(21) Hildebrand, J. H.; Scott, R. L. *Regular Solutions.* Prentice Hall, Englewood Cliffs, NJ, 1962.

(22) Landolt-Börnstein: Zahlenwerte und Funktionen aus Physik, Chemie, Astronomie, Geophysik, und Technik. Springer, Berlin, 6th Ed., 1951.

(23) McClellan, A. *Tables of Experimental Dipole Moments.* Vol. 1, W. H. Freeman, 1963; Vol. II, Rahara Enterprises, 1974.

Chapter 5

Kinetic study

Chapter 5: Kinetic Study

5.1 Introduction

Many important chemical processes involve mass transfer of components from a gaseous phase to a liquid phase. When these processes involve a reaction, species from the gas phase are transferred to the liquid phase and then take part in a chemical reaction with species already present in the liquid phase. Typical examples of industrially important processes where this happens include gas purification, oxidation, chlorination, hydrogenation and hydroformylation processes. In industrial plants, these gas-liquid reactions frequently take place in bubble columns, stirred tank reactors and absorption units[1]. Many investigations have been dedicated to the study of the kinetics of gas-liquid reactions because a detailed knowledge of kinetics is essential for the appropriate design of the reactor and for the prediction of reactor performance; inaccurate estimation of reaction rates may well lead to significant errors in reactor design.

Absorption and reaction experiments are thus performed on a laboratory scale to obtain a fundamental understanding of these reactions, to study the effect of the mass transfer on reaction kinetics, and to describe the reaction rate as a function of process variables such as temperature, pressure, reactor design, reactant concentration, etc. These bench-scale kinetic experiments are performed at the conditions typical for the consequent

industrial process. Several experimental methods have been used to obtain kinetic data for such systems[2, 3, 4, 5]. Two sorts of contactors are routinely used in such studies: in the first class, the flow pattern is well defined, for instance, in wetted-wall columns, wetted-sphere contactors, and laminar jet absorbers; in the second class, the flow pattern is not well established, examples being stirred cell reactors[6, 7, 8, 9, 10], and mechanically agitated contactors. In some designs, for example wetted wall and wetted sphere contactors, the mass transfer interfacial area is geometrically simple and therefore known. In all experimental designs gaseous components must be transported into the liquid phase both before, and during, the reaction, and so equilibrium and mass transfer considerations must be taken into account in designing the kinetic study. Alternatively there are experimental procedures without a phase transition, where two liquid phases are brought together and rapidly mixed, with the gas to be studied dissolved in one phase and a chemically active solvent present in the other phase [1, 11, 12]. Mass transfer is not considered in these methods, and the kinetic parameters are defined from the rate of the homogeneous reaction.

In this project the novel NMR bubble column reactor described in Chapter 2, rather than one of the previous designs, has been used. The reason for the use of this novel system is that ultimately it was hoped to combine the kinetic study with NMR characterization of the active species. Bubble columns[13, 14, 15] are not used for kinetic studies of gas-liquid reactions

because the contact interfacial area is not easily determined and the reactor design is difficult due to the continuous gas feed bubbling into the liquid phase. However it is a more realistic design from the industrial point of view. Bubble column reactors are used industrially to perform non-catalytic and homogeneously catalyzed gas-liquid reactions, such as Fischer-Tropsch and methanol syntheses. The processes taking place in a bubble column include mass transfer between the gas and liquid phase combined with chemical reaction in the liquid film and in the liquid bulk.

Stirred cell reactors are widely used and they are batch-operated devices, which have the advantage that no analysis of the liquid phase is needed; only the pressure history of the gas phase is required for the determination of the kinetic parameters. However, in industrial practice it is common that the pressure in the reactor is kept constant as well as the gas phase composition by a continuous gas feed stream. The bubble column experimental system proposed is thus as similar as possible to an industrial design. It is a semi batch reactor; a continuous gas feed is bubbled through the stationary liquid phase in the reaction cell, and so the reaction rate is not obtained from the pressure in the reaction cell, which is kept constant, but from direct measurements of compositions of the liquid phase by NMR. Stirred reactors may give good conditions for fast mass transfer because of the thorough mixing of gas and liquid phases, but there are experimental difficulties in the implementation of a mechanically stirred

NMR HP reactor such as technical and experimental complexity associated with the manufacture and implementation. There are design restraints imposed by the limited bore diameters of superconducting magnets. The mechanical agitator, which should be made of a non magnetic material, needs an electric motor which is clearly incompatible with a strong magnetic field. Too violent agitation in the NMR cell can lead to poor spectral resolution. Hence, an elegant design device would require great skill in design, manufacture, maintenance and operation.

Conventional theoretical modelling of gas-liquid reactors has focused on the bulk liquid phase mass balances while the mass transfer enhanced by chemical reaction in the liquid film is usually solved analytically for simple reaction kinetics (Danckwerts[16], 1970; Charpentier[17], 1982) or treated with approximate methods (van Krevelen and Hoftijzer[18], 1948; Hikita and Asai[19], 1966). Recently there has been an increasing interest in modelling gas-liquid reactions more thoroughly and more complex models have been determined for some particular cases with complicated reaction kinetics. However, we are not interested here in developing or applying a general model, but rather, in the investigation and understanding of the kinetics of the methoxycarbonylation of ethylene in a bubble column reactor. Hence, knowledge about how mass transfer processes can affect reaction kinetics is needed but the application of complex balances needed for the determination of a general model is not required.

When reaction occurs in the liquid phase two distinct physical phenomena, interfacial mass transfer between gas and liquid, and reaction in the liquid phase occur simultaneously. Thus, for the overall process rate determination it is necessary to consider two different resistances, that of mass transport, and the resistance of the chemical reaction process. The relative values of these resistances will define the kinetic regime of the overall process. Therefore, if the mass transfer process is very slow relative to the reaction, the overall process will be governed by the mass transfer step. On the other hand, in a slow chemical reaction with fast mass transfer, the overall rate observed will correspond with the chemical reaction kinetics. These two extreme cases have simple resolution because the overall rate will be reduced to the definition of only one or other single process, mass transfer or kinetic reaction. However, in general the behaviour of gas-liquid reactions falls in an intermediate regime where both, mass transfer and chemical reaction resistances are significant. In that case the reaction occurs at the interface as well as in the bulk of liquid. Hence, understanding mass transfer between the gas and the liquid phase is crucial to understand the operating kinetic regime. Danckwerts (1970)[17] and Doraiswamy and Sharma[20] (1984) summarized the theory of mass transfer in chemical reactions and suggested general models that can be employed to study the kinetics of gas–liquid reaction systems.

5.1.1. Mass transfer

The mass transfer rate of the gas components into the liquid phase will depend on: the physical properties of the gas and liquid phases, the concentration difference, the interface contact area, and the degree of turbulence. Consequently, the reactor must be designed to give a large area of contact between the phases, and to create turbulence in order to attain fast mass transfer, to make the reaction the rate controlling process, and avoid mass transfer limitation of the reaction rate.

Different mechanisms have been proposed to represent conditions in the region of phase boundary. The first is the two-film theory developed by Whitman[21] (1923) who suggested that mass transfer in each phase could be considered to proceed via stationary molecular diffusion in a thin film close to the interface. The turbulence in the bulk is considered to vanish in the interfacial films. In 1935 Higbie[22] suggested that the transfer process was mostly attributable to fresh material being transported to the interface by currents caused by turbulence, where a process of non-steady state transfer took place for a period of time at the freshly exposed surface, this theory is generally known as the penetration theory. Danckwerts[23] (1951) suggested a modification of this theory in which it is considered that the material brought to the surface will remain there for varying periods of time, and a probability of replacement is introduced, to approximate the random age distribution of such elements from which transfer occurs by a

non-steady state process to the liquid phase. This is the surface renewal model. In brief, the two-film model presumes the presence of a liquid film, while the penetration model and the surface renewal model define gas-liquid mass transfer using dynamic absorption in small liquid elements at the contact surface. Later, Toor and Marchello[24] proposed a more general theory, the film-penetration theory, and showed that each of the earlier theories corresponds to a particular limiting case.

Thus, gas-liquid mass transfer has been under scientific study for a long period of time. In spite of this, there still exist no satisfactory general design criteria for all phenomena of gas-liquid mass transfer that may occur. In well-mixed gas-liquid reactors, the most frequently applied model is the two-film model[25, 26, 27]. In most situations it is found that the Higbie penetration model gives similar results as compared to the two-film theory[28].

In two-film theory when mass transfer occurs through an interface separating both gas and liquid phases, the resistance to mass transfer causes a concentration gradient as shown by full lines in Figure 5.1. The concentration gradient is linear near the interface, and becomes progressively smaller at larger distances.

The basis of the two-film theory is the supposition that the regions where the resistance to transfer occurs can be represented by two imaginary films, one on each side of the interface, in which the mass transfer occurs entirely

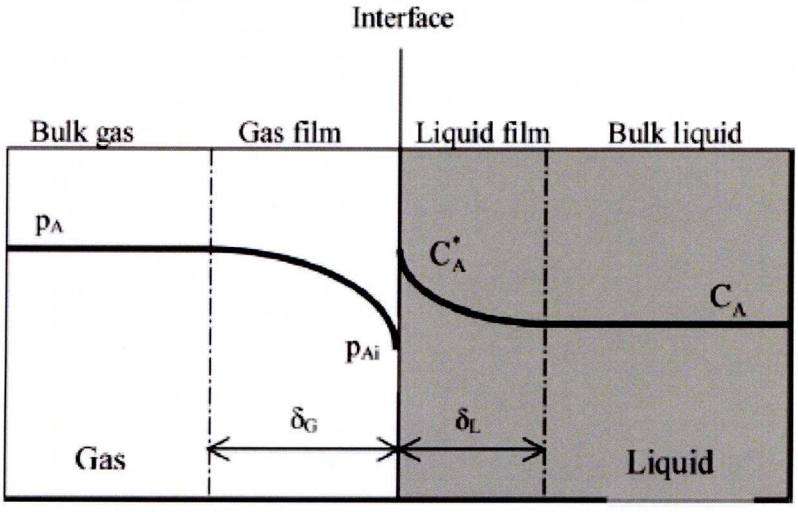

Figure 5.1. Two-film theory.[2]

by molecular diffusion. Outside the films, in the bulk fluid phases, turbulence eliminates the composition gradient. Equilibrium is assumed to exist at the interface and therefore the values of concentration and partial pressure at the interface are determined by thermodynamic equilibrium relations (Henry's law).

5.1.2. Mass transfer coefficients

For diluted systems the mass transfer rate is proportional to the driving force, expressed as a molar concentration difference. Due to the one dimensional nature of the film model, the amount of solute transferred from the bulk gas phase to the interface must equal the amount transferred from the interface to the bulk liquid, and hence, the following relation holds:

$$N_A = k_L(C_{Ai} - C_A) = k_G(p_A - p_{Ai}) \qquad 5.1$$

Where N_A is the mass transfer rate expressed as moles of solute transferred per unit time per unit area; p_A and p_{Ai} are the partial pressures of the solute in the gas phase and the interface; and C_A and C_{Ai} ($\equiv C_A^*$) are the molar concentrations of the solute in the liquid bulk and the interface respectively. The liquid-side mass transfer coefficient k_L represents the amount of solute (here denoted by A) transferred through the liquid film per unit time, per unit area, per driving force unit in terms of liquid concentration. Similarly, the gas-side mass transfer coefficient k_G is the amount of solute transferred through the gas film per unit time, per unit area, per driving force unit in terms of pressure. In some simple situations mass transfer coefficients can be calculated from basic principles. For the different models shown earlier, the two-film, the penetration, and the surface renewal theories try to extend these theoretical calculations to more complex situations. Although these models are not usually very precise, they are very useful for obtaining a physical idea of the mass transfer coefficient variations. Hence, in the two-film theory, k_L is directly proportional to the solute diffusivity in the liquid and inversely proportional to the liquid film thickness. According to the penetration theory it is proportional to the square root of the diffusivity and, when all surface elements are exposed for an equal time, it is inversely proportional to the square root of time of exposure; when random surface renewal is assumed, it is proportional to the square root of the rate of renewal. In the film-penetration theory, the mass transfer coefficient is a complex function

of the diffusivity, the film thickness, and either the time of exposure or the rate of renewal of surface.

Due to the importance of mass transfer coefficients in modelling mass transfer processes many correlations[29], based either on experimental or theoretical evidence, have been developed for different geometries and working conditions. These correlations, usually based on non-dimensional numbers as Schmidt, Reynolds, etc., allow the calculation of diffusivities and mass transfer coefficients of single and multicomponent systems in gas and liquid phases.

5.1.3. Effect of chemical reaction in mass transfer

For slow gas-liquid reactions the dissolved solute molecules are transported deep into the bulk of the liquid before the reaction starts. Therefore the overall absorption rate is not increased considerably because of chemical reaction, being the rate of mass transfer controlled by the driving force (concentration difference between the interface and the bulk liquid). For very fast gas-liquid reactions, the solute molecules only penetrate slightly into the liquid film before the reaction begins, the diffusion path of the solute is very small when compared to the distance it travels in simple physical absorption. Reaction rates vary greatly from one chemical reaction system to another, from very slow to essentially instantaneous reactions. When the reaction rate is comparable to that of the mass transfer through the diffusion film, interactions must be taken into

account. The interactions can be delineated as five regimes, as shown in Figure 5.2. These are identified by the value of the Hatta number, *Ha*, which is defined as the square root of the ratio of the diffusion time, t_D, to the reaction time, t_R. For a reaction of the type

$$nA + mB \rightarrow \text{products}$$

These are defined as follows:

$$t_D = \frac{D_{AB}}{k_L^2} \qquad 5.2$$

$$t_R = \frac{n+1}{2k_{mn}C_{AL}^{n-1}C_{BL}^{m}} \qquad 5.3$$

The Hatta[30] number represents the ratio of maximal possible conversion in the film (due to reaction) to the maximum mass transfer by diffusion through the film. Thus it is possible to distinguish between very slow, slow, fast, and instantaneous reactions, with respect to physical mass transfer, depending on the value of the Hatta number[21].

For design purposes it is important to catalogue gas-liquid reactions by the magnitude of the Hatta number. Hence, for a value of $Ha > 2$ the reaction is considered to be fast and occurs completely in the gas-liquid interface, while for $Ha < 0.02$ the reaction is slow with respect to mass transfer rate and takes place principally in the liquid bulk. For reactions with $0.02 < Ha < 2$, which are very common in chemical processes, the reaction takes

place mainly in the liquid film and the process is diffusion controlled, happening some of reaction also in the liquid bulk.

	REGIME	CONDITIONS	IMPORTANT VARIABLES	CONCENTRATION PROFILES
I	*Kinetic control* Slow reaction	$\sqrt{\frac{t_D}{t_R}} < 0.02$	Rate α ϵ_L α k_{nm} α $(C^*_{AL})^n$ α $(C_{BL})^m$ Independent of *a* (if a adequate) Independent of k_L	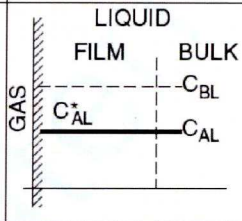
II	*Diffusion control* Moderately fast reaction in bulk of liquid $C_{AL} \approx 0$	$0.02 < \sqrt{\frac{t_D}{t_R}} < 2$ Design so that $\frac{\epsilon_L}{a} > 100 \frac{D_{AL}}{k_L}$	Rate α a α k_L α C^*_{AL} Independent of k_{nm} Independent of ϵ_L (if ϵ_L adequate)	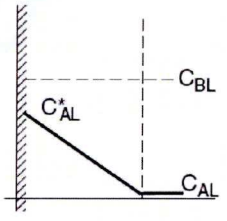
III	*Fast reaction* Reaction in film $C_{AL} \approx 0$ (pseudo first order in A')	$2 < \sqrt{\frac{t_D}{t_R}} < \frac{C_{BL}}{qC^*_{AL}}$ $C_{BL} >> C^*_{AL}$	Rate α a α $\sqrt{k_{nm}}$ α $(C^*_{AL})^{(n+1)/2}$ Independent of k_L Independent of ϵ_L	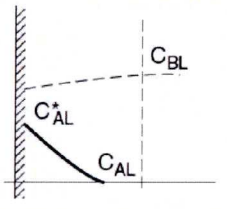
IV	*Very fast reaction* General case of III	$2 < \sqrt{\frac{t_D}{t_R}}$ $C_{BL} \sim C^*_{AL}$	Rate α a depends on k_L, k_{nm}, C^*_{AL}, C_{BL} Independent of ϵ_L	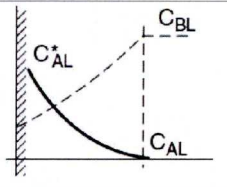
V	*Instantaneous reaction* Reaction 'at interface'. Controlled by transfer of B to interface from bulk. $J \alpha k_L a$	$\sqrt{\frac{t_D}{t_R}} >> \frac{C_{BL}}{qC^*_{AL}}$	Rate α a α k_L Independent of C^*_{AL} Independent of k_{nm} Independent of ϵ_L	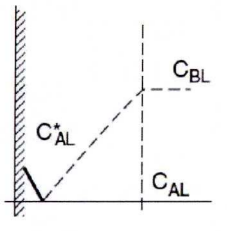

Figure 5.2. Regimes of gas–liquid mass transfer with reaction.[31] $C^*_{AL} \equiv C_{Ai}$.

31

Thus, the Hatta number defines the region where the reaction takes place from the relation of the rates of reaction and mass transport. For regimes III and IV the reaction effectively enhances the mass transfer rate, and an "enhanced" effective value of k_L is often used, defined as k^*_L.

$$k_L^* = \left[\frac{2D_{AB} k_{mn} (C_{Ai} - C_{AL})^{n-1} C_{BL}^m}{n+1} \right]^{0.5} \qquad 5.4$$

The enhancement factor, q, is defined as the ratio of the mass flux of component A through the interface with chemical reaction and driving force (C_{Ai}-C_{AL}) to the mass flux through the interface without chemical reaction, but with the same driving force. For an instantaneous reaction it can be expressed by:[16]

$$q = 1 + \left(\frac{nC_{BL}}{mC_{Ai}} \frac{D_B}{D_A} \right) \qquad 5.5$$

Hence, when q is multiplied by the physical mass transfer coefficient, the observed mass transfer coefficient in the presence of reaction is obtained.

5.2. Experimental system

5.2.1. Design: Relaxation agent appropriate for monitoring reaction

The experimental system used for the determination of gas solubility in a working catalytic reaction is that described in Chapter 2 called "NMR + GC bubble column flow system". It is based on that used for the determination of gas solubility in equilibrium (without reaction) with the addition of a GC in the return gas line, for the determination of the composition of the gas phase with time, and a forward pressure controller in the feed gas cylinder for assuring a constant pressure and gas phase composition in the reactor.

An additional design concern emerges when adding a catalyst to the four components chemical system, the use of a relaxation agent that does not affect the catalyst performance. The need for a relaxation agent to ensure the NMR measurements are quantitative has been explained in Chapter 3. The relaxation agent used for the equilibrium compositions determination, $Cr(acac)_3$ was expected to be chemically "innocent", because acetylacetonate (acac) is a chelating ligand and it should be strongly bound to the Cr(III) centre. This serves two purposes: (i) it prevents the catalyst system reacting with the Cr(III) centre, and (ii) it prevents the acac ligating the Pd(II). However, initial kinetic experiments revealed that this did not happen and this relaxation agent showed a strong negative effect on the

catalyst activity. A likely reason is that the acac dissociated from the Cr(III). This could be because the catalyst system contains a strong acid (methanesulfonic acid), which could protonate the acac to give acetylacetone acacH, which is a poor ligand for Cr(III) but might be good enough for Pd(II). In any event there would be also present "unprotected" Cr(III) present, which might do any number of unwanted reactions.

Therefore, several potential relaxation agents were screened firstly to assess their relaxation capability and secondly to determine their effect on the catalysis. The ideal situation would be that the catalyst complex itself acted as a good relaxation agent since the problem would be solved without the need of adding any additional species to the reaction media. Hence the T_1 constant, which defines the delay between pulses necessary for allowing all the spins to relax (five times T_1 approx.), of the solvents species was determined applying a saturation recovery fourier transform method (Chapter 3):

	C(O)OR	**OMe1**	**OMe2**	**CH_2**	**CH_3**
T_1 (s)	32.6	5.7	10.8	8.8	4.9

Table 5.1. T1 relaxation time constants for solvents species **without any added species.**

The carbonyl group in the methyl propanoate molecules has the longest T_1 and it would define a pulse delay between pulses of approximately 3 minutes, which is so long delay that each measurement, 64 scans, would

take 3 hours, before which time the reaction would certainly have finished. After adding the catalyst complex, in the appropriate concentration for a good reaction performance (5 ppm of Pd), the relaxation time constants T_1 were measured again, Table 5.2.

	C(O)OR	OMe1	OMe2	CH_2	CH_3
T_1 (s)	20.9	2.9	3.4	3.2	1.2

Table 5.2. T1 relaxation time constants for solvents species with **catalyst complex added**.

The catalyst Pd-complex shows a reasonably good relaxation capacity for all but the ester carbonyl C. However, it is the longest T_1 that determine the required pulse delay. Thus a delay of ca. 2 minutes between pulses is still required.

So an additional relaxation agent is needed, one that will not affect the catalyst activity and at the same time give efficient relaxation of all carbons, allowing a short delay between pulses. Gd^{3+} is another standard NMR relaxation agent and has a high magnetic moment so should have a greater "relaxing" effect than Cr^{3+}, and perhaps allow the use of lower concentrations.

The first compound tried was gadolinium chloride ($GdCl_3.8H_2O$) because it is readily available. Short relaxation time constants T_1 were observed, Table 5.3.

	C(O)OR	OMe1	OMe2	CH_2	CH_3
T_1 (s)	0.72	0.96	0.005	0.95	1

Table 5.3. T1 relaxation time constants for solvents species with **6 g/L of $GdCl_3.8H_2O$**.

$GdCl_3.8H_2O$ causes very efficient relaxation, allowing pulse delays of only 5 seconds. Unfortunately, when added to the catalyst system no reaction occurred, which is attributed to the presence of the Cl^- anion. The anion has a major impact on the catalysis, thus $GdCl_3.8H_2O$ kills the catalyst by coordination to Pd(II). However, the Gd^{3+} seems to be a good relaxation agent, so the aim at this point was to find an anion that coordinated to Gd^{3+} but did not affect the catalyst activity.

Gadolinium methanesulfonate was thought to be a good possibility since methanesulfonic acid was already present in the reaction media, hence the methanesulfonate should not affect the catalyst negatively. On adding 6 g/L of Gd-methanesulfonate, the relaxation time constants T_1 observed were (Table 5.4):

	CO	C(O)OR	C_2H_4	OMe1	OMe2	CH_2	CH_3
T_1 (s)	2.8	0.41	1.5	1.4	0.008	1.9	1.5

Table 5.4. T1 relaxation time constants for solvents species with **6 g/L of $Gd(CH_3SO_3)_3$**.

Now the highest time constant is shown by CO, defining a delay between pulses of 15 seconds, allowing liquid composition measurements each 15 minutes, which is good enough. This relaxation agent, as it was expected, did not affect the catalyst activity as confirmed by analysis performed in Lucite International laboratories at Wilton Research Centre. Hence, the Gd-methanesulfonate is a good relaxation agent for monitoring the methoxycarbonylation of ethylene reaction by NMR. Now the experimental system, after some modifications explained in Chapter 2, and the research carried out on relaxation agents appropriate for the catalyst system, is completely setup and ready for studying the reaction kinetics.

5.2.2. Experimental procedure

The experimental system and procedure used was analogous to that described in Chapter 2. Firstly the mixed solvent system for the catalytic reaction and comprising a mixture of methyl propanoate, 70 %, and methanol, 30 % mass composition, and a relaxation agent, gadolinium methanesulfonate, 6 g/L, was prepared.

The catalyst was then prepared *in situ* by the addition of the bidentate phosphine ligand 1,2-bis(di-*tert*-butylphosphinomethyl)benzene (L_2) and $[Pd_2(dba)_3]$ (dba = *trans,trans*-dibenzylideneacetone) to the solvent system to give the complex $[L_2Pd(dba)]$. Treatment of this complex with methanesulfonic acid (MsOH) generates a complex capable of converting ethylene, carbon monoxide, and methanol to methyl propanoate[32]. The

compositions of the catalyst species in the final reacting solution are: *[Pd] = 5-15 ppm*; *[L_2] = 40-50 ppm*; *[MsOH] = 2000 ppm*. The reaction solution was prepared and kept under nitrogen due to the sensitivity of the catalyst complex to oxygen.

A volume of 4 mL of the reacting solution was introduced, under nitrogen, into the reaction cell (consisting of a sapphire tube connected to the gas recirculation system described in Chapter 2). The system was then sealed, to avoid evaporation the liquid solution was frozen, and the apparatus evacuated. The reaction cell and rest of the system was then pressurized to 15 - 20 bar with a mixture of ethylene: ^{13}CO [4:1 molar ratio]. The reaction gas was then pumped at a flow rate of 30 mL/min through the reaction solution. The reaction cell was then introduced into the NMR magnet, and composition measurements taken. The reaction was initiated by raising the reactor temperature to 373 K (100 °C). Gases consumed by reaction were replenished from a ballast cylinder via a forward pressure regulator containing a mixture of ethylene: ^{13}CO [1:1 molar ratio] so that the composition of the gas phase and the total pressure of the system was constant.

The composition of the reacting solution was monitored with time by NMR. Figure 5.3 presents the NMR spectra recorded during a typical reaction. The peak at 173 ppm approx. due to the carbonyl group [$^{13}C(O)OR$] of MeP grows in intensity as the reaction proceeds. The large

magnitude of this peak with respect to the others is because of the use of ^{13}CO enriched as gas reactant.

The formation of MeP, which corresponds with the consumption of MeOH, CO, and C_2H_4, can thus be easily followed with time and the reaction rate calculated. The reaction cannot be followed so clearly using the peaks of the alkyl groups (8 and 26 ppm approx.) of MeP because these carbons are not enriched in ^{13}C, and so are of much lower intensity.

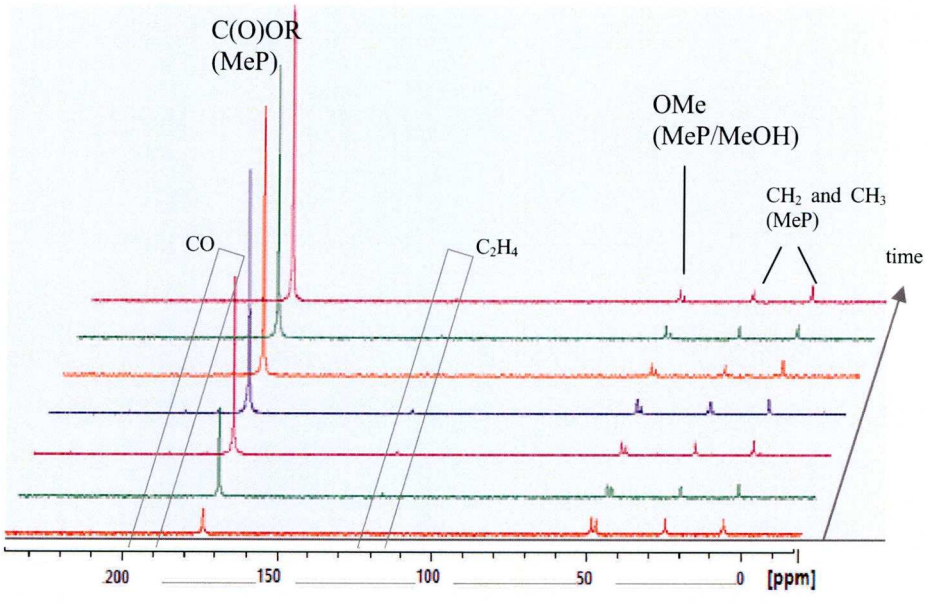

Figure 5.3. NMR spectra recorded during reaction showing production of MeP.

The increase with time in the composition of MeP can also be observed in the peaks of the methoxy groups (50 ppm approx.), present in the MeP and MeOH molecules. The ratio of the peak corresponding to the methoxy group of MeP (left) to that of MeOH (right) increases with time due to the production of MeP and consequent consumption of MeOH. The peaks of

the gaseous components, ethylene and CO, dissolved in the liquid phase are of very low intensity, and appear in the positions marked by the rectangles in Figure 5.3.

5.3. Kinetic observations.

The determination of liquid composition with time allows the calculation of the reaction rate, and so a further investigation and understanding of the reaction system. Hence, the aim of the experiments described here is the investigation of the parameters affecting the reaction rate, as well as to define the kinetic regime of the reaction in terms of which process controls the overall rate, mass transfer or reaction kinetics, and so understand where the reaction happens. The kinetic study comprises the experimental observation of how several variables affect the reaction rate. For that the initial reaction rate is experimentally determined keeping all variables constant except one, which is modified for each rate measurement. The variables investigated will be the area of contact between gas and liquid phases, the concentration of carbon monoxide in the film, and the catalyst concentration.

Reaction rates were calculated by monitoring the liquid phase concentration during reaction measured by NMR. Hence, from the increase in the MeP peak between two measurements, the time passed between them, and the total liquid volume present in the reaction cell (4 mL), values of the averaged reaction rate between two experimental measurements were performed in $^{mol}/_{L \cdot \min}$ units. The reaction rate was higher at the beginning of the reaction, as more concentration of reactants was present.

Hence, measurements performed during the first 30 minutes, when the reaction rate values were not falling yet, were used for the calculation of initial reaction rates.

5.3.1. Contact area between phases

The initial reactions performed used a flow rate of 12 mL/min and a simple PTFE dip tube to deliver gas to the reaction. No standing concentration of carbon monoxide was observed in the liquid bulk. This fact can only be explained by slow mass transfer compared with reaction, i.e. carbon monoxide is so rapidly consumed by reaction that it does not reach the bulk of the liquid reacting phase. This is an indication that under these system conditions, with slow mass transfer, the reaction happens in the liquid film. The mass transfer rate can be increased by increasing the contact surface between phases, i.e. delivering the maximum gas possible in the smallest bubbles achievable. Hence, the gas flow rate was increased to 30 mL/min, the maximum achievable before the system became so turbulent that the liquid solution was pushed out of the reaction cell, and the resolution in the NMR spectra degrades. The gas delivery tube was modified to reduce the size of the bubbles. An open ended tube delivers large gas bubbles (6 mm diameter approx). In contrast, a tube with a sealed end and perforated by two small holes at the bottom section of the tube delivers smaller bubbles (3.2 mm diameter approx) with little coalescence up through the reacting solution from the bottom to the top of the reaction cell. The change in the

contact surface area between gas and liquid with gas flow rate and bubble size is evident in Figure 5.4 which shows pictures of the reaction bubble cell at flow rates of 20, 30 and 40 mL/min using the original (right) and modified (left) gas delivery tube.

The effect of the contact surface area on the reaction rate has been determined. Two reactions have been performed, the first using the original delivery tube, i.e. with large gas bubbles, and a second identical reaction but using the modified tube, i.e. with small bubbles. The contact surface area between gas and liquid was determined by measuring the average diameter of the bubbles, and counting the number of

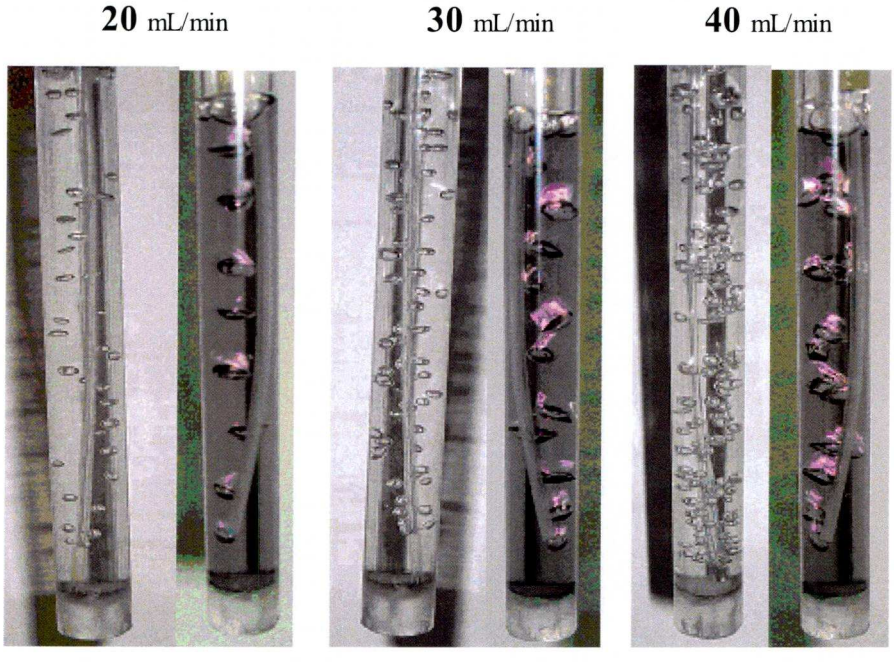

Figure 5.4. Illustrating the increase of the contact surface area by increasing the gas flow rate and decreasing bubble size.

bubbles in the reaction cell. In the first reaction the contact area between

phases was $1.1 \cdot 10^{-3}$ m^2, while for the second (small bubble size) it was $1.9 \cdot 10^{-3}$ m^2. The initial rates obtained were $2.51 \cdot 10^{-3}$ *moles MeP/h,* and $5.29 \cdot 10^{-3}$ *moles MeP/h* respectively for the two reactions, i.e. the reaction rate is proportional to the area of contact between the gas and liquid phases. This indicates that reaction takes place in the liquid film, indicating a high reaction rate with respect to mass transport.

However, this change in mass transfer rate did not affect the composition of the gaseous components dissolved in the liquid bulk. For very slow mass transfer, that is large bubbles, no carbon monoxide is dissolved in the liquid bulk because it is all reacted in the liquid film. With improved mass transfer, i.e. when small bubbles are used, a very small concentration of CO dissolved in the bulk of the liquid can be observed at the very beginning of the reaction, which disappears very quickly.

Thus, from these batch reactions examining mass transfer effects, an initial understanding of the kinetic regime of the process has been obtained. Nevertheless, a number of continuous gas feed reactions were performed changing the gas feed flowrate (20, 30, 40 mL/min), and keeping the rest of conditions the same: small size of bubbles, 1.2 bar of partial pressure of CO, 8.2 M of methanol concentration, and 5 ppm of Palladium; to obtain more evidence of the effect of the area of contact between phases in reaction rate using always small bubbles, Figure 5.5.

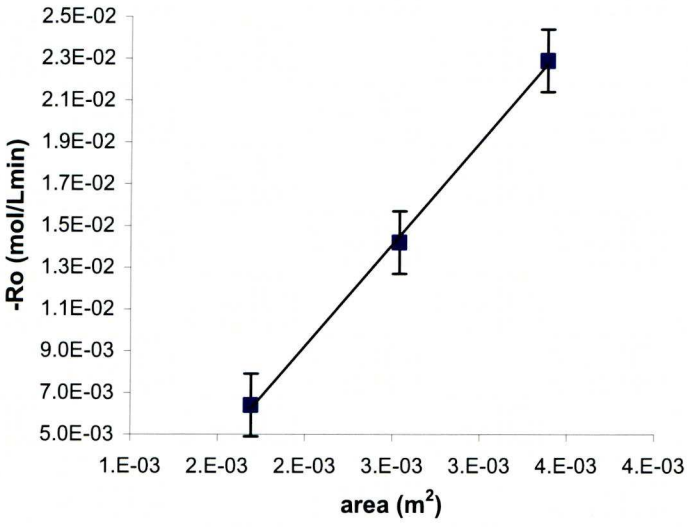

Figure 5.5. Effect of contact area between gas and liquid phases in reaction rate.

A linear relationship between reaction and contact area between phases is observed in Figure 5.5, which shows that reaction rate increased more than proportionally with area of contact between phases, i.e. doubling the area of contact, the rate increased by more than the double. This can only be explained by the fact that the area of contact was increased by increasing the volumetric flow of gas into the reaction cell, hence producing more bubbles, and therefore more area of contact with the liquid phase. But this increase in flow means also less time of residence of bubbles in the reacting solution, and so the time of reaction was shorter and the conversion achieved lower. Hence, the higher concentration of gaseous reactants (CO and C_2H_4) present gave higher reaction rates.

From Figure 5.2, this linear relation between reaction rate and area of contact leads to an initial conclusion that reaction happens in the liquid

film, with diffusion the controlling process. Under this diffusion controlled condition it is not possible to observe experimentally real kinetics and therefore no determinations of reaction rate constants can be performed. Without kinetic reaction constant values the calculation of the Hatta number is not possible, however, it is possible to determine the reaction regime from how different parameters affect the observed rate.

At this point four possible regimes must be considered depending on the reaction rate, Figure 5.2, II: moderately fast reaction, III: fast reaction, IV: very fast reaction, or V: instantaneous reaction. Hence, the next parameter to study is that of the concentration of carbon monoxide in the liquid film. If the reaction rate is not affected by its concentration we know we have an instantaneous reaction, and then the regime would be defined.

5.3.2. Concentration of CO in the liquid film

Of the two gaseous components participating in reaction, the carbon monoxide is the limiting one because its equilibrium concentration at working conditions, which will correspond with the concentration in the liquid film, is much lower than that of ethylene, which is always present in the liquid bulk.

For the investigation of the effect on reaction rate of the concentration of CO in the liquid film different determinations of the initial rate of reaction were done at different initial compositions of the gas phase. The

concentration of CO in the liquid film is the concentration at equilibrium for the conditions of temperature, pressure, and composition for each reaction rate determination. The equilibrium compositions were calculated using the thermodynamic model described in detail in Appendix A and validated in Chapter 4 by good agreement with experimental results. Hence, the equilibrium concentration of CO is varied by changing the partial pressure of CO in the gas phase. The rest of the reaction conditions are kept constant for all rate measurements, 30 mL/min of gas feed flowrate, 8.2 M of methanol concentration, small bubble size, and 5 ppm of palladium concentration.

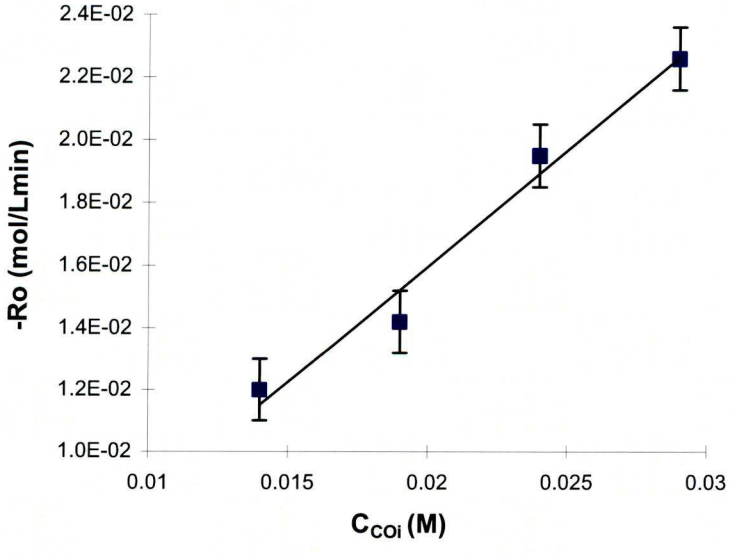

Figure 5.6. Effect of carbon monoxide film concentration in reaction rate.

A linear relation between the concentration in the liquid film of CO and the reaction rate is observed, Figure 5.6. This result eliminates the possibility of an instantaneous reaction, leaving the options of regimes II, III, and IV.

For regimes with fast reaction (III, and IV) the mass transfer process is enhanced by the presence of a reaction, so it is necessary to increase the reaction rate and see if it has any influence in the mass transfer rate.

5.3.3. Mass transfer rate enhancement by reaction

The increase in reaction rate is obtained by the increase in the catalyst concentration in the reaction media. The mass transfer rate is easily calculated from the experimental determinations applying a mass balance to carbon monoxide. Hence, the quantity of carbon monoxide transferred from the gas phase to the liquid phase equals the quantity of CO consumed in the reaction plus the quantity of CO dissolved in the liquid bulk. From the mass transfer rate calculated from experimental values applying a mass balance to CO, a mass transfer coefficient, k_{Lobs}, can be calculated, which may not be the real mass transfer coefficient since reaction can affect its value. The mass transfer rate, in terms of moles of CO transferred per time and interface unit area, divided by the driving force, in terms of the difference between the equilibrium concentration of CO and that present in the liquid bulk, gives a value for the observed mass transfer coefficient.

Now, on changing the metal concentration and keeping the rest of conditions constant, different initial rates are obtained experimentally, Figure 5.7. Actually the reaction rate increases linearly with palladium concentration, as expected, since the greater the concentration of palladium, the more active centres are present for the insertion of

methanol, carbon monoxide, and ethylene, and so faster formation of methyl propanoate results.

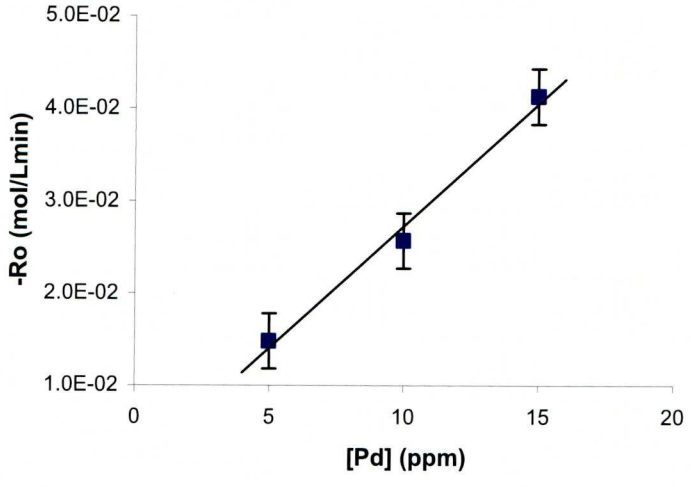

Figure 5.7. Effect of Pd concentration in reaction rate.

For each of previous reactions, a value of the observed mass transfer coefficient, k_{Lobs}, was calculated applying equation 5.1, dividing the mass transfer rate of CO by the difference between the liquid film and bulk CO concentration. The number of moles transferred from the gas to the liquid phase between two experimental measurements was equal to the difference between the moles of CO in the liquid bulk in each experimental determination, determined by NMR, plus the moles of CO reacted, which from reaction stoichiometry are identical in number to the moles of MeP produced, also calculated from NMR spectrum and liquid sample volume. Hence, dividing the moles of CO transferred by the time passed between measurements, and by the area of contact between phases ($3 \cdot 10^{-3}$ m^2), mass transfer reaction values were obtained in $mol/m^2 s$ units. With these

values of mass transfer rates, the concentration of CO in the liquid bulk determined by NMR, the concentration of CO in the liquid film calculated with the thermodynamic model developed for equilibrium calculations, and applying equation 5.1, values of k_{Lobs} in *m/s* units were obtained.

The results in Figure 5.8 show that faster mass transfer occurs with faster reaction rates. The fact that the CO transferred is rapidly consumed makes the gradient of CO concentration through the liquid film high at all times resulting in the increase of mass transfer. This result reduces the possibilities to regimes III and IV, with fast reaction rate. As the concentration of CO in the liquid film is much lower than the concentration of methanol in the reaction media, it is concluded that the regime observed in this gas-liquid reaction is III, that of fast pseudo first order in CO reaction in the liquid film (Figure 5.2).

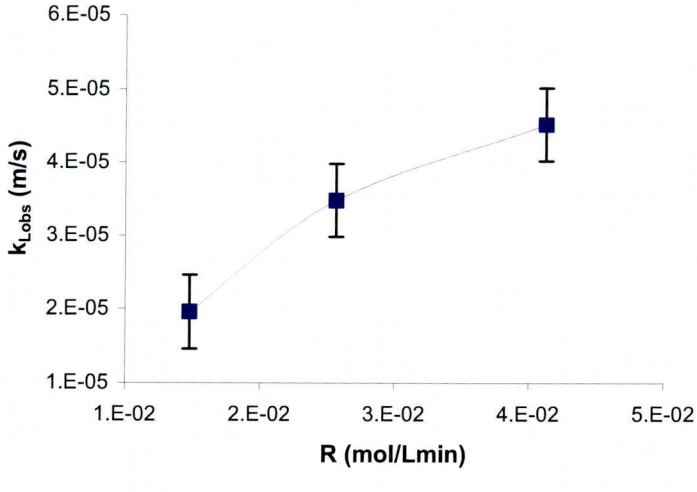

Figure 5.8.Mass transfer coefficient as a function of reaction rate.

Note that regime III, as defined in Figure 5.2, does not depend on mass transfer coefficient k_L. Figure 5.8 shows that reaction rate depends on k_{Lobs} but this does not mean that k_L affects reaction rate. In fact, k_{Lobs} is an observed mass transfer coefficient. In fact, it is defined as the theoretical coefficient, k_L, affected by the reaction "enhancement factor", which accounta for the influence of reaction in mass transfer rate, as shown in equations 5.4 and 5.5. Hence, reaction rate affects the "enhancement" factor and so k_{Lobs} values, but it does not depend on k_L.

We cannot calculate Hatta numbers from experimental results because of the diffusion controlled regime, but we know from experimental observations that the value of the Hatta number for this catalytic gas-liquid reaction performed in the bubble column used in this project must be higher than 2.

5.4. Conclusions

The methoxycarbonylation of ethylene in a bubble column reactor has been studied using the NMR technique. After an investigation of relaxation agents, searching for one which did not affect the catalyst performance, $Gd(MeSO_3)_3$ was found to allow for frequent NMR composition measurements not affecting the reaction. Some modifications of the gas delivery tube to improve the mass transfer were done. The effects on reaction rates observed of the area of contact between gas and liquid phases, and the composition of CO in the liquid film were investigated, as well as the enhancement in mass transfer due to reaction. These experimental observations allowed the definition of the reaction regime in terms of mass transport and reaction rates, concluding that the reaction occurs in the liquid film because of the slow mass transport with respect to reaction rate.

5.5. References

(1) Astarita, G.; Savage, D. W.; Bisio, A. *Gas Treating with Chemical Solvents*. John Wiley & Sons, New York, 1983.

(2) Vaidya, P. K.; Kenig, E. Y. Gas–liquid reaction kinetics: A review of determination methods. *Chem. Eng. Commun.* **2007**, *194 (10-12)*, 1543.

(3) Blauwhoff, P.M.M.; Versteeg, G.F.; van Swaaij, W.P.M. A study on the reaction between CO_2 and alkanolamines in aqueous solutions. *Chem. Eng. Sci.* **1984**, *39 (2)*, 207.

(4) Cullen, E.J.; Davidson, J.F. Absorption of gases in liquid jets. *Trans. Faraday Soc.* **1957**, *53*, 113.

(5) Nijsing, R.A.T.O.; Hendriksz, R.H.; Kramers, H. Absorption of CO_2 in jets and falling films of electrolyte solutions with and without chemical reaction. *Chem. Eng. Sci.* **1959**, *10*, 88.

(6) Laddha, S.S.; Danckwerts, P.V. Reaction of CO_2 with ethanolamines: kinetics from gas-absorption. *Chem. Eng. Sci.* **1981**, *36 (3)*, 479.

(7) Littel, R.J.; van Swaaij, W.P.M.; Versteeg, G.F. Kinetics of carbon dioxide with tertiary amines in aqueous solution. *AIChE J.* **1990**, *36 (11)*, 1633.

(8) Pani, F.; Gaunand, A.; Cadours, R.; Bouallou, C.; Richon, D. Kinetics of absorption of CO_2 in concentrated aqueous methyldiethanolamine solutions in the range of 296 K to 343 K. *J. Chem. Eng. Data.* **1997**, *42 (2)*, 353.

(9) Rangwala, H.A.; Morrell, B.R.; Mather, A.E.; Otto, F.D. Absorption of CO_2 into aqueous tertiary amine/MEA solutions. *Can. J. Chem. Eng.* **1992**, *70 (3)*, 482.

(10) Xu, S.; Wang, Y.W.; Otto, F.D.; Mather, A.E. Kinetics of the reaction of carbon dioxide with 2-amino-2-methyl-1-propanol solutions. *Chem. Eng. Sci.* **1996**, *51 (6)*, 841.

(11) Hikita, H.; Asai, S.; Ishikawa, H.; Honda, M. The kinetics of reactions of carbon dioxide with monoethanolamine, diethanolamine and triethanolamine by a rapid mixing method. *Chem. Eng. J.* **1977**, *13*, 7.

(12) Barth, D.; Tondre, C.; Delpuech, J.J. Stopped-flow investigations of the reaction kinetics of carbon dioxide with some primary and secondary alkanolamines in aqueous solution. *Int. J. Chem. Kinet.* **1986**, *18 (4)*, 445.

(13) Romanien, J. J.; Salmi, T. The effect of reaction kinetics, mass transfer and pattern on non-catalytic and homogeneously catalyzed gas-liquid reactions in bubble columns. *Chem. Eng. Sci.* **1992**, *47 (9-11)*, 2493.

(14) Maalej, S.; Benadda, B.; Otterbein, M. Interfacial area and volumetric mass transfer coefficient in a bubble reactor at elevated pressures. *Chem. Eng. Sci.* **2003**, *58 (11)*, 2365.

(15) Stegeman, D.; Knop, P. A.; Wijnands, A. J. G.; Westerterp, K. R. Interfacial area and gas holdup in a bubble column reactor at elevated pressures. *Ind. Eng. Chem. Res.* **1996**, *35 (11)*, 3842.

(16) Danckwerts, P. V. *Gas-Liquid Reactions*. McGraw-Hill, New York, 1970.

(17) Charpentier. J. C. What's new in absorption with chemical reaction? *Trans. IChemE.* **1982**, *60*, 131.

(18) Van Krevelen, D. W.; Hoftijzer. P.J. Kinetics of gas- liquid reactions. Part I: General Theory. *Rec. Trav. Chim. Pays-Bas.* **1948**, *67*, 563.

(19) Hikita, H.; Asai. S. Gas Absorption with (m,n)-th order. Irreversible chemical reaction. *Int. J. Chem. Eng.* **1964**, *4*, 332.

(20) Doraiswamy, L. K.; Sharma, M. M. *Heterogeneous Reactions: Analysis, Examples and Reactor Design*. John Wiley & Sons, New York, Vol. 2, 1984.

(21) Whitman, W. G. The two-film theory of gas absorption. *Chem. Met. Eng.* **1923**, *29 (4)*, 147.

(22) Higbie, R. The rate of absorption of pure gas into a still liquid during

short periods of exposure. *Trans. AIChE J.* **1935**, *31*, 365.

(23) Danckwerts, P. V. Significance of liquid film coefficients in gas absorption. *Ind. Eng. Chem.* **1951**, *43 (6)*, 1460.

(24) Toor, H. L.; Marchello, J. M. Film-penetration model for mass and heat transfer. *AIChE J.* **1958**, *4*, 97.

(25) Westerterp, K.R.; van Swaaij, W.P.M.; Beenackers, A.A.C.M. *Chemical Reactor Design and Operation*. 2nd Edition. John Wiley & Sons, New York, 1984.

(26) Landau, L. Desorption with a chemical reaction. *Chem. Eng. Sci.* **1992**, *47 (7)*, 1601.

(27) Parulekar, S.J.; Saidina Amin, N.A. Complex gas-liquid reactions: Feedback from bulk liquid to liquid-side film. *Chem. Eng. Sci.* **1996**, *51 (10)*, 2079.

(28) Elk, E. P. Gas-liquid reactions. Influence of liquid bulk and mass transfer on process performance. *PhD Thesis, Twente University*. **2001**.

(29) Perry, R. H.; Green, D. W. *Perry's chemical engineers handbook.* McGraw-Hill, New York, 7th Ed., Vol. 1. 2001.

(30) Hatta, S. On the absorption velocity of gases by liquids. *Tech. Rep. Tohoku Imp. Univ.* **1932**, *10*, 119.

(31) Middleton, J. C.; Harnby, N.; Nienow, A. W.; Edwards, M. F. *Mixing in the Process Industries. Gas–liquid dispersion and mixing.* 2nd Edition. Butterworth-Heinemann, Oxford, 1997.

(32) Clegg, W.; Eastham, G. R.; Elsegood, M. R. J.; Tooze, R. P.; Wang, X. L.; Whiston, K. Highly active and selective catalysts for the production of methyl propanoate via the methoxycarbonylation of ethene. *Chem. Commun.* **1999**, 1877.

Chapter 6

Conclusions

Chapter 6: Conclusions

6.1. Overall conclusions

A novel High Pressure NMR bubble column has been designed for the study of gas solubilities in working catalytic reactions. Specifically, the project has focused on the Alpha process for the production of methyl propanoate via the methoxycarbonylation of ethylene using a palladium-based phosphine ligand catalyst.

The interest of driving force for the development of the new HPNMR bubble column system was the problem of gas starvation observed in previous gas solubility determinations in reacting gas-liquid systems, and the lengthy equilibration times necessary in studies in which a much simpler sapphire NMR tube system was used.[1] This novel experimental design avoids both these problems and also allows easy control of working conditions. The system has been validated by the reproduction of gas solubilities results reported in the literature.[2, 3, 4]

A crucial design issue encountered with the new NMR bubble column was the need for a condenser to avoid loss of liquid solvent due to evaporation at high temperatures. Therefore, a copper tube, with cooling water flowing through it, is wound around the exit gas line, cooling it and allowing the solvent to condense. It was also found necessary to increase the diameter of the exhaust gas line, allowing unconstrained drainage of condensed fluids

back into the equilibrium cell, so that the exit gas flowing upwards did not drag droplets of liquid condensate further up the exit gas lines.

The chemical system studied consisted of a gas phase formed by carbon monoxide and ethylene, and a liquid solvent mixture of MeP:MeOH [70:30 % wt.]. The low solubility of carbon monoxide, coupled with the low NMR sensitivity of carbon at natural abundance (^{13}C = 1.1%) led to the use of ^{13}C enriched carbon monoxide to amplify its NMR peak intensity, allowing accurate experimental determination of the liquid composition. A standard NMR relaxation agent, $Cr(acac)_3$, was needed to level and reduce the spin-lattice relaxation times, making quantitative NMR measurements feasible within a practical timescale.

A thermodynamic model based on the Redlich-Kwong[5] equation of state and the UNIQUAC[6] activity coefficient method, to resolve the gas and the liquid phases respectively, was developed to perform vapour-liquid equilibrium calculations. Results from these calculations, performed with Aspen Plus, were compared with the experimental results in order to validate the model which was found to be reliable across the full range of working conditions.

The experimental measurements of equilibrium liquid phase composition were performed using the HPNMR bubble column, whilst the experimental determination of gas phase composition required the design of a new independent experimental system. The latter was achieved by replicating

the equilibrium conditions in an analogous bubble column experimental system but using on-line Gas Chromatography as the analytical technique instead of NMR.

Gas solubility is a crucial parameter affecting gas-liquid reaction performance given that the gaseous components must dissolve in the reacting liquid solution for the reaction to happen. If gases are too soluble they might have an adverse on the catalyst activity, e.g. high concentrations of CO can lead to deactivation/decomposition of the palladium-based phosphine ligand catalyst. On the other hand, if the gas solubilities are too low the reaction might be controlled by mass transfer processes and not by kinetics. Thus, a detailed study of the vapour-liquid equilibrium of the four-component chemical system of interest was performed to understand the saturation conditions before any reaction kinetic observations were done.

Meaningful comparisons of solubilities of CO and C_2H_4 in MeP:MeOH [70:30% wt.] were made by evaluation of their Henry's coefficient values. First experimental observations showed that the solubility of CO was much lower than that of C_2H_4 in the solvent mixture MeP:MeOH [70:30 % wt.]. The observation that the solubilities of CO and C_2H_4 showed different behaviour with temperature, i.e. the solubility of CO increased with increasing temperature, whilst that of C_2H_4 decreased at higher temperatures added to the interest and complexity of the study. An

investigation of the thermodynamics of mixing[7] led to the explanation that the different behaviour with temperature was due to opposite changes in entropy and enthalpy occurring during the process of dissolution of CO and C_2H_4 in the liquid solvent. The use of the computer calculations using the thermodynamic model showed that the dissolution of CO in MeP:MeOH [70:30 % wt.] was an endothermic process with a positive change in entropy, whereas it was exothermic, with a negative entropy change, for C_2H_4.

Carbon monoxide and ethylene solubilities showed different trends when mixed at different gas phase compositions. The solubility of CO decreased at high composition in the gas phase, whilst ethylene was more soluble when concentrated. Deviations from ideality confirm this observation, i.e. CO activity coefficient is lower than unity, leading to negative deviations from ideality, but the C_2H_4 activity coefficient is larger than unity, resulting in positive deviations.

After this detailed study and consequent understanding of the equilibrium conditions of the gas-liquid system under study, reaction kinetics and gas solubilities during reaction were investigated.

The first concern for the kinetic study, arose from the high reaction rate, thus an NMR relaxation agent which did not affect the catalyst activity yet afforded fast spin-lattice relaxation was needed. $Cr(acac)_3$, the standard NMR relaxation agent used in the VLE studies, proved to be a catalyst

poison. Therefore other relaxation agents were investigated including gadolinium chloride and gadolinium methanesulfonate. Gadolinium methanesulfonate, $Gd(CH_3SO_3)_3$, was chosen as the relaxation agent since it did not affect catalyst activity and it gave short relaxation times at low concentration.

In gas-liquid reactions, the gaseous components dissolve in the liquid reacting solvent as the reaction occurs. Hence, mass transfer should be increased to the maximum possible so that the overall process is controlled by the reactions kinetics. In fact, the first reactions performed showed that no CO was present in the bulk liquid during reaction, meaning that mass transfer was limiting the overall process. To increase mass transfer, the gas flow rate was increased to 30 mL/min, the maximum flow possible without losing NMR spectral resolution, and the gas delivery PTFE dip tube was modified so that it produced much smaller bubbles, therefore increasing the surface of contact between phases. Some further modifications were made to the HPNMR bubble column system to allow constant gas phase composition, by replenishing the gas consumed by reaction, and a GC was introduced in the return gas line from the reaction cell to measure experimentally gas composition at all times. These modifications enabled the monitoring of liquid and gas phase composition during reaction, required for reaction rate calculations.

The kinetic study consisted of the investigation of different parameters affecting the reaction rate in order to find the process controlling the overall rate. It was found that the reaction rate was enhanced by increasing the contact area between phases, which led to the initial conclusion that mass transfer was the controlling process in this study. The linear relationship between the concentration of CO in the liquid film (considered to be at equilibrium condition) and the reaction rate is most consistent with reaction occurring in the liquid film. Finally, a faster mass transfer rate was observed at higher catalyst concentrations (faster reaction), consistent with a reaction of pseudo-first order in CO in the liquid film in which the mass transfer is enhanced by chemical reaction.

6.2. Future work

The work done in this project could be completed by further investigating the reaction kinetics. A new experimental design allowing for faster composition measurements during reaction, so that more compositions could be retrieved at the initial stage of the reaction, would be an interesting progress for the investigation, as well as would be achieving faster mass transfer allowing for the determination of true reaction kinetics not affected by mass transfer.

Fast NMR experiments could be achieved by reducing the spin relaxation time. A new reaction cell design, "draught tube", in which the NMR coil region, where the sample is excited, is continuously replenished with relaxed solution could allow for fast relaxation and rapid pulse repetition. This new design could be as represented in Figure 6.1.

The gas bubbles (black arrows) would be introduced into the liquid above the NMR region, flowing upwards within a concentric inner tube generating a continuous flow of liquid solution (red arrows) within the reaction cell. The green area, NMR region, would be continuously fed with relaxed material (light blue). This is just an initial idea that could be further developed.

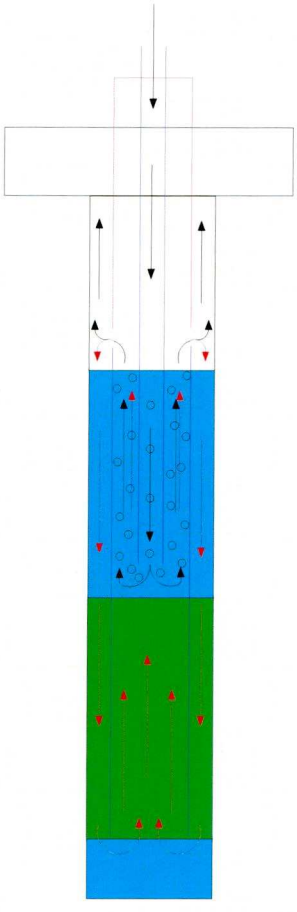

Figure 6.1. Draught tube.

For increasing the mass transfer rate would be necessary to get smaller bubbles, more area of contact between phases, and better mixing. Smaller bubbles could probably be obtained doing some modifications to the gas delivery tube. Smaller bubbles could also allow higher volumetric rates of gas fed to the reaction cell and better mixing, hence increasing the mass transfer rate. Another option could be to slow down the reaction rate, instead of increasing the mass transfer. Parameters affecting the reaction rate have been identified in this project. A study of exactly how these variables affect the reaction, by obtaining accurate relations, combined

with a sufficiently fast mass transfer, might give the possibility of controlling the reaction rate, slowing it down and looking at true reaction kinetics not affected by mass transfer.

6.3. References

(1) Roe, D. C.; Kating, P. M.; Krusic, P. J.; Smart, B. E. High resolution NMR techniques in catalysis. *Top. Catal.* **1998**, *5 (1-4)*.

(2) Konobeev, B. I.; Lyapin, V. V. Solubility of ethylene and propylene in organic solvents. *Khim. Prom. Ukr.* **1967**, *43*, 144.

(3) Liu, Q.; Takemura, F.; Yabe, A. Solubility and diffusivity of carbon monoxide in liquid methanol. *J. Chem. Eng. Data.* **1996**, *41 (3)*, 589.

(4) Tonner, S. P.; Wainwright, M. S.; Trimm, D. L. Solubility of carbon monoxide in alcohols. *J. Chem. Eng. Data.* **1983**, *28*, 59.

(5) Redlich, O.; Kwong, J. N. S. On the Thermodynamics of solutions V. An equation-of-state. Fugacities of gaseous solutions. *Chem. Rev.* **1979**. *44*, 223.

(6) Abrams, D. S.; Prausnitz, J. M. Statistical thermodynamics of liquid mixtures: A new expression for the excess Gibbs energy of partly or completely miscible systems. *AIChE J.* **1975**, *21*, 116.

(7) Prausnitz, J. M. et al. *Molecular thermodynamics of fluid-phase equilibria.* 3rd Edition. Prentice Hall, Englewood Cliffs, NJ, 1999.

Appendix

Appendix A: Thermodynamic model calculations

The activity coefficient model proposed in Chapter 1 is based on following equilibrium relations:

$$f_i^v = f_i^l \tag{1.15}$$

$$\varphi_i^v y_i P = \gamma_i x_i f_i^{0l} \tag{1.16}$$

Fugacity coefficient

The vapour phase fugacity coefficient, φ_i^v, is calculated according to following expression:

$$\ln \varphi_i^v = \frac{1}{RT} \int_V^\infty \left[\left(\frac{\partial P}{\partial n_i} \right)_{T,V,n_j} - \frac{RT}{V} \right] dV - \ln Z \tag{1.17}$$

Where V is the gas phase volume. The fugacity coefficient is then resolved applying the Redlich-Kwong equation of state:

$$P = \frac{RT}{\overline{V} - b} - \frac{a}{\overline{V}\left(\overline{V} + b\right)} \tag{1.18}$$

where $\overline{V}$ is the gas phase molar volume.

Alternatively it can be given in terms of the compressibility factor Z:

$$Z = \frac{P\overline{V}}{RT} \tag{1.19}$$

$$Z = \frac{\overline{V}}{\overline{V} - b} - \frac{a\overline{V}}{RT(\overline{V}^2 + b\overline{V})} \qquad 1.20$$

The two parameters a and b are given by:

$$a = \frac{0.42748R^2T_c^{2.5}}{P_cT^{0.5}} \qquad 1.21$$

$$b = \frac{0.08664RT_c}{P_c} \qquad 1.22$$

where P_c and T_c are the critical pressure and temperature respectively. For multi-component systems mixing rules are used to determine the parameter values. The mixing rules used are:

$$\sqrt{a} = \sum_i y_i \sqrt{a_i} \qquad 1.23$$

$$b = \sum_i y_i b_i \qquad 1.24$$

The pure component saturated volume is given by the Rackett equation:

$$\overline{V} = \frac{RT_c\left(Z^{RA}\right)^{\left[1+(1-T_r)^{2/7}\right]}}{P_c} \qquad 1.36$$

where Z^{RA} is the Rackett compressibility factor. Liquid mixture molar volumes are calculated by using the ideal mixing rules (the total volume of the mix is the addition of the volumes of its components).

	CO	C_2H_4	MeOH	MeP
Tc (K)	132.92	282.34	512.64	530.6
Pc (Pa)	349.9+06	5.040+06	8.097+06	4.004+06
Z_{RA}	0.2896	0.2808	0.2353	0.2566

Table A.1. Values of T_c, P_c, and Z_{RA} used in the calculations.

Hence, for the resolution of the fugacity coefficient (1.17) it is necessary to resolve first $\left(\frac{\partial P}{\partial n_i}\right)_{T,V,n_j}$:

$$\left(\frac{\partial P}{\partial n_i}\right)_{T,V,n_j} = \frac{\partial\left(\frac{RT}{V/n - b}\right)_{T,V,n_j}}{\partial n_i} - \frac{\partial\left(\frac{a}{\left(V/n\right)^2 + bV/n}\right)_{T,V,n_j}}{\partial n_i} =$$

$$= RT\frac{\partial\left(\frac{n}{V - nb}\right)_{T,V,n_j}}{\partial n_i} - \frac{\partial\left(\frac{an^2}{V^2 + nb}\right)_{T,V,n_j}}{\partial n_i} =$$

$$= RT\frac{\partial(n)_{T,V,n_j}/\partial n_i \cdot (V - nb) - n \cdot \partial(V - nb)_{T,V,n_j}/\partial n_i}{(V - nb)^2} -$$

$$- \frac{\partial(an^2)_{T,V,n_j}/\partial n_i \cdot (V^2 + nbV) - an^2 \cdot \partial(V^2 + nbV)_{T,V,n_j}/\partial n_i}{(V + nbV)^2} \qquad \text{A.1}$$

Developing separately each derivation:

$$\Rightarrow \frac{\partial(n)_{T,V,n_j}}{\partial n_i} = \frac{\partial\left(\sum_i^{NC} n_i\right)_{T,V,n_j}}{\partial n_i} = \frac{\partial n_i}{\partial n_i} = 1$$

$$\Rightarrow \frac{\partial(b)_{T,V,n_j}}{\partial n_i} = \frac{\partial\left(\sum_i^{NC} y_i b_i\right)_{T,V,n_j}}{\partial n_i} = b_i \frac{\partial(y_i)_{T,V,n_j}}{\partial n_i} + \sum_{j\neq i}^{NC-1} b_j \frac{\partial(y_j)_{T,V,n_j}}{\partial n_j} =$$

$$= b_i \frac{\partial\left(n_i/n\right)_{T,V,n_j}}{\partial n_i} + \sum_{j\neq i}^{NC-1} b_j \frac{\partial\left(n_j/n\right)_{T,V,n_j}}{\partial n_j} = b_i \frac{n-n_i}{n^2} + \sum_{j\neq i}^{NC-1} b_j \frac{-n_j}{n^2} =$$

$$= \frac{(n-n_i)b_i - \sum_{j\neq i}^{NC-1} b_j n_j}{n^2} = \frac{b_i - b}{n}$$

$$\Rightarrow \frac{\partial(V-nb)_{T,V,n_j}}{\partial n_i} = -\left(\frac{\partial(n)_{T,V,n_j}}{\partial n_i}\cdot b + n\cdot\frac{\partial(b)_{T,V,n_j}}{\partial n_i}\right) = -b - n\frac{b_i - b}{n} = -b_i$$

$$\Rightarrow \frac{\partial(a)_{T,V,n_j}}{\partial n_i} = \frac{\partial\left(\left(\sum_i^{NC} y_i\sqrt{a_i}\right)^2\right)_{T,V,n_j}}{\partial n_i} = 2\cdot\sum_i^{NC} y_i\sqrt{a_i}\cdot\frac{\partial\left(\sum_i^{NC} y_i\sqrt{a_i}\right)_{T,V,n_j}}{\partial n_i} =$$

$$= 2\sqrt{a}\cdot\left(\sqrt{a_i}\cdot\frac{\partial(y_i)_{T,V,n_j}}{\partial n_i} + \frac{\partial\left(\sum_{j\neq i}^{NC-1} y_j\sqrt{a_j}\right)_{T,V,n_j}}{\partial n_i}\right) = 2\sqrt{a}\left(\sqrt{a_i}\left(\frac{n-n_i}{n^2}\right) - \sum_{j\neq i}^{NC-1}\frac{n_j\sqrt{a_j}}{n^2}\right) =$$

$$= 2\sqrt{a}\left(\sqrt{a_i}\left(\frac{1-y_i}{n}\right) - \sum_{j\neq i}^{NC-1}\frac{y_j\sqrt{a_j}}{n}\right) = \frac{2\sqrt{a}}{n}\left(\sqrt{a}_i - \sqrt{a}\right)$$

$$\Rightarrow \frac{\partial\left(an^2\right)_{T,V,n_j}}{\partial n_i} = \frac{\partial(a)_{T,V,n_j}}{\partial n_i}\cdot n^2 + a\cdot\frac{\partial\left(n^2\right)_{T,V,n_j}}{\partial n_i} = 2n\sqrt{a}\cdot\left(\sqrt{a_i}-\sqrt{a}\right)+2na = 2n\sqrt{a}\sqrt{a_i}$$

$$\Rightarrow \frac{\partial\left(V^2+nb\right)_{T,V,n_j}}{\partial n_i} = V\left(\frac{\partial(n)_{T,V,n_j}}{\partial n_i}\cdot b + n\cdot\frac{\partial(b)_{T,V,n_j}}{\partial n_i}\right) = V\left(b+n\frac{b_i-b}{n}\right) = Vb_i$$

Hence, equation A.1 can be rewritten as follows:

$$\left(\frac{\partial P}{\partial n_i}\right)_{T,V,n_j} = \frac{RT}{(V-nb)^2}\left(V-nb+nb_i\right)-\frac{2\sqrt{a}\sqrt{a_i}\cdot n\left(V^2+nbV\right)-an^2\cdot Vb_i}{\left(V^2+nbV\right)^2}$$

Rewriting now equation 1.17 defining the fugacity coefficient:

$$\ln\varphi_i^v = \frac{1}{RT}\int_V^\infty\left[\frac{RT\left(V-nb+nb_i\right)}{(V-nb)^2}-\frac{2\sqrt{a}\sqrt{a_i}\cdot n\left(V^2+nbV\right)}{\left(V^2+nbV\right)^2}-\frac{ab_in^2V}{\left(V^2+nbV\right)^2}\right]dV-\ln Z =$$

$$=\frac{1}{RT}\left[RT\left(\frac{-nb}{V-nb}+\ln(V-nb)+\frac{nb}{V-nb}\right)+\left(\frac{-RTnb_i}{V-nb}\right)--2\sqrt{a}\sqrt{a_i}\cdot n\left(\frac{1}{nb}\ln\left(\frac{V}{V+nb}\right)\right)-\right.$$
$$\left.-ab_in^2\left(\frac{1}{nb(nb+V)}+\frac{1}{n^2b^2}\ln\left(\frac{V}{V+nb}\right)\right)-RT\ln V\right]_V^\infty-\ln Z =$$

$$=\left[\ln(V-nb)-\frac{nb_i}{V-nb}-\frac{2\sqrt{a}\sqrt{a_i}}{RTb}\ln\left(\frac{V}{V+nb}\right)-\frac{ab_in}{b(V+nb)}-\frac{ab_i}{b^2}\ln\left(\frac{V}{V+nb}\right)-\ln V\right]_V^\infty-\ln Z$$

By definition, the limit $V\to\infty$ corresponds with:

$$P\to 0\Leftrightarrow Z\to 1\Leftrightarrow\varphi_i^v\to 1\Leftrightarrow\ln\varphi_i^v\to 0$$

Hence, the value of the equation between brackets at the boundary $V \to \infty$ equals $(\ln Z)$ and so:

$$\ln \varphi_i^v = \ln Z - \ln\left(\overline{V} - b\right) + \frac{b_i}{\overline{V} - b} + \left(\frac{2\sqrt{a}\sqrt{a_i}}{RTb} + \frac{ab_i}{b^2}\right)\ln\left(\frac{\overline{V}}{\overline{V} + b}\right) + \frac{ab_i}{b\left(\overline{V} + b\right)} - \ln \overline{V} - \ln Z$$

$$\boxed{\ln \varphi_i^v = \ln\left(\frac{\overline{V}}{\overline{V} - b}\right) + \frac{2b\sqrt{a}\sqrt{a_i} + RTab_i}{RTb^2}\ln\left(\frac{\overline{V}}{\overline{V} + b}\right) + \frac{b_i}{\overline{V} - b} + \frac{ab_i}{b\left(\overline{V} + b\right)}} \qquad \text{A.2}$$

Liquid phase activity coefficient

The liquid phase activity coefficient is given by the UNIQUAC equation:

$$\ln \gamma_i = \ln\left(\frac{\Phi_i}{x_i}\right) + \frac{z}{2} q_i \ln\left(\frac{\theta_i}{\Phi_i}\right) + l_i - \frac{\Phi_i}{x_i}\sum_j x_j l_j +$$

$$+ q_i\left[1 - \ln\left(\sum_j^{NC} \theta_j \tau_{ji}\right) - \sum_j^{NC} \frac{\theta_j \tau_{ij}}{\sum_k^{NC} \theta_k \tau_{kj}}\right] \qquad 1.25$$

Where:

$$\Phi_i = {r_i x_i}/{r_T} \; ; \; r_T = \sum_k^{NC} r_k x_k \qquad \theta_i = {q_i x_i}/{q_T} \; ; \; q_T = \sum_k^{NC} q_k x_k$$

$$l_i = \frac{z}{2}\left(r_i - q_i\right) + 1 - r_i \qquad \tau_{ij} = \exp\left(a_{ij} + {b_{ij}}/{T} + c_{ij} \ln T + d_{ij} T + {e_{ij}}/{T^2}\right)$$

$z = 10$

r_i = pure component property, van der Waals volume parameter for molecule i (Table A.2).

q_i = pure component property, van der Waals surface area parameter for molecule i (Table A.2).

T = absolute temperature.

a_{ij}, b_{ij}, c_{ij}, d_{ij} and e_{ij} are binary parameters (Table A.3).

	CO	C_2H_4	*MeOH*	*MeP*
r_i	1.0679	1.57416	1.43111	3.47858
q_i	1.112	1.488	1.432	3.116

Table A.2. Values used for the resolution of the UNIQUAC equation.

i	*CO*	*CO*	*CO*	*CO*	*C2H4*	*C2H4*	*C2H4*	*C2H4*
j	*CO*	*C2H4*	*MeOH*	*MeP*	*CO*	*C2H4*	*MeOH*	*MeP*
aij	0	0	0	0	0	0	0	0
bij	0	0	0	0	0	0	-144.865	0
cij	0	0	0	0	0	0	0	0
dij	0	0	0	0	0	0	0	0
eij	0	0	0	0	0	0	0	0
i	*MeOH*	*MeOH*	*MeOH*	*MeOH*	*MeP*	*MeP*	*MeP*	*MeP*
j	*CO*	*C2H4*	*MeOH*	*MeP*	*CO*	*C2H4*	*MeOH*	*MeP*
aij	0	0	0	0.29199	0	0	0.010522	0
aij	0	0	0	0.29199	0	0	0.010522	0
bij	0	-13023.2	0	-408.75	0	0	22.382	0
cij	0	0	0	0	0	0	0	0
dij	0	0	0	0	0	0	0	0
eij	0	0	0	0	0	0	0	0

Table A.3. Values of binary coefficients used for resolution of UNIQUAC equation.

Henry's constant

For light dissolved gases the reference state is defined to be at infinite dilution and at the temperature and pressure of the mixtures. The liquid

phase reference fugacity is defined as the Henry's constant for that component in the mixture. Thus, the phase equilibrium relationship for a dissolved gas becomes:

$$\varphi_i^v y_i P = x_i \gamma_i^0 H_i \qquad 1.28$$

where

$$\gamma_i^0 = \frac{\gamma_i}{\gamma_i^\infty} \qquad 1.29$$

where γ_i^∞ is the activity coefficient of component *i* at infinite dilution.

Henry's constant is calculated for a dissolved gas component *i,* for one or more solvents (*A,B*), by the following:

$$\ln\left(H_i / \gamma_i^\infty\right) = \sum_A w_A \ln\left(H_{iA} / \gamma_{iA}^\infty\right) \qquad 1.31$$

where $\gamma_i^\infty \equiv \gamma_i$ at $x_i = 0$

$$w_A = \frac{x_A (V_{cA})^{2/3}}{\sum_B x_B (V_{cB})^{2/3}} \qquad 1.32$$

$$\ln H_{iA}\left(T, p_A^0\right) = a_{iA} + b_{iA}/T + c_{iA} \ln T + d_{iA} T + e_{iA}/T^2 \qquad 1.33$$

	CO	C_2H_4	*MeOH*	*MeP*
Vc (m^3/kmol)	0.0944	0.131	0.1180	0.282

Table A.4. Critical volume values of pure components used in simulations.

i *j*	*CO* *MeOH*	*CO* *MeP*	C_2H_4 *MeOH*	C_2H_4 *MeP*
aij *(K)*	86.9474	16.7289	20.6312	15.4734
bij *(K)*	-3113.31	509.750	-1054.03	-719.82
cij *(K)*	-10.0276	0	0	0.15527
dij *(K)*	0	0	0	0.005046
eij *(K)*	0	0	0	0

Table A.5. Parameters for the Henry's coefficient calculation (1.33).

The vapour pressure of a pure component, p_i^0, is calculated using the extended Antoine equation:

$$\ln p^0 = c_1 + \frac{c_2}{T + c_3} + c_4 T + c_5 \ln T + c_6 T^{c_7} \qquad 1.39$$

where c_i are experimentally determined constants.

	CO	C_2H_4	*MeOH*	*MeP*
c_1 (Pa)	45.698	74.242	81.768	70.717
c_2 (K)	-1076.6	-2707.2	-6876	-6439.7
c_3 (K)	0	0	0	0
c_4 (K)	0	0	0	0
c_5 (K)	-4.8814	-9.8462	-8.7078	-6.9845
c_6 (K)	7.5673e-05	2.2457e-02	7.1926e-06	2.0129e-17
c_7 (K)	2	1	2	6

Table A.6. Parameters for the calculation of the vapour pressure with the Antoine equation.

The Henry's constant can be corrected for pressure by the Poynting factor:

$$H_{iA}(T,P) = H_{iA}(T,p_A^0)\exp\left(\frac{1}{RT}\int_{p_A^0}^{P} V_{iA}^{\infty}\,dp\right) \qquad 1.18$$

where V_{iA}^{∞} is the volume of supercritical component *i* at infinite dilution in pure solvent *A* and is obtained from the Brelvi O'Connel model.

The general form of the Brelvi-O'Connell model is:

$$\frac{V_{iA}^{\infty}}{Z_A^{RA} RT} = 1 - C_{12}^0$$

Where Z_A^{RA} is the Rackett compressibility of the pure solvent, and C_{12}^0 is calculated by the following relation:

$$\ln\left[-C_{12}^0\left(\frac{V_A^{BO}}{V_i^{BO}}\right)^{0.62}\right] = -2.4467 + 2.12074\cdot\tilde{\rho} \qquad 2 \le \tilde{\rho} \le 2.785$$

$$= 3.012214 - 1.87085\cdot\tilde{\rho} + 0.71955\cdot\tilde{\rho}^2 \qquad 2.785 \le \tilde{\rho} \le 3.2$$

Where $\tilde{\rho} = \rho_A V_A^{BO}$ is the density of the pure solvent reduced by its characteristic volume (V_A^{BO}). This characteristic volume for simple substances corresponds with the critical volume.

	CO	C_2H_4	*MeOH*	*MeP*
V_i^{BO} (m^3/kmol)	0.0932441	0.12868	0.117916	0.282

Table A.7. Characteristic volume for the Brelvi-O'Connel model.

The pure component liquid density is given by the DIPPR equation:

$$\rho_l = \frac{c_1}{c_2^{\left(1+(1-T/c_3)^{c4}\right)}} \qquad 1.37$$

	CO	C_2H_4	MeOH	MeP
c_1 (m^3/kmol)	2.897	2.0961	2.288	0.9147
c_2 (K)	0.27532	0.27657	0.2685	0.2594
c_3	132.92	282.34	512.64	530.6
c_4 (K)	0.2813	0.29147	0.2453	0.2774

Table A.8. Parameters for the resolution of the DIPPR equation for the liquid density.

Hence summarising, looking at the equation of equilibrium (1.28): $\varphi_i^v y_i P = x_i \gamma_i^0 H_i$, the fugacity coefficient in the gas phase, φ_i^V, has been defined as a function of the composition of the gas phase, y_i (A1.2), via the Redlich-Kwong equation of state; the activity coefficient, γ_i^0, is a function of the liquid phase composition, y_i (1.,25), via the UNIQUAC equation; and the Henry's constant is calculated as a function of the liquid phase composition as well with equation 1.31. Therefore, at a fixed temperature and pressure, the only unknown variables are the compositions of the liquid and gas phases.

Flash calculation

Applying a mass balance to the flash block where the equilibrium takes place, and knowing the initial compositions x_i^F and y_i^F, it is possible to calculate the compositions of the gas and liquid phases in equilibrium by an iterative calculation. The component mass balance to the flash block is as follows:

$$Fz^F = L_F x_i^F + V_F y_i^F = L x_i + V y_i$$

So it is possible to express the composition of a component in one phase related to its component in the other phase. The flash calculation is defined by *T, P,* and *V/L* ratio. Hence, knowing T_c, P_c, and $\overline{V}$, the fugacity and activity coefficient are calculated using the known initial feed compositions. For the calculation of H_i is also necessary the determination of the vapour pressure with the Antoine equation, the supercritical components volumes at infinite dilution via the Brelvi-O'Connel model, and the liquid density calculated with the DIPPR equation.

$$\varphi_i^v\left(y_i^F\right)y_i P = x_i \gamma_i^0\left(x_i^F\right)H_i$$

$$x_i = \frac{Fz^F - Vy_i}{L}$$

All flows/quantities *L*, *V*, and *F* are known. Hence, from the equilibrium relation above and the component mass balance it is possible to calculate the compositions of NC-1 (all components except one). The last component composition is calculated by:

$$x_j = 1 - \sum_{i \neq j}^{NC-1} x_i$$

Then it is checked if the compositions calculated are equal to those used for the calculation of the fugacity and activity coefficient (feed compositions in this case). If the compositions do not correspond with

those used for the calculations, another calculation is performed using the new values of the compositions obtained:

$$\varphi_i^v\left(y_i^j\right)y_i^{j+1}P = x_i^{j+1}\gamma_i^0\left(x_i^j\right)H_i$$

$$x_i^{j+1} = \frac{Fz^F - Vy_i^{j+1}}{L}$$

This is how the compositions of the liquid and gas phases in equilibrium are calculated with the thermodynamic model proposed. These calculations are performed in Aspen Plus defining a flash block as shown in Figure A.1:

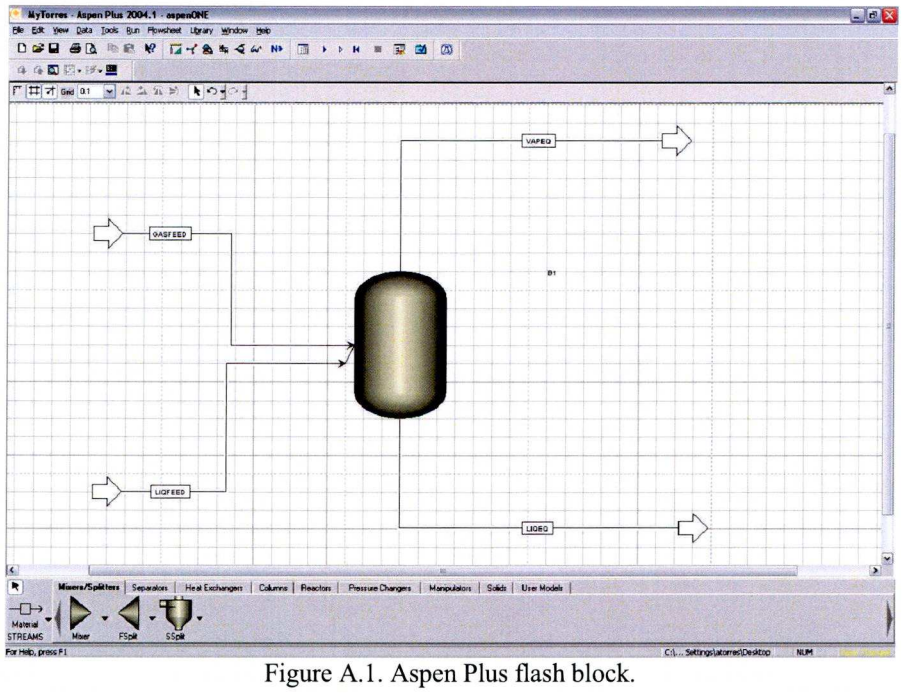

Figure A.1. Aspen Plus flash block.

The property method Redlich Kwong equation of state combined with UNIQUAC activity coefficient method and Henry's supercritical components are defined:

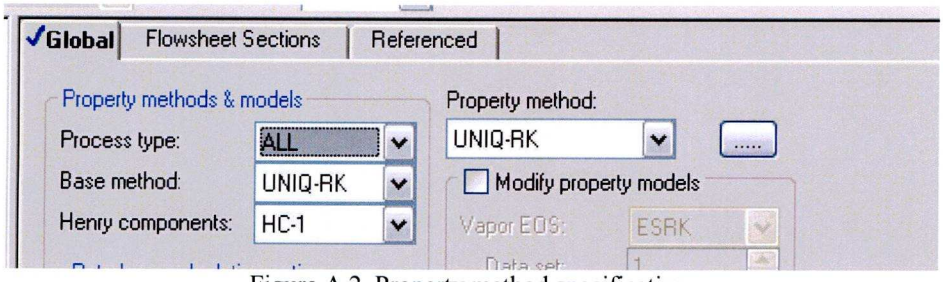

Figure A.2. Property method specification.

The characterization of the feed gas and liquid streams is done as shown in following figures:

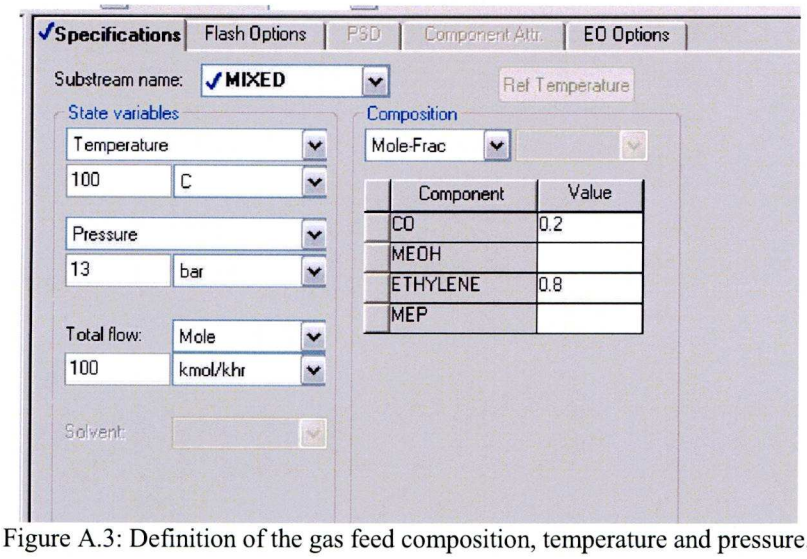

Figure A.3: Definition of the gas feed composition, temperature and pressure.

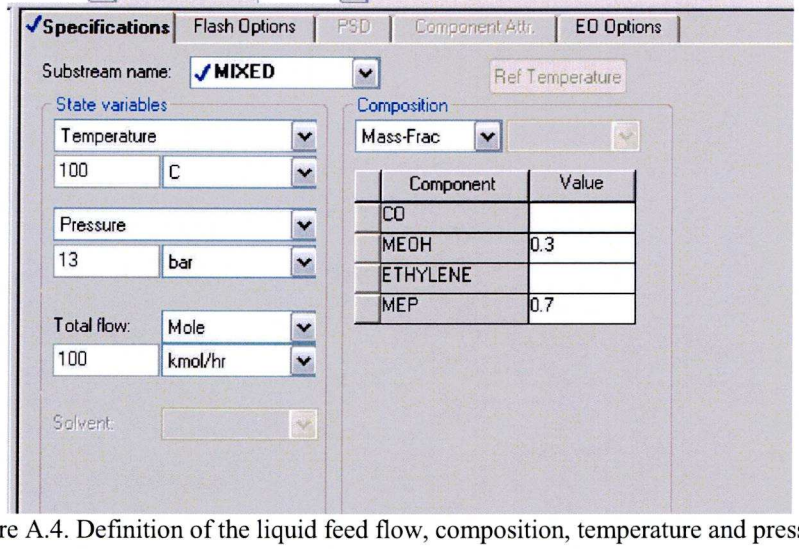

Figure A.4. Definition of the liquid feed flow, composition, temperature and pressure.

The next step is to define the conditions within the flash block. As explained in Chapter 1 (pages 42 - 44) the conditions fixed within the flash block are temperature, pressure, and L/V ratio. In the flash block determination Aspen Plus allows fr the definition of two of these conditions, and so pressure and L/V ratio are defined.

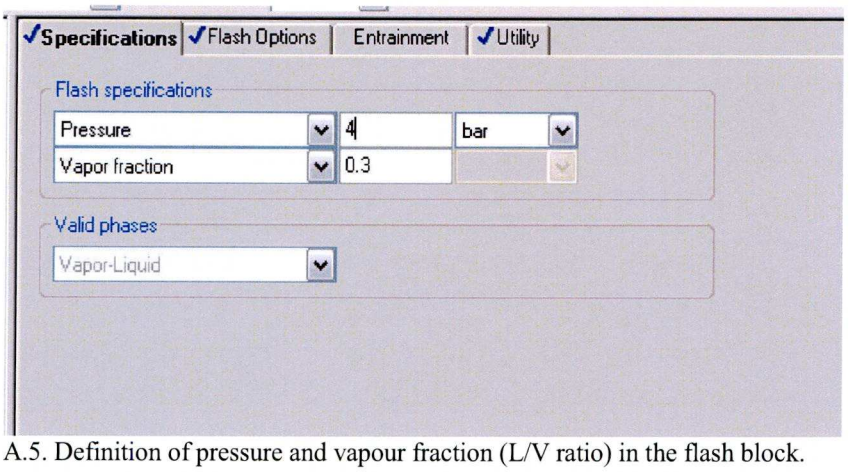

Figure A.5. Definition of pressure and vapour fraction (L/V ratio) in the flash block.

The temperature of equilibrium is fixed through the hot gas feed flow with the design specification tool.

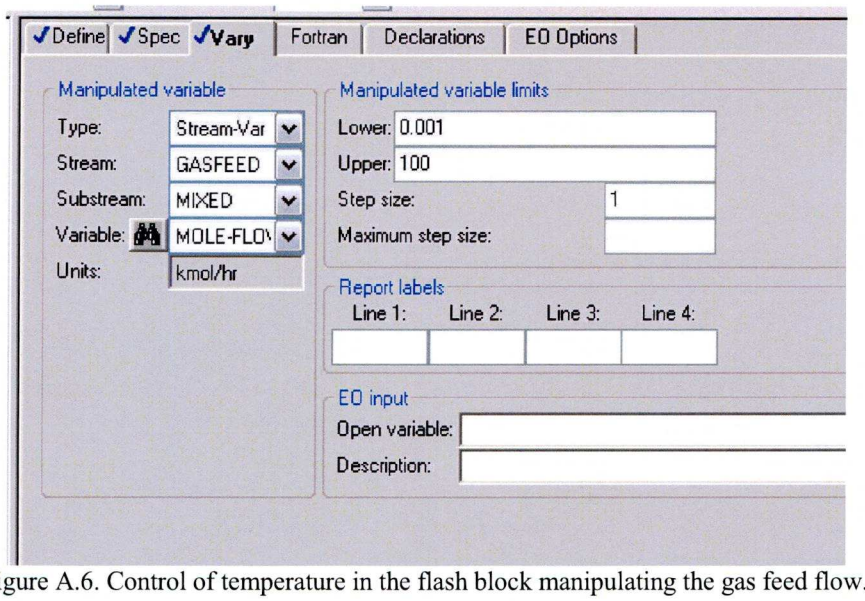

Figure A.6. Control of temperature in the flash block manipulating the gas feed flow.

Finally, a report with the results is obtained after running the simulator. In figure A.7 is represented the convergence report of the design specification and in figure A.8 the stream results:

```
CONVERGENCE STATUS SUMMARY
 -------------------------

   DESIGN-SPEC SUMMARY
   ===================

   DESIGN                                                          CONV
   SPEC       ERROR          TOLERANCE     ERR/TOL       VARIABLE   STAT  BLOCK
   ------     -----          ---------     -------       --------   ----  -----
   DS-3      -0.81683E-04   0.10000E-02 -0.81683E-01    25.408      #    $OLVER01

   #  = CONVERGED
   *  = NOT CONVERGED
   LB = AT LOWER BOUNDS
   UB = AT UPPER BOUNDS

 DESIGN-SPEC:  DS-3
 ------------------

   SAMPLED VARIABLES:
     TEMP      : TEMPERATURE IN STREAM LIQPROD SUBSTREAM MIXED

   SPECIFICATION:
     MAKE TEMP APPROACH 70.0000
     WITHIN           0.0010000

   MANIPULATED VARIABLES:
     VARY      : TOTAL MOLEFLOW IN STREAM GASFEED SUBSTREAM MIXED
     LOWER LIMIT =           0.0010000                 KMOL/HR
     UPPER LIMIT =         100.000                     KMOL/HR
     FINAL VALUE =          25.4077                    KMOL/HR

   VALUES OF ACCESSED FORTRAN VARIABLES:
     VARIABLE       VALUE AT START      FINAL VALUE      UNITS
                       OF LOOP
     --------       --------------      -----------      -----
     TEMP            -22.0505            69.9999         C
```

Figure A.7. Control loop convergence report.

GASFEED GASPROD LIQFEED LIQPROD

STREAM ID	GASFEED	GASPROD	LIQFEED	LIQPROD
FROM :	----	B1	----	B1
TO :	B1	----	B1	----
SUBSTREAM: MIXED				
PHASE:	VAPOR	VAPOR	LIQUID	LIQUID
COMPONENTS: KMOL/HR				
CO	16.4985	16.3582	0.0	0.1403
C2H4	8.9092	8.4388	0.0	0.4704
MEPROP.	0.0	4.3080	43.0000	38.6920
METHANOL	0.0	8.5173	57.0000	48.4827
COMPONENTS: MOLE FRAC				
CO	0.6494	0.4348	0.0	1.5980-03
C2H4	0.3507	0.2243	0.0	5.3581-03
MEPROP.	0.0	0.1145	0.4300	0.4408
METHANOL	0.0	0.2264	0.5700	0.5523
COMPONENTS: KG/HR				
CO	462.1290	458.1997	0.0	3.9293
C2H4	249.9367	236.7411	0.0	13.1955
MEPROP.	0.0	379.5610	3788.5718	3409.0107
METHANOL	0.0	272.9120	1826.4031	1553.4911
COMPONENTS: MASS FRAC				
CO	0.6490	0.3401	0.0	7.8907-04
C2H4	0.3510	0.1757	0.0	2.6499-03
MEPROP.	0.0	0.2817	0.6747	0.6846
METHANOL	0.0	0.2025	0.3253	0.3120
TOTAL FLOW:				
KMOL/HR	25.4077	37.6223	100.0000	87.7854
KG/HR	712.0656	1347.4139	5614.9749	4979.6266
CUM/HR	60.0451	263.2836	7.2264	6.1559
STATE VARIABLES:				
TEMP C	100.0000	69.9999	100.0000	69.9999
PRES BAR	13.0000	4.0000	13.0000	4.0000
VFRAC	1.0000	1.0000	0.0	0.0
LFRAC	0.0	0.0	1.0000	1.0000
SFRAC	0.0	0.0	0.0	0.0
ENTHALPY:				
KJ/KMOL	-5.0850+04	-1.2878+05	-3.2342+05	-3.2883+05
KJ/KG	-1814.4202	-3595.7544	-5759.9201	-5796.8742
KW	-358.8851	-1345.8248	-8983.8352	-8018.4081
ENTROPY:				
KJ/KMOL-K	31.0353	-41.7354	-311.4066	-325.3426
KJ/KG-K	1.1074	-1.1653	-5.5460	-5.7354
DENSITY:				
KMOL/CUM	0.4231	0.1429	13.8382	14.2605
KG/CUM	11.8589	5.1177	777.0126	808.9249
AVG MW	28.0256	35.8142	56.1497	56.7250

Figure A.8. Stream results report.

Here has been presented an example of an equilibrium calculation for a gas feed composition of C_2H_4:CO 4:1 molar ratio, a liquid feed of MeP:MeOH 70:30 % wt., at a pressure of 4 bar and 70 ºC of temperature.

Appendix B: Gas Chromatography

The GC used consists on a 1 meter long Silco steel column (Hayesep D 80-100 Lot 174). The carrier gas (Helium) pressure is 1.4 bar with a flowrate of 20.5 mL/min. Volume of Valco 314U sample valve is 2 microliters. A typical spectrum recorded for the four components chemical system: CO, C2H4, MeOH, MeP, is shown in following picture.

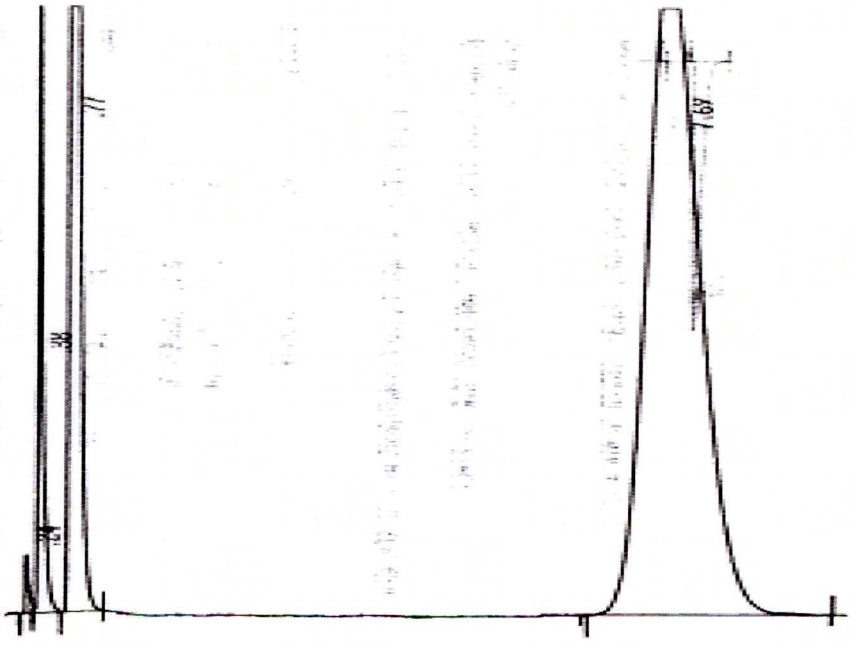

Figure B.1. Typical GC spectrum.

Appendix C: Heat of solution of gases

This appendix shows the derivation of equations 4.5 and 4.6 based in the development found in a publication by Sherwood and Prausnitz (reference 12 in Chapter 4).

The total differential of the chemical potential of a component (2) in a homogeneous phase of two components is given by:

$$d\mu_2 = -\bar{s}_2 dT + \bar{v}_2 dP + \left(\frac{\partial \mu_2}{\partial \ln x_2}\right)_{T,P} d\ln x_2 \qquad \text{C.1}$$

Writing Eq. B.1 for both liquid and vapour phases:

$$d\left(\mu_2^l - \mu_2^g\right) = -\left(\bar{s}_2^l - \bar{s}_2^g\right)dT + \left(\bar{v}_2^l - \bar{v}_2^g\right)dP + \left(\frac{\partial \mu_2^l}{\partial \ln x_2}\right)_{T,P} d\ln x_2 - \left(\frac{\partial \mu_2^g}{\partial \ln y_2}\right)_{T,P} d\ln y_2 \qquad \text{C.2}$$

For both phases in equilibrium: $\mu_2^l = \mu_2^g$ and since the identity: $\mu_2^l = \bar{h}_2 - T\bar{s}_2$ can be written for both phases:

$$\bar{s}_2^l - \bar{s}_2^g = \frac{\bar{h}_2^l - \bar{h}_2^g}{T} \equiv \frac{\Delta \bar{h}_2}{T} \qquad \text{C.3}$$

The chemical potential in the liquid phase is related to the liquid phase activity coefficient.

$$d\mu_2^l = RTd\ln\gamma_2$$

$$\left(\frac{\partial \mu_2^l}{\partial \ln x_2}\right)_{T,P} = RT\left[1+\left(\frac{\partial \ln \gamma_2}{\partial \ln x_2}\right)_{T,P}\right] \qquad \text{C.4}$$

Similarly it can be related to the vapour phase fugacity coefficient.

$$d\mu_2^g = RTd\ln \phi_2 y_2 P$$

$$\left(\frac{\partial \mu_2^g}{\partial \ln y_2}\right)_{T,P} = RT\left[1+\left(\frac{\partial \ln \phi_2}{\partial \ln y_2}\right)_{T,P}\right] \qquad \text{C.5}$$

Substituting equations B.4, B.4, and B.5 into B.2 and rearranging:

$$\frac{\Delta \bar{h}_2}{R} = \left[1+\left(\frac{\partial \ln \phi_2}{\partial \ln y_2}\right)_{T,P}\right]\cdot\left(\frac{\partial \ln y_2}{\partial 1/T}\right)_P - \left[1+\left(\frac{\partial \ln \gamma_2}{\partial \ln x_2}\right)_{T,P}\right]\cdot\left(\frac{\partial \ln x_2}{\partial 1/T}\right)_P \qquad \text{C.6}$$

Assuming that the solvent is essentially non-volatile and the activity coefficient of the solute is independent of the composition due to its low solubility:

$$\left(\frac{\partial \ln y_2}{\partial 1/T}\right)_P = 0 \quad \text{and} \quad \left(\frac{\partial \ln \gamma_2}{\partial \ln x_2}\right)_{T,P} = 0$$

And hence it is obtained the final expression:

$$\left(\frac{\partial \ln x_2}{\partial 1/T}\right)_P = -\frac{\Delta \bar{h}_2}{R} \qquad 4.6$$

From equation B.3 the entropy of mixing is related to the enthalpy by:

$$\Delta\bar{s}_2 = \frac{\Delta\bar{h}_2}{T} \text{ and so } \quad \left(\frac{\partial \ln x_2}{\partial \ln T}\right)_P = \frac{\Delta\bar{s}_2}{R} \qquad 4.5$$

Appendix D: Experimental results

D.1. CO and C_2H_4 solubility in MeOH

T / K	P / barA	literature *x(ethene)*	experimental *x(ethene)*
313	2.90	0.0080	0.0080
	8.24	0.024	0.024
	17.80	0.057	0.060
333	2.90	0.0050	0.0050
	8.29	0.019	0.018
	17.95	0.048	0.048

T / K	P / barA	literature *x(CO)*	experimental *x(CO)*
300	5.19	1.93E-03	2.00E-03
373	5.86	3.18E-03	2.90E-03
323	9.66	3.80E-03	3.90E-03
344	10.35	4.10E-03	4.30E-03
333	14.90	5.20E-03	5.90E-03
323	20.05	8.07E-03	7.90E-03

Table D.1. Experimentally determined CO and C_2H_4 solubilties in MeOH compared with literature reported values.

D.2. CO solubility in MeP/MeOH [70:30 % wt.]

T / K	P/ barA	X(CO)
323	0.60	0.00E+00
	1.64	6.89E-04
	2.74	1.37E-03
	4.67	2.74E-03
	6.23	4.08E-03
	7.65	5.14E-03
343	1.40	0.00E+00
	1.50	0.00E+00
	2.60	1.15E-03
	4.11	1.88E-03
	6.19	3.61E-03
	8.16	4.99E-03
363	2.70	0.00E+00
	3.25	2.64E-04
	4.90	1.68E-03
	6.06	2.16E-03
	8.73	4.43E-03

Table D.2. Solubility of CO in liquid solvent MeP/MeOH [70:30 % wt.] experimentally measured in the sapphire tube 'static' experimental system.

T / K	P / barA	P_{CO} / bar	x(CO)
323	0.62	0.02	0.00E+00
	4.92	4.32	3.31E-03
	9.12	8.52	6.99E-03
	11.87	11.28	9.38E-03
	14.77	14.18	1.19E-02
	17.79	17.20	1.41E-02
343	1.35	0.05	0.00E+00
	4.89	3.59	2.89E-03
	9.14	7.86	6.78E-03
	11.86	10.58	9.21E-03
	14.83	13.56	1.19E-02
	17.86	16.58	1.45E-02
373	3.66	0.18	0.00E+00
	4.90	1.45	1.58E-03
	9.08	5.67	5.66E-03
	11.89	8.50	8.50E-03
	14.89	11.49	1.13E-02
	17.92	14.52	1.38E-02

Table D.3. Solubility of CO in liquid MeP/MeOH [70:30 % wt.] measured using the NMR bubble column flow system.

D.3. C_2H_4 solubility in MeP/MeOH [70:30 % wt.]

T / K	P / barA	P_{ethene} / bar	x(C_2H_4)
323	0.62	0.02	0.00E+00
	4.97	4.38	2.99E-02
	8.31	7.75	5.49E-02
	12.96	12.41	8.77E-02
	15.32	14.78	1.04E-01
	19.13	18.61	1.34E-01
343	1.35	0.05	0.00E+00
	5.05	3.77	1.87E-02
	8.44	7.20	4.24E-02
	13.07	11.86	6.78E-02
	15.49	14.30	8.19E-02
	19.28	18.12	1.08E-01
373	3.66	0.18	0.00E+00
	5.14	1.72	1.19E-02
	8.58	5.23	2.44E-02
	13.22	9.91	4.64E-02
	15.69	12.44	5.81E-02
	19.47	16.28	7.63E-02

Table D.4. Solubility of C_2H_4 in liquid MeP/MeOH [70:30 % wt.] measured using the NMR bubble column flow system.

D.4. CO/C_2H_4 solubility in MeP/MeOH [70:30 % wt.]

y_{C2H4}/y_{CO} = 0.5

T / K	P / barA	x(CO)	$x(C_2H_4)$
323	0.62	0.00E+00	0.00E+00
	2.14	6.61E-04	4.00E-03
	4.76	2.24E-03	7.83E-03
	9.28	4.78E-03	1.89E-02
	15.06	8.37E-03	2.70E-02
343	1.35	0.00E+00	0.00E+00
	2.20	5.01E-04	8.76E-05
	4.80	2.01E-03	6.77E-03
	9.36	5.04E-03	1.46E-02
	15.12	8.09E-03	2.34E-02
373	3.66	0.00E+00	0.00E+00
	4.86	9.58E-04	2.13E-03
	9.46	3.88E-03	8.16E-03
	15.20	7.50E-03	1.51E-02

Table D.5. Solubility of C_2H_4 and CO mixed in a molar ratio 1:2, respectively, in solvent MeP/MeOH [70:30 % wt.] using the NMR bubble column flow system at different temperatures and pressures.

y_{C2H4}/y_{CO} = 2.5

T / K	P / barA	x(CO)	$x(C_2H_4)$
323	0.62	0.00E+00	0.00E+00
	2.54	5.47E-04	8.11E-03
	4.22	8.03E-04	1.59E-02
	4.22	7.88E-04	1.54E-02
	7.22	1.55E-03	2.93E-02
	9.87	2.43E-03	4.43E-02
	13.03	3.42E-03	5.86E-02
	15.84	4.28E-03	7.11E-02
343	1.35	0.00E+00	0.00E+00
	2.61	3.34E-04	4.96E-03
	4.28	6.75E-04	1.12E-02
	7.29	1.58E-03	2.35E-02
	9.94	2.43E-03	2.97E-02
	13.12	3.31E-03	4.28E-02
	15.94	4.17E-03	5.76E-02
373	3.66	0.00E+00	0.00E+00
	4.34	3.02E-04	2.01E-03
	7.40	1.13E-03	1.03E-02
	10.04	1.93E-03	2.11E-02
	13.23	2.89E-03	2.90E-02
	16.06	3.62E-03	3.68E-02

Table D.6. Solubility of C_2H_4 and CO mixed in a molar ratio 2.5:1, respectively, in solvent MeP/MeOH [70:30 % wt.] using the NMR bubble column flow system at different temperatures and pressures.

y_{C2H4}/y_{CO} = 5.7

T / K	P / barA	x(CO)	$x(C_2H_4)$
323	0.62	0.00E+00	0.00E+00
	2.51	2.51E-04	9.80E-03
	4.62	5.92E-04	2.12E-02
	7.39	9.80E-04	3.18E-02
	10.35	1.55E-03	5.22E-02
	12.74	1.99E-03	6.68E-02
	12.77	1.92E-03	5.96E-02
	12.78	2.00E-03	6.44E-02
	14.97	2.36E-03	7.61E-02
	17.97	3.04E-03	9.58E-02
	23.57	4.00E-03	1.21E-01
343	1.35	0.00E+00	0.00E+00
	2.59	1.78E-04	4.50E-03
	4.68	4.67E-04	1.40E-02
	7.546	9.06E-04	2.57E-02
	10.43	1.39E-03	3.77E-02
	12.87	1.92E-03	4.91E-02
	12.90	1.83E-03	4.93E-02
	15.10	2.24E-03	6.25E-02
	18.10	2.85E-03	7.56E-02
	23.71	3.90E-03	9.52E-02
373	3.66	0.00E+00	0.00E+00
	7.55	6.17E-04	1.64E-02
	10.56	1.17E-03	2.41E-02
	13.03	1.62E-03	3.08E-02
	13.04	1.56E-03	3.17E-02
	15.27	1.90E-03	4.03E-02
	18.27	2.50E-03	5.07E-02
	23.90	3.60E-03	7.62E-02

Table D.7. Solubility of C_2H_4 and CO mixed in a molar ratio 5.7:1, respectively, in solvent MeP/MeOH [70:30 % wt.] using the NMR bubble column flow system at different temperatures and pressures.

y_{C2H4}/y_{CO} = 7.8

T / K	P / barA	x(CO)	$x(C_2H_4)$
323	0.62	0.00E+00	0.00E+00
	2.18	1.40E-04	7.45E-03
	4.11	3.56E-04	1.58E-02
	7.25	7.40E-04	4.21E-02
	9.74	9.71E-04	5.66E-02
	12.12	1.21E-03	6.54E-02
	15.29	1.66E-03	9.32E-02
	17.98	2.11E-03	1.06E-01
343	1.35	0.00E+00	0.00E+00
	2.26	7.87E-05	3.94E-03
	4.18	2.46E-04	1.16E-02
	7.33	5.94E-04	2.85E-02
	9.79	8.78E-04	4.16E-02
	12.15	1.21E-03	5.36E-02
	15.44	1.57E-03	6.73E-02
	18.16	2.05E-03	9.05E-02
373	3.66	0.00E+00	0.00E+00
	4.22	9.70E-05	4.36E-03
	7.43	3.74E-04	1.34E-02
	9.90	7.00E-04	2.13E-02
	12.26	1.08E-03	3.06E-02
	15.48	1.47E-03	4.67E-02
	18.33	1.94E-03	6.36E-02

Table D.8. Solubility of C_2H_4 and CO mixed in a molar ratio 7.8:1, respectively, in solvent MeP/MeOH [70:30 % wt.] using the NMR bubble column flow system at different temperatures and pressures.

y_{C2H4}/y_{CO} = 14

T / K	P / barA	x(CO)	$x(C_2H_4)$
323	0.62	0.00E+00	0.00E+00
	2.26	9.47E-05	9.79E-03
	4.28	2.34E-04	2.14E-02
	6.92	4.28E-04	3.52E-02
	9.34	5.50E-04	5.15E-02
	11.71	7.20E-04	7.00E-02
	14.23	9.45E-04	8.73E-02
343	1.35	0.00E+00	0.00E+00
	4.33	2.03E-04	1.68E-02
	7.01	3.59E-04	2.94E-02
	9.39	5.29E-04	3.83E-02
	11.80	7.54E-04	5.11E-02
	14.31	9.47E-04	6.38E-02
373	3.66	0.00E+00	0.00E+00
	4.41	1.18E-04	6.12E-03
	7.13	2.35E-04	1.43E-02
	9.49	4.34E-04	2.35E-02
	11.92	6.27E-04	3.32E-02
	14.42	7.99E-04	4.13E-02
	17.00	9.85E-04	5.57E-02

Table D.9. Solubility of C_2H_4 and CO mixed in a molar ratio 14:1, respectively, in solvent MeP/MeOH [70:30 % wt.] using the NMR bubble column flow system at different temperatures and pressures.

y_{C2H4}/y_{CO} = 25

T / K	P / barA	x(CO)	$x(C_2H_4)$
323	0.62	0.00E+00	0.00E+00
	3.10	3.26E-05	1.41E-02
	4.58	7.69E-05	2.30E-02
	6.29	1.48E-04	3.30E-02
	8.33	2.66E-04	4.78E-02
	10.07	3.02E-04	6.16E-02
	12.26	3.96E-04	7.73E-02
	12.34	3.86E-04	7.70E-02
	14.86	5.51E-04	9.39E-02
	17.88	6.58E-04	1.17E-01
	23.49	9.18E-04	1.50E-01
343	1.35	0.00E+00	0.00E+00
	6.37	1.20E-04	2.63E-02
	8.43	2.18E-04	3.92E-02
	10.17	2.46E-04	4.57E-02
	12.54	3.61E-04	6.16E-02
	15.02	4.89E-04	7.14E-02
	18.09	6.13E-04	9.04E-02
	23.65	8.73E-04	1.25E-01
373	3.66	0.00E+00	0.00E+00
	8.56	2.05E-04	2.06E-02
	10.31	2.35E-04	2.88E-02
	12.75	2.77E-04	3.63E-02
	15.22	4.95E-04	4.42E-02
	18.30	6.30E-04	6.04E-02
	23.85	8.51E-04	8.30E-02

Table D.10. Solubility of C_2H_4 and CO mixed in a molar ratio 25:1, respectively, in solvent MeP/MeOH [70:30 % wt.] using the NMR bubble column flow system at different temperatures and pressures.

D.5. Gas phase equilibrium composition for liquid solvent MeP/MeOH [70:30 % wt.] and gas phase C_2H_4/CO [5:1 molar ratio] system.

T = 323 K				
P / barA	**y(CO)**	**y(C_2H_4)**	**y(MeOH)**	**y(MeP)**
0.43	0.000	0.000	0.574	0.426
0.43	0.000	0.000	0.592	0.408
0.44	0.000	0.000	0.673	0.327
0.44	0.000	0.000	0.707	0.293
0.45	0.000	0.000	0.706	0.343
0.64	0.000	0.207	0.389	0.287
0.87	0.000	0.436	0.288	0.199
1.12	0.054	0.515	0.199	0.171
1.58	0.075	0.584	0.145	0.115
1.94	0.087	0.583	0.124	0.094
2.65	0.105	0.631	0.093	0.078
3.17	0.114	0.629	0.077	0.078
3.64	0.123	0.691	0.069	0.068
4.24	0.135	0.684	0.073	0.057
4.96	0.134	0.678	0.050	0.051
5.94	0.145	0.731	0.064	0.028
6.36	0.145	0.735	0.058	0.022
7.04	0.150	0.784	0.065	0.031
7.47	0.156	0.777	0.059	0.037
7.81	0.162	0.770	0.056	0.009
8.68	0.159	0.749	0.046	0.016
9.38	0.157	0.758	0.040	0.032
9.97	0.167	0.763	0.043	0.011
11.00	0.168	0.765	0.035	0.009
12.44	0.141	0.778	0.031	0.008
12.48	0.146	0.776	0.032	0.008
13.22	0.145	0.781	0.030	0.000

Table D.11. Compositions of the gas phase initially formed by a a molar ratio C_2H_4:CO 5:1 in solvent MeP:MeOH (70:30% wt.) at 323 K.

T = 343 K				
P / barA	**y(CO)**	**y(ethene)**	**y(MeOH)**	**y(MeP)**
1.03	0.017	0.000	0.525	0.422
1.54	0.043	0.313	0.352	0.252
1.75	0.054	0.365	0.310	0.230
1.99	0.066	0.415	0.280	0.205
2.17	0.072	0.474	0.256	0.166
2.48	0.095	0.486	0.234	0.173
2.74	0.112	0.506	0.209	0.173
3.01	0.115	0.533	0.192	0.160
3.33	0.109	0.565	0.166	0.124
3.47	0.119	0.565	0.166	0.150
4.14	0.124	0.601	0.146	0.128
4.29	0.121	0.606	0.143	0.088
5.44	0.132	0.647	0.121	0.091
5.97	0.146	0.666	0.111	0.077
6.51	0.142	0.678	0.103	0.068
7.67	0.145	0.708	0.081	0.064
7.93	0.141	0.708	0.081	0.070
8.39	0.156	0.728	0.075	0.048
9.03	0.157	0.735	0.067	0.050
9.62	0.160	0.731	0.059	0.056
10.02	0.164	0.740	0.054	0.042
10.23	0.144	0.744	0.063	0.049
10.52	0.164	0.739	0.049	0.048
11.38	0.172	0.745	0.045	0.038
12.08	0.173	0.747	0.043	0.037
12.84	0.178	0.753	0.040	0.030
13.50	0.180	0.750	0.038	0.032
14.22	0.184	0.750	0.036	0.031
14.66	0.192	0.756	0.025	0.027

Table D.12. Compositions of the gas phase initially formed by a a molar ratio C_2H_4:CO 5:1 in solvent MeP:MeOH (70:30% wt.) at 343 K.

T = 363 K				
P / barA	**y(CO)**	**y(ethene)**	**y(MeOH)**	**y(MeP)**
1.70	0.000	0.000	0.615	0.385
1.80	0.000	0.000	0.614	0.450
2.10	0.002	0.017	0.618	0.363
2.10	0.005	0.033	0.613	0.350
3.30	0.039	0.264	0.445	0.252
3.35	0.043	0.287	0.445	0.243
4.70	0.083	0.396	0.360	0.189
5.75	0.115	0.482	0.294	0.147
6.80	0.097	0.552	0.221	0.129
7.60	0.098	0.560	0.218	0.122
8.40	0.099	0.567	0.214	0.120
9.45	0.138	0.601	0.194	0.099
10.30	0.140	0.628	0.178	0.097
11.90	0.146	0.642	0.140	0.086
12.23	0.144	0.645	0.132	0.076
14.10	0.157	0.685	0.106	0.072
14.40	0.157	0.684	0.101	0.071
14.90	0.158	0.686	0.094	0.069
15.20	0.160	0.691	0.090	0.049
17.20	0.172	0.712	0.091	0.053
17.80	0.173	0.713	0.091	0.055

Table D.13. Compositions of the gas phase initially formed by a a molar ratio C_2H_4:CO 5:1 in solvent MeP:MeOH (70:30% wt.) at 363 K.

D.6. Initial reaction rate determination for the methoxycarbonylation of ethylene.

[Pd] / ppm	G-L contact area / m^2	C_{MeOH}^0 / M	C_{CO} / M	$-R^0$ / mol MeP /Lmin	
5	1.7E-03	8.2	0.018	6.4E-03	
5	2.5E-03	8.2	0.019	1.4E-02	
5	3.4E-03	8.2	0.017	2.3E-02	
5	2.5E-03	8.2	0.014	1.2E-02	
5	2.5E-03	8.2	0.019	1.4E-02	
5	2.5E-03	8.2	0.024	2.0E-02	
5	2.5E-03	8.2	0.029	2.3E-02	k_{Lobs} / m/s
5	2.5E-03	7.7	0.033	1.5E-02	2.0E-05
10	2.5E-03	7.8	0.034	2.6E-02	3.5E-05
15	2.5E-03	7.7	0.031	4.1E-02	4.5E-05

Table D.14. Initial rates for the methoxycarbonylation of ethylene at 373 K and 15 barA; as a function of catalyst concentration, gas-liquid contact area, and CO film concentration.